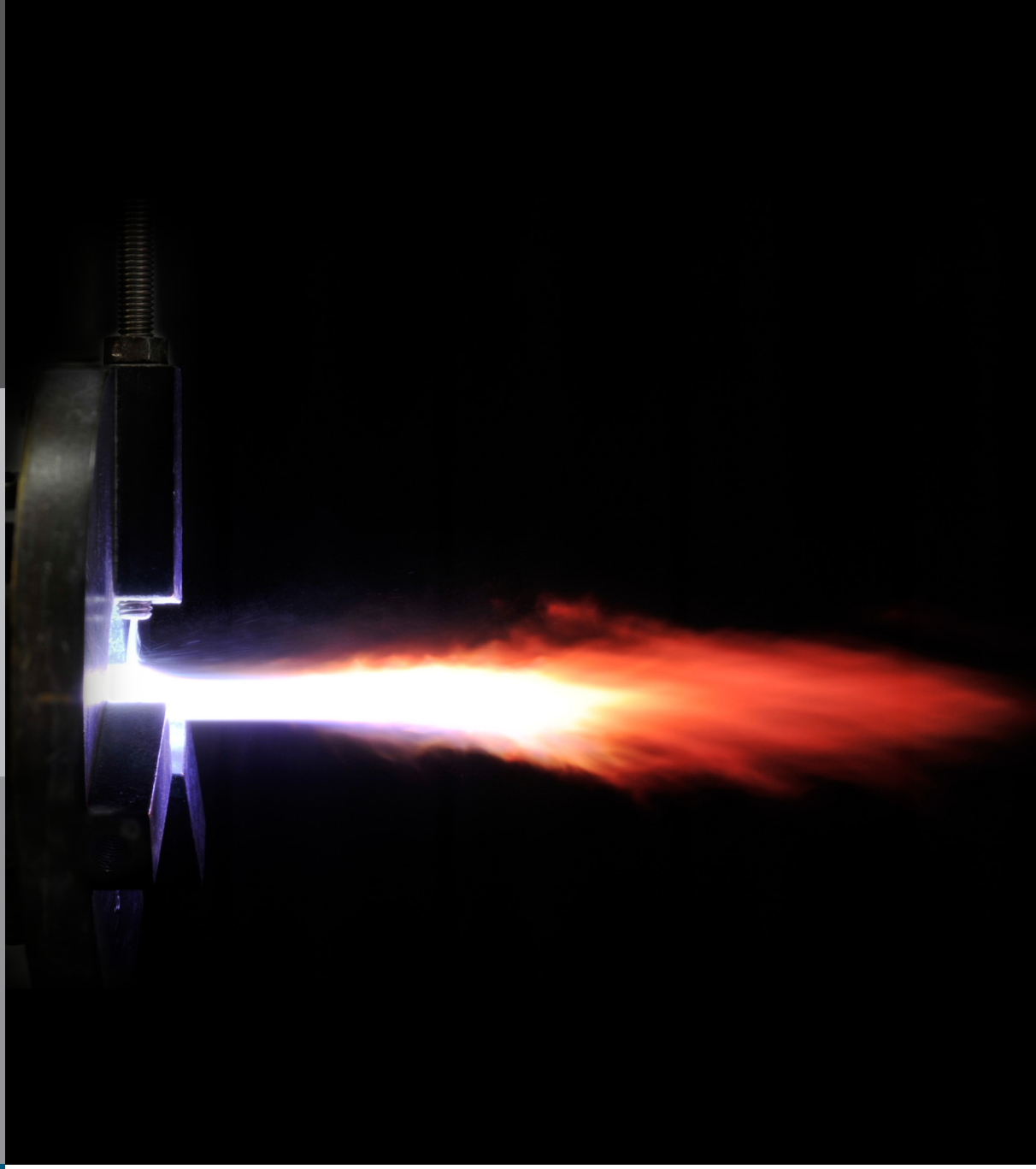

Development of thermal spray processes with liquid feedstocks

Alexandre Guignard

Mitglied der Helmholtz-Gemeinschaft

JÜLICH
FORSCHUNGSZENTRUM

Schriften des Forschungszentrums Jülich
Reihe Energie & Umwelt / Energy & Environment Band / Volume 141

Forschungszentrum Jülich GmbH
Institute for Energy and Climate Research (IEK)
Materials Synthesis and Processing (IEK-1)

Development of thermal spray processes with liquid feedstocks

Alexandre Guignard

Schriften des Forschungszentrums Jülich
Reihe Energie & Umwelt / Energy & Environment Band / Volume 141

ISSN 1866-1793 ISBN 978-3-89336-788-7

Bibliographic information published by the Deutsche Nationalbibliothek.
The Deutsche Nationalbibliothek lists this publication in the Deutsche Nationalbibliografie; detailed bibliographic data are available in the Internet at http://dnb.d-nb.de.

Publisher and Distributor:	Forschungszentrum Jülich GmbH Zentralbibliothek 52425 Jülich Phone +49 (0) 24 61 61-53 68 · Fax +49 (0) 24 61 61-61 03 e-mail: zb-publikation@fz-juelich.de Internet: http://www.fz-juelich.de/zb
Cover Design:	Grafische Medien, Forschungszentrum Jülich GmbH
Printer:	Grafische Medien, Forschungszentrum Jülich GmbH
Copyright:	Forschungszentrum Jülich 2012

Schriften des Forschungszentrums Jülich
Reihe Energie & Umwelt / Energy & Environment Band / Volume 141

D 294 (Diss., Bochum, Univ., 2012)

ISSN 1866-1793
ISBN 978-3-89336-788-7

The complete volume is freely available on the Internet on the Jülicher Open Access Server (JUWEL) at http://www.fz-juelich.de/zb/juwel

Abstract

The manufacture of submicrometer-structured coatings by thermal spraying is currently a subject of increasing research efforts in order to obtain unique and often enhanced properties compared to conventional coatings. Injecting suspensions of submicron ceramic particles into the plasma jet or the flame enables to deposit finely-structured coatings. Such fine microstructures are desired for a large range of applications, such as in the field of thermal barrier coatings (TBCs) for gas turbines. Suspension plasma sprayed (SPS) TBCs show unique mechanical, thermal and optical properties compared to conventional atmospheric plasma sprayed (APS) TBCs. They have thus the potential of providing increased TBC performances under severe thermo-mechanical loading.

The benefits of SPS-deposited yttria-stabilized zirconia (YSZ) TBCs are demonstrated, such as very fine porosity, high segmentation crack density and low Young's modulus. Although segmentation cracks survive during thermal cycling at 1400°C, it was shown that the sintering tendency is high at such temperature exposure. An improvement of the SPS YSZ microstructure was realized by reducing significantly the fraction of unmolten clusters. However, this improvement was not reflected in thermal cycling performances in a burner rig. Further experimental investigations with modified spraying parameters yielded a columnar-structured YSZ coating. This type of microstructure is advantageous for TBC applications since intercolumnar voids can comply with in-plane stresses during thermal cycling, similar to electron beam physical vapor deposited (EB-PVD) TBCs.

Further investigations on the SPS process with lanthanum zirconate ($La_2Zr_2O_7$) as a new promising material for TBCs yielded almost stoichiometric coatings by preventing lanthania evaporation with at the same time columnar-type structure being promising in terms of compliance.

The deposition of TiO_2 coatings by SPS was also investigated. A large range of various microstructures was produced and specific anatase phase content can be tailored. Tree-like columnar structures are particularly attractive for their large surface area that promotes photoactivity. SPS appears as a highly versatile process with great potential for the manufacture of these coatings.

Kurzfassung

Die Herstellung von Schichten mit einer Mikrostruktur im Submikrometer-Bereich mittels thermischen Spritzens ist derzeit ein wichtiges Forschungsthema, um einzigartige und oft verbesserte Schichteigenschaften im Vergleich zu herkömmlichen Schichten zu erzeugen. Das Injizieren von Suspensionen mit keramischen Partikeln im Submikrometer-Bereich in den Plasmastrahl oder die Flamme ermöglicht es, feinstrukturierte Schichten abzuscheiden. Solche feinen Mikrostrukturen sind für eine Vielzahl von Anwendungen erwünscht, zum Beispiel im Bereich von Wärmedämmschichten (WDS) für Gasturbinen. Suspensionsplasmagespritzte (SPS) WDS zeigen einzigartige mechanische, thermische sowie optische Eigenschaften im Vergleich zu herkömmlichen mittels atmosphärischen Plasmaspritzens (APS) hergestellten WDS. Deshalb haben sie das Potenzial, unter hohen thermomechanischen Belastungen erhöhte WDS-Leistungen zu erreichen.

Die Vorteile von SPS WDS aus Yttriumoxid stabilisiertem Zirkonoxid (YSZ) werden dargestellt, zum Beispiel ihre sehr feine Porosität, ihre hohe Segmentierungsrissdichte und ihr niedriges Elastizitätsmodul. Obwohl die Segmentierungsrisse die Thermozyklierung bei 1400°C aushalten, wurde gezeigt, dass die Sinterneigung bei solchen Temperaturen hoch ist. Eine Verbesserung der SPS YSZ Mikrostruktur wurde durch eine deutliche Verringerung des Anteils an unaufgeschmolzenen Clustern erreicht. Allerdings hat sich diese Verbesserung nicht im Thermozyklierverhalten widergespiegelt. Durch weitere experimentelle Entwicklungen konnte mittels modifizierter Spritzparameter eine YSZ Schicht mit kolumnarer Mikrostruktur erzeugt werden. Diese Art von Mikrostruktur ist für WDS-Anwendungen vorteilhaft, da durch interkolumnare Hohlräume Dehnungen in Zugrichtung in der Schichtebene während der Thermozyklierung ertragen werden können, ähnlich wie bei WDS, die mittels „electron beam physical vapor deposition“ (EB-PVD) hergestellt werden.

Weitere Entwicklungen des SPS Prozesses mit Lanthan-Zirkonat ($La_2Zr_2O_7$), einem neuen vielversprechenden Material für WDS, führten zu Schichten, die durch die Verringerung der Lanthanoxid-Verdampfung fast stöchiometrisch sind, bei gleichzeitig kolumnar-artiger Mikrostruktur, die im Hinblick auf die Dehnungstoleranz vielversprechend ist.

Weiterhin wurde die Herstellung von Schichten aus Titanoxid mittels SPS untersucht. Ein breites Spektrum von Mikrostrukturen mit spezifischem Anatas-Gehalt konnte erreicht werden. Baumartige kolumnare Mikrostrukturen sind wegen ihrer hohen spezifischen Oberfläche im Hinblick auf eine hohe Photoaktivität besonders attraktiv. SPS erwies sich als vielseitiger Prozess mit einem hohen Potenzial für die Herstellung solcher Schichten.

Table of contents

1. Introduction

1.1. Subject

Thermal spray processes are commonly applied in the industry for the production of advanced coatings. These coatings are manufactured for example to improve the performance of a component, such as in the case of thermal barrier coatings (TBCs) for gas turbines. Thermal spray processes involve usually the injection of a powder feedstock into a flame or a plasma jet. In the case of the conventional plasma spray process referred to as atmospheric plasma spray (APS), the powder particles must have a diameter in the range 10-100 μm to be flowable. This limitation in the feedstock particle size leads to a limitation in the possibilities of the process. With APS, it is difficult to obtain nanostructured coatings with very fine microstructure and/or to manufacture very thin coatings (below approx. 10 μm in thickness) as at least several lamellae piled up on each other are necessary to form a coating.

On the other hand, nanostructured materials have been under consideration these last decades because of their improved properties. Nanomaterials are attractive in the area of surface treatments and coatings technology as well. As a result, processes that enable to manufacture nanostructured coatings are being investigated in current research efforts. One possible method to spray submicron particles is to use agglomerated nano-powders. However, the most promising approach is to use a carrier liquid to inject directly the individual submicron particles into the plasma jet. Referred to as suspension plasma spray (SPS), this relatively novel process is very promising for the manufacture of nanostructured coatings for a large range of applications.

1.2. Aim of the work

The specific aims of this work are to develop submicrometer-structured ceramic coatings by employing the relatively novel suspension plasma spray process (SPS). The main focus is on the manufacture of yttria-stabilized zirconia (YSZ) coatings for applications as thermal barrier coatings (TBCs) for gas turbines. The fine microstructures of the coatings will be investigated and relevant coating properties will be characterized. Advantages compared to conventional atmospheric plasma sprayed (APS) coatings will be pointed out. With regard to TBC performances in thermal cycling conditions, the aim is to understand the underlying mechanisms that limit the lifetime and to improve coating performances. The approach is to improve the coating deposition process through a better understanding of the complex phenomena that take place in SPS. A further aim is to investigate the potential of depositing columnar-type coating structures with the SPS process in order to benefit from the unique properties related to this kind of microstructure similar to that of coatings produced by electron beam physical vapor deposition (EB-PVD).

In a second part of the work, the fabrication of $La_2Zr_2O_7$ coatings by SPS is investigated. This constitutes a new promising material for TBCs, having better thermal stability than conventional YSZ. The main issue of this material when being plasma sprayed with APS is that it is prone to La_2O_3 loss during spraying. The experimental investigations will demonstrate the potential of the SPS process for the production of these new TBCs with regard to this main issue.

The third part of this work focuses on the field of photocatalytic coatings. The SPS process is employed to manufacture TiO_2 coatings with the aim of yielding large surface areas and specific phase compositions in order to enhance the photoactivity of the coatings.

2. Background

2.1. Theoretical background

2.1.1. Thermal spray

Thermal spray is a surface coating technique. In the field of materials engineering, it is often an advantage to separate the base material which constitutes most of the mass of the component and its surface state. The base material plays mostly the role of fulfilling the component's structural properties such as its strength, its ductility and its weight. It contributes also mostly to the cost of the component and must therefore often be chosen accordingly to maintain its cost as low as possible. On the other hand the surface properties of the component can be advantageously determined by applying one or several coatings on its surface. This approach enables e.g. to add one or several functions to the component or to improve considerably its performances.
There is a large range of coating processes that provide various types of coating materials such as metals, oxides or carbides. The deposition processes can be e.g. of chemical nature, of mechanical nature or of thermal nature. Common processes are e.g. wet chemical methods as dip-coating, chemical vapor deposition (CVD), physical vapor deposition (PVD) and thermal spray.

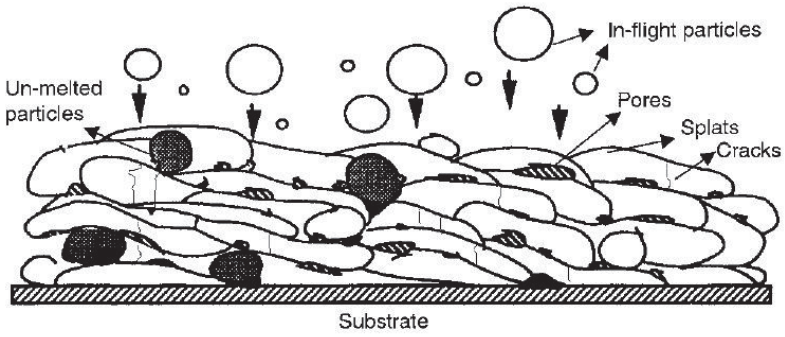

Fig. 1: Schematic of a thermal spray coating showing typical microstructural features such as splats, pores, cracks and unmolten particles [Kucuk '01].

In thermal spray processes, particles of a metallic or non-metallic material are heated by a heat source up to a molten or semi-molten state and accelerated by a flow until the impact on the substrate [Fauchais '01, Pawlowski '95]. The solidification of the obtained splats leads to the formation of the coating (Fig. 1). The heat source employed in thermal spray can be a combustion flame or an electric arc. In the combustion flame spraying, the chemical energy of the combustion of a fuel gas in oxygen is used to melt the material. The materials that can be deposited by this process are usually metals, alloys, cermets or ceramics with a low melting point. In the cases where an electric arc is used as heat source, much higher temperatures can be obtained, enabling to deposit ceramic materials with a higher melting point. The electric arc is either a direct current arc (d.c.) or a radiofrequency arc (r.f.) [Fauchais '04a]. In most cases, a d.c. arc is used, i.e. with a cathode (or three cathodes, e.g. in Triplex torches, leading to three arcs) and a circular anode (nozzle). The electric arc discharge between the cathode and the anode is in contact with a gas flow which is thus heated (Joule effect) and ionized, leading to the formation of a plasma. The electric energy of the current generator is converted into thermal energy. The plasma exits through the nozzle and expands to form a plasma jet. In the case of conventional plasma spray, the plasma jet is used in the ambient air at atmospheric pressure and the process is referred to as atmospheric plasma spraying (APS).

Depending on the experimental conditions, the plasma jet has very high temperatures (higher than about 8000 K in the core [Fauchais '02]) and velocities that can be above 2000 $m.s^{-1}$ at the nozzle exit. The feed material (usually a powder in a carrier gas) is injected into the plasma jet, typically perpendicularly to the plasma jet axis. The particles (typical size range between 10 and 100 μm) are melted and accelerated in the plasma up to a high velocity (typically several hundreds of $m.s^{-1}$) [Fauchais '00] and eventually impact the substrate, which is situated at a given distance from the plasma gun nozzle exit. The molten particles flatten and solidify to form lamellae or “splats” [Fauchais '04b]. The obtained coating is the build-up from these lamellae and has a thickness typically between 50 μm and a few mm, featuring many micron-size defects such as pores, cracks and unmolten particles. The plasmagenic gas is usually a mixture of two gases: a primary gas with a high density such as Ar or N_2 for the momentum transfer between the plasma and the sprayed particles and a secondary gas such as H_2 or He improving the heat transfer between the plasma and the particles.

Usually the surface of the substrate has to be previously roughened by sand blasting in order to obtain a high adhesion of the deposited coating.

2.1.2. Thermal barrier coatings (TBCs)

Thermal barrier coatings (TBCs) are commonly used to provide a thermal insulation on components in gas turbines, for both power generation and aerospace engines [Miller '97]. The efficiency of gas turbines is increased with higher entry gas temperature [Perepezko '09] and leads thus to lower fuel consumption and less emissions. The use of TBCs enables to decrease the metal surface temperature by up to approx. 200°C [Miller '87], thus allowing operating temperatures higher than the melting point of the nickel-based superalloy underneath. In addition to higher efficiencies, the lifetime of the coated components can also be significantly improved.

TBCs are bilayer systems containing one ceramic layer referred to as the topcoat, typically made of yttria partly stabilized zirconia (YSZ) [Clarke '03] with 7-8 wt.% Y_2O_3 [Stecura '86] to provide a thermal insulation, and one bondcoat sub-layer enabling a good adhesion between the ceramic layer and the coated metallic component and to increase the resistance to oxidation [Meier '91] and hot corrosion (Fig. 2). The bondcoat (typically made of a MCrAlY alloy) is aluminum-rich so that a protecting alumina layer appears in operating conditions due to the oxygen diffusion through the ceramic topcoat. This layer is referred to as the thermally grown oxide layer (TGO) and often plays an important role in the most common failure mechanisms of TBCs in thermal cycling conditions [Evans '01, Rabiei '00, Vaßen '04b].

Two coating techniques are commonly used at the industrial scale to produce the ceramic topcoat in TBCs: electron beam physical vapor deposition (EB-PVD) and atmospheric plasma spray (APS). These two processes yield very different microstructures (Fig. 3) and resultant coating properties. EB-PVD TBCs have a characteristic columnar structure yielding high strain tolerance. The voids between the columns can open and close and this lateral compliance reduces in-plane stresses during thermal cycling operations [Schulz '00]. On the other hand, EB-PVD TBCs

show a relatively high thermal conductivity (in the range of 1.8-2.0 W/m.K) [Schulz '04] since the intercolumnar gaps are parallel to the heat flow. APS TBCs contain interlamellar pores lying perpendicular to the heat flow, thus yielding low thermal conductivities that can reach values below 1.0 W/m.K [Mauer '09]. However they have a lower lateral compliance than EB-PVD TBCs. The APS technique induces much lower costs than EB-PVD. Therefore, APS TBCs are advantageous for large components such as combustion chambers. They are mostly applied in land-based gas turbines for power generation, in which operating times are long and thermal cycling is limited. On the contrary, the high costs and low deposition rates of EB-PVD tend to restrict its application for the most critical components in a gas turbine in which high lateral compliance is highly demanded, mostly in aerospace gas turbines where more frequent thermal cycling operations occur. They are also appropriate for rotating components such as turbine blades. Nowadays, more APS TBCs than EB-PVD ones are being developed due to the significant improvements that were realized on the APS process [Mauer '11]. One of the main challenges in the field of TBCs is to manufacture coatings having both good insulating properties and a high cycling lifetime at high temperatures. Innovative thermal spray processes are expected to yield a solution to these issues. Besides, current TBC developments tend to focus as well on new oxides to substitute YSZ because of its limited temperature capability above 1200°C [Clarke '05, Stöver '04, Vaßen '10a].

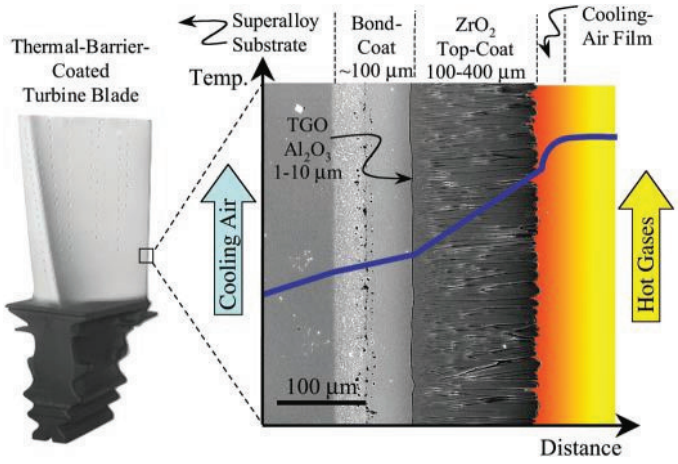

Fig. 2: Structure of a thermal barrier coating (TBC) [Padture '02].

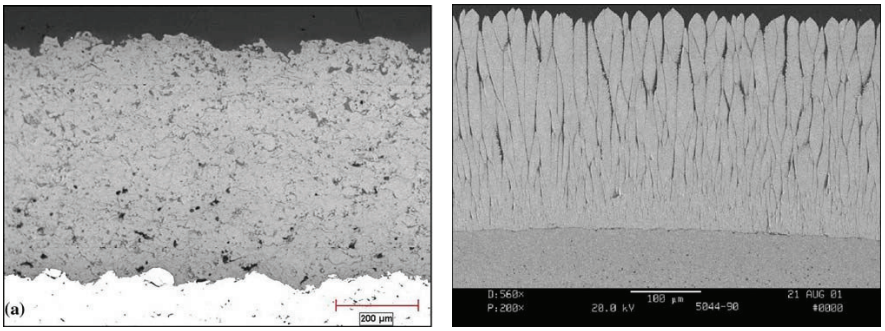

Fig. 3: Microstructure of TBCs: deposited by atmospheric plasma spraying (APS) (left) and by electron beam physical vapor deposition (EB-PVD) (right) [Feuerstein '08].

2.1.3. Suspension plasma spray (SPS)

By using nanostructured materials, the performance of engineering components can be increased. Many properties of nanostructured materials differ from conventional ones due to the larger volume fraction of internal surfaces. Therefore, these nanomaterials are widely used in different areas of application. In the field of thermal spray, the conventional APS process does not permit to deposit nanostructured coatings due to its restrictions in the particle diameter of the powder feedstocks. The feed material must be an easily flowable powder with a typical size range of 10-100 µm. In order to produce nanostructured coatings, submicron powders or nanopowders have to be used instead. However, these powders are not flowable enough and tend to agglomerate in conventional powder feeders employed for thermal spray, leading to clogging or irregular feed rates [Fauchais '10b]. As a result, submicrometer-sized powders cannot be directly used in thermal spray. This constitutes a restriction in the range of achievable microstructures since the sizes of feedstocks typically determine the microstructural scale of the deposited coatings.

An appropriate solution to this issue is to use a carrier liquid instead of the carrier gas to transport the fine particles into the plasma jet. The submicrometer-sized particles in a carrier liquid form a suspension. This technique is thus referred to as suspension plasma spraying (SPS). Particle diameters in the suspension feedstock are typically

between a few up to several hundred nanometers. Fig. 4 shows a micrograph of submicron particles used in the SPS process compared to a typical coarse flowable powder used in the APS process.

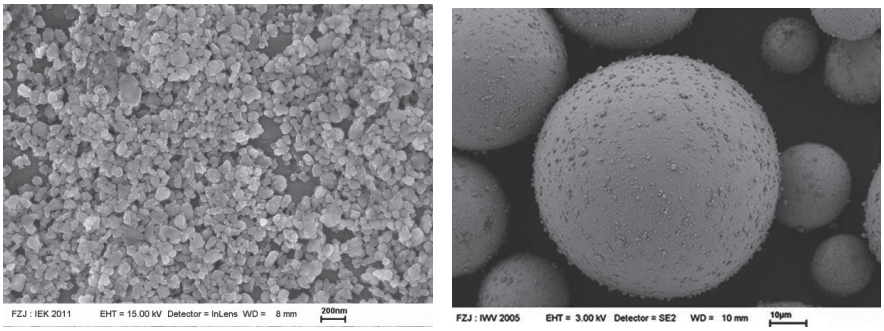

Fig. 4: Submicrometer-sized YSZ particles used for suspension plasma spraying (SPS) (left) compared to typical micrometer-sized particles (Sulzer Metco AG, Wohlen, Switzerland) used in conventional atmospheric plasma spraying (APS) (right). The left SEM micrograph is from the own work; the right one is from [Kaßner '08a].

The fine particles for SPS are dispersed in a solvent with a solid fraction commonly in the range 5-30 wt.% and the formulated suspension is directly injected into the plasma jet. Liquid injection can be realized as a coherent stream or as atomized droplets [Rampon '08b]. When entering the plasma jet, the liquid is subjected to a fragmentation due to the plasma jet shear effects, yielding even smaller suspension droplets [Fazilleau '06]. The solvent is rapidly vaporized and the particles located in a single droplet form an agglomerate (Fig. 5). The obtained solid agglomerates are accelerated and melted in the plasma jet [Delbos '06], transforming into ceramic molten droplets, and eventually impact onto the substrate surface. The deposited splats have very small dimensions (diameter from 0.2 to 6 µm and thickness of 20-300 nm [Kaßner '08a]) compared to typical APS splats having thicknesses of about 2-5 µm. As a result, SPS coatings have an increased number of lamellae and present significantly finer microstructures with the potential of improved properties. Fig. 6 illustrates the particle agglomeration phenomenon in the plasma by showing on the one hand YSZ primary particles contained in a suspension prior to spraying and on the other hand sprayed particles collected in water. The spherical shape reveals that

the particles reach the molten state during flight. Besides, the much larger particle diameter compared to the primary particles of the suspension points out that the particles collected in water are molten agglomerates. This experiment illustrates clearly the agglomeration phenomenon that occurs upon vaporization of the solvent in the plasma jet. The size of the agglomerates and hence the size of the YSZ molten droplets impinging the substrate are correlated to the diameter of the suspension droplets after the secondary fragmentation in the plasma. It is also observed in Fig. 6 that a fraction of the primary particles can still be seen after spraying into water. Due to their very fine size and hence their low momentum, this fraction of particles did not penetrate into the core of the plasma jet and thus were located in the fringes of the jet during flight. They do not reach the molten state and can be partly embedded in the coating as unmolten clusters of poorly bonded very fine particles. These unmolten clusters constitute non-negligible microstructural features that are mostly considered to be detrimental to the overall mechanical stability of the coating.

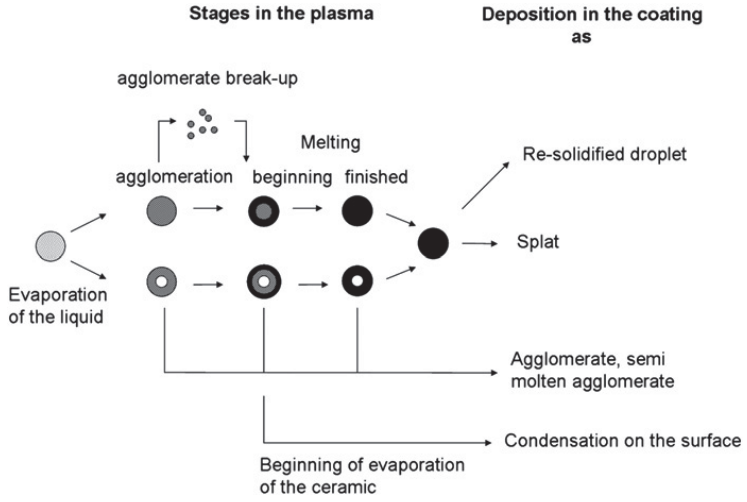

Fig. 5: Schematic of the droplet and particle stages during flight and at deposition for SPS [Kaßner '08c].

Due to the low thermal inertia of the nano-scaled particles, the spraying distance (distance from the nozzle exit to the substrate surface) is typically shorter than for APS (typically below 80 mm). Another closely related thermal spray process employs also liquid feedstocks and is referred to as solution precursor plasma spray (SPPS). In

this case, a solution containing a chemical precursor is used as feedstock instead of a suspension. The precursor is heated in the plasma jet and pyrolized to form submicrometer-sized particles in flight that are eventually deposited onto the substrate [Fauchais '08b].

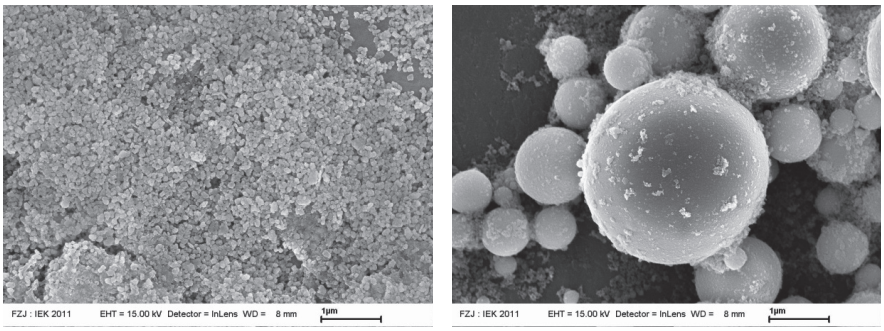

Fig. 6: YSZ primary particles contained in a suspension prior to spraying (left); sprayed particles collected in water (right). The two images have the same magnification to illustrate clearly the agglomeration phenomenon that occurs in SPS upon spraying.

The attractiveness of the SPS process for the deposition of a large range of coatings for various applications turned it into a currently active research field. Current developments by a large number of research groups are presented in the following section.

2.2. Literature review: recent developments on SPS coatings

The rapid development of thermal spray processes using liquid feedstock is reflected by a large number of review papers published since 2006 by Fazilleau et al. [Fazilleau '06], Delbos et al. [Delbos '06], Fauchais et al. [Fauchais '08a, Fauchais '08b], Pawlowski [Pawlowski '08, Pawlowski '09], and more recently in 2010 and 2011 by Fauchais et al. [Fauchais '10a, Fauchais '11a, Fauchais '11b].

There is a large variety of potential and emerging applications for coatings produced with suspension plasma spraying (SPS). The following literature review includes some new applications for wear-resistant, thermal barrier, corrosion-resistant, bioactive, photocatalytic, and electrochemically functional coatings manufactured by SPS and also by solution precursor plasma spraying (SPPS). The author's work in this review was already published as part of a journal article in 2011 [Killinger '11].

2.2.1. Yttria-stabilized zirconia (YSZ) and NiO/YSZ

Yttria-stabilized zirconia (YSZ) coatings deposited by SPS and/or SPPS were subjected to intensive research for several applications, mostly for thermal barrier coatings (TBCs) or solid oxide fuel cells (SOFCs).

Suspension plasma spraying experiments for YSZ TBCs were performed by Kaßner [Kaßner '09a, Vaßen '09c]. On the basis of diagnostic measurements [Mauer '10], the optimum spray distance was found at 65 mm where the particles just begin to solidify and their velocity is still high. Shorter stand-off distances run the risk of overheating the substrates. Applying these process parameters for turbine components, homogeneous microstructures with an evenly distributed pore network were obtained. At a larger spray distance of 75 mm and in particular at 85 mm, very large pores were observed. Above 85 mm globular re-solidified particles were incorporated. Further downstream at 95 mm, the coating consisted mainly of re-solidified material. At the same time, the deposition efficiency dropped continuously.

Furthermore, at a spray distance of 65 mm, Kaßner already achieved high segmentation crack densities at small coating thicknesses. Such segmented TBCs offer good thermal shock resistance, but if they are manufactured by APS their thermal conductivity is significantly higher compared to conventional porous APS

TBCs [Vaßen '10b]. In contrast, the suspension-plasma-sprayed TBCs show a high porosity and thus a low thermal conductivity as well as many segmentation cracks at the same time. Kaßner achieved the best lifetime results in thermal cycling tests for samples with medium porosity (23%) and a high segmentation crack density (approximately 11 cracks/mm) [Kaßner '08a]. An example is given in Fig. 7. The segmentation cracks and the evenly distributed porosity are obvious. Compared to APS coatings, the much larger fraction of small pores <1 µm is typical. These micropores provide not only low thermal conductivity but also considerably improved reflectivity and lowered transmittance in the near-infrared wavelength range between 0.5 µm and 2.5 µm since they act as scattering centers reducing the semi-transparency of YSZ. This is relevant for the reduction of the radiative heat load of turbine components [Vaßen '08].

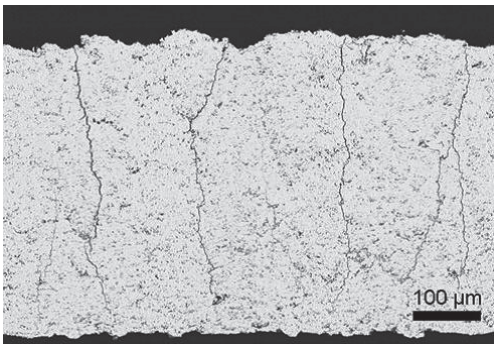

Fig. 7: Suspension-plasma-sprayed thermal barrier coating with medium porosity and high segmentation crack density [Kaßner '08a].

Ben-Ettouil et al. reported on the manufacture of SPS-deposited YSZ TBCs by using two different commercial powders of different particle size distributions for the preparation of the sprayed suspensions [Ben-Ettouil '09]. The deposited coatings were submitted to a series of thermal shock tests. It was shown by the authors that the suspension with a lower average particle size and a narrower particle size distribution led to better results. However, the absence of bond coat in the tested TBC samples combined with the pre-polishing of the steel substrates might have promoted the early spallation of the coating and thus have been detrimental to the thermal shock performances.

Research activities on the SPS and SPPS processes for SOFC applications are reflected by several recent papers, which are described in Table 1.

Table 1: Overview of the recent research activities on SPS and SPPS for SOFCs

SOFC component	Process investigated	Main statements	Ref.
YSZ electrolyte	SPS	The best results in coating gas tightness were obtained with the F4MB torch at a spraying distance of 30 mm leading to a gas permeability of 4.16×10^{-16} m², which is still poor compared to data from the literature for APS coatings. This is explained by the presence of columnar stacking defects due to the scale difference between the very low average size of the feedstock (50 nm) and the average roughness of the porous substrates used for permeability measurements (2.5 µm).	[Brousse '09]
YSZ electrolyte	SPS (axial injection)	The focus was placed on the optimization of the feedstock suspension and the effects of solid loadings, dispersant type and dispersant concentration on suspension viscosity and coating characteristics. Optimum dispersant concentration ranges were determined for three different dispersants.	[Waldbillig '09]
YSZ electrolyte	SPS	Optimization of the spray parameters showed that the density of electrolyte coatings was increased with higher plasma torch input power.	[Wang '10b]
NiO/YSZ anode	SPS	The porosity of the anode was increased by a higher suspension feed rate while it was reduced by higher plasma gas flow and higher spraying distance.	[Wang '10b]

NiO/YSZ anode	SPS	The nature of the solvent as well as the atomizing gas rate in the two-fluid atomizing nozzle have major effects on the coating porosity. Better performances of the layers were achieved when using a low atomizing gas flow rate and an ethanol-based suspension.	[Marchand '10]
La_2NiO_4 cathode	SPS	In contrast to the NIO/YSZ anode, the La_2NiO_4 cathode showed better characteristics when sprayed with a water-based suspension.	[Marchand '10]
NiO/YSZ anode	SPS and SPPS	Both SPS and SPPS routes enable a homogeneous distribution of NiO in the YSZ matrix. However, while SPS presented injection problems associated with the dispersion and stabilization of the fine powder in the suspension solvent, SPPS enabled an intimate mixing of the salts in the solution. Thus, SPPS was suggested as a good alternative to circumvent poor stability and fast sedimentation of the suspension in SPS.	[Michaux '10]
gadolinia-doped ceria electrolyte as an alternative material to YSZ	SPS and SPPS	Gadolinia-doped ceria ($Ce_{0.8}Gd_{0.2}O_{1.9}$) has a higher ionic conductivity than YSZ but tends to show electric conductivity. It is presented as an alternative material for intermediate temperature SOFCs (IT-SOFCs). While SPPS led to a globular microstructure and an increased porosity, SPS enabled more homogeneous and much denser deposited layers, thus providing improved gas tightness. The fine SPS particles penetrated into the pores and cracks of the anode substrate upon impact. This yielded an improved adhesion between the electrolyte and the anode.	[Jia '10]
$Sm_{0.5}Sr_{0.5}CoO_3$ cathode	SPPS	In IT-SOFCs, the cathode polarization is critical for fuel cell performance as it increases	[Wang '10a]

		dramatically at reduced operating temperatures. In this regard, materials with high performance at low temperatures such as $Sm_{0.5}Sr_{0.5}CoO_3$ are considered as cathode materials. The fine particles in the SPPS-deposited layers contributed to reducing the cathode polarization (characterized by electrochemical impedance measurements). However, it remained large compared to other data in the literature so that this seems still not to be practicable.	

An assessment of these recent SPS and SPPS activities for SOFC components reveals that these investigations are still at an early stage since high performance cells were not reached up to now with these processes.

Another application of the SPS process was presented by Vert et al. [Vert '10]. A 4th generation nuclear reactor (gas-cooled fast reactor) requires the development of a protective coating able to resist high temperatures, high pressure variations and wear. In this specific application, the superalloy substrates need to be thin (1 mm in thickness) and thus do not permit grit-blasting prior to coating deposition. Nevertheless, good coating adhesion has to be ensured even on such smooth substrates. SPS was assessed here to be a promising candidate since the small size of the sprayed particles is likely to be adapted to the low substrate roughness. The authors investigated the deposition of YSZ coating by SPS and focused on the effect of the spray parameters on coating adhesion.

2.2.2. Alumina, alumina-zirconia and alumina-titania

Alumina (Al_2O_3) is widely applied for wear-resistant and electrically insulating coatings. Toma et al. provided an overview of suspension-sprayed Al_2O_3 coatings [Toma '10]. SPS of Al_2O_3 is focused to retain to the greatest possible extent of the only thermodynamically stable α-phase as conventional APS processes mainly

produce metastable phases, e.g. γ- or δ-Al_2O_3, with disadvantages regarding long-term stability in humid environments or electrical insulating properties. Furthermore, nanostructured Al_2O_3 coatings with improved mechanical characteristics have attracted interest.

Research activities on wear-resistant coatings fabricated by SPS are reflected in several recent papers, which are summarized in Table 2.

Table 2: Overview of the recent research activities on SPS-deposited wear-resistant coatings

Material	Main statements	Ref.
Al_2O_3	It is shown that SPS coatings had higher microhardness than APS coatings under all loads, due to their reduced grain size. The indentation fracture toughness was also found to be higher for SPS coatings. This was attributed by the authors to the finer structure and the stronger interlamellar cohesion due to the fine SPS particles being melted to a larger extent. The bonding strength to the substrate was also better for SPS. Because of the improved mechanical properties of SPS-deposited coatings the authors assumed that their behavior under abrasive wear and sliding friction will be better than for APS coatings.	[Oliker '09]
Al_2O_3 and Al_2O_3-ZrO_2	The decrease of the spraying distance, the solid mass ratio or the nozzle internal diameter yielded a reduction of the number of poorly treated particles in the coating structure, thus leading to lower stacking defect density and denser coatings. Some preliminary characterizations of the wear behavior showed a low friction coefficient and good wear resistance. The tribological behavior of Al_2O_3-ZrO_2 coatings was found to be even better than that of the Al_2O_3 coatings. Fig. 8 shows a typical micrograph of an Al_2O_3-ZrO_2 composite coating.	[Tingaud '10a]

Al_2O_3, Al_2O_3-ZrO_2 and Al_2O_3-SiC	SPS enabled the feedstock composition to be preserved, even with material displaying high vapor pressure such as SiC. The most important parameters with respect to coating microstructure and mechanical properties were found to be feedstock size distribution and plasma gases. This study confirmed that a reduced feedstock size led to a lower friction coefficient. The latter could also be decreased by the addition of SiC in the Al_2O_3 matrix. Besides, the Al_2O_3-ZrO_2 composite coatings showed higher wear resistance than the Al_2O_3 coatings.	[Darut '10a]
Al_2O_3 and Al_2O_3-TiO_2	It was found that the phase composition of the feedstock was partially retained in the deposited coating. The operating parameters were optimized and it was demonstrated that a reduced spraying distance (30 mm) and an increased plasma mass enthalpy were necessary to deposit dense and cohesive coatings.	[Darut '10b]

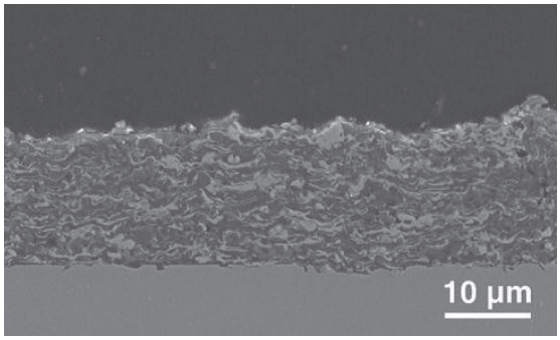

Fig. 8: Rather dense Al_2O_3-ZrO_2 composite coating manufactured by SPS [Tingaud '10a].

Qiu et al. found that the quality of SPS-deposited Al_2O_3 coatings is strongly dependent on plasma power, spraying distance, suspension solvent, suspension concentration, inner diameter of the suspension injection needle and injection pressure [Qiu '09]. The optimized conditions were determined for each parameter. The authors demonstrated that a low suspension concentration yielded decreased droplet sizes,

thus enabling better melting and finally a smoother coating surface. Spraying distance had an effect on the phase transformation of Al_2O_3. It was found that an ethanol-based suspension provided better results while water-based suspensions resulted in unmelted particles.

In order to better understand the coating manufacturing mechanisms occurring with SPS, Tingaud et al. performed spraying experiments with Al_2O_3 suspensions and studied the effects of several operating parameters [Tingaud '09]. Spray beads (see Trifa et al. in [Tingaud '09]) were sprayed onto polished stainless steel plates by consecutive passages of the torch in front of the plates. The spray bead profile and its surface roughness were characterized with a surface profilometer. The authors found that the thickness of the deposited bead was significantly dependent on the spraying distance and developed non-linearly in the investigated range of spraying distances.

The investigations on spray bead profiles by Tingaud et al. were continued by studying the effect of different plasma gas mixtures [Tingaud '10b]. The main characteristics of the different plasma flows at the nozzle exit were determined by using an analytical model according to the specific enthalpy and the thermophysical properties. The authors showed that the choice of the plasma gas mixture had a great effect on the spray bead thickness and microstructure. The obtained results yielded a better understanding of the process manufacturing mechanisms and enabled a wide range of coatings with different microstructures to be sprayed. Then the authors applied these findings to manufacture three types of Al_2O_3-ZrO_2 coatings with different architectures: graded coatings, composite coatings and finely structured multilayers.

Al_2O_3-ZrO_2 composite coatings were studied by Chen et al. [Chen '09a, Chen '09b]. The authors stated that the preparation of crystalline nanosized powders, often used in both APS and SPS processes, appears to be rather expensive due to the high temperature and long heat treatment required. In contrast, the preparation of amorphous powders should be cheaper thanks to the low temperature and short heat treatment. Therefore, in this investigation, an amorphous powder was produced and then dispersed in ethanol for SPS. The coating obtained was composed of α-Al_2O_3 and tetragonal ZrO_2 phases and showed a very homogeneous phase distribution compared to coatings sprayed with crystalline powder by SPS or APS.

Tarasi et al reported on the deposition of Al_2O_3/YSZ nanocomposite coatings by SPS using the Axial III™ torch, for a potential application as TBCs [Tarasi '10]. The authors investigated the phase formation in the coating and found that the in-flight particle velocity (measured by Accura-Spray G2 from Tecnar Automation, Canada) was the crucial parameter. Low particle velocities led to stable phases while high velocities yielded metastable phases. The particle velocity was controlled by the plasma auxiliary gas and the plasma power. It was found that the particle temperature does not play an important role in the phase formation as long as it is high enough to reach complete particle melting.

2.2.3. Titanium oxide

Titanium oxide films and coatings have been studied frequently within the time scope of this review because of their interesting physical, chemical and electrical properties. Thus, the application of TiO_2 coatings as hydrogen and oxygen sensors, self-cleaning and photocatalytic surfaces, to degrade organic pollutants but also as electron emitters for light-emitting devices has been considered [Jaworski '10]. When thermal spraying TiO_2, an important issue is always the phase composition of the deposit. It is generally assumed that anatase has a higher photocatalytic activity than rutile. Furthermore, microstructural features such as porosity and specific surface are essential. Hence, suspension thermal spraying offers a large potential to manufacture efficient TiO_2 coatings.

Toma et al. compared the photocatalytic behavior of titanium oxide coatings deposited by SPS as well as by HVOF suspension spraying [Toma '09, Toma '10]. The feedstock material contained about 80% anatase with 25 nm average crystallite size. The largest anatase contents (67 to 80 vol.%) were found in the SPS coatings while 26.8 to 41.5 vol.% were identified in the HVOF suspension spray deposits. Based on dye decoloration and pollutant degradation experiments, the authors proposed a threshold of 65% anatase to achieve sufficient photocatalytic performance. In the case of SPS, the coatings consisted to a great extent of non-melted regions. Thus, the authors assumed that the high anatase content was due to the fact that anatase was retained from the feedstock. However, as a consequence they also found only poor adhesion of the coatings.

A comparison between external atomization and internal continuous stream injection of water-ethanol based TiO_2 suspensions into the plasma torch was presented by Kozerski et al. [Kozerski '10b]. The feedstock material was rutile with a volume-to-surface mean diameter of 0.33 µm. The external atomizer produces distinctly smaller droplets than the continuous jet breakup occurring with use of the internal injector so that considerably smaller agglomerates are expected to form upon evaporation of the liquid. For such conditions, higher anatase contents were detected. However, they were still small (< 15.4 vol.%) and did not show a significant correlation with the photocatalytic activity. The authors suggest that the particle-size-dependent solidification conditions on the substrate are responsible for the amount of anatase.

High anatase contents and nanocrystalline microstructures were also the reason to apply SPS for the manufacture of TiO_2 photovoltaic Graetzel cells [Vaßen '09d]. The feedstock material was anatase with a mean particle size of 60 nm. In preliminary experiments, the best results were achieved from SPS at low substrate temperatures. An alternative SPPS approach yielded only low deposition rates. Thus, cold SPS parameters were developed since it was assumed that the phase transformation from anatase to rutile mainly took place on the hot substrates. The results were highly porous TiO_2 coatings with anatase contents of about 90% and crystallite sizes well below 50 nm. However, the photovoltaic cell design still had to be optimized to achieve sufficient efficiencies.

Titania's ability to absorb light energy also makes it a viable material to implant in a matrix of crystalline silicon in order to increase the efficiency of appropriate photovoltaic cells. Moroz et al. presented such an approach based on a liquid titanium isopropoxide precursor coaxially fed with ethanol into the plasma torch while silicon powder was externally injected downstream [Moroz '10]. Dense composite coatings 75-150 µm in thickness were obtained containing nanosized titania particles. Both the TiO_2 phases anatase and rutile were observed. Furthermore, axial precursor injection was compared to external atomizing feeding. The latter produced considerably smaller particle sizes. In this case, the authors obtained the most predominant anatase contents in the titania nanoparticles.

Furthermore, as another application, TiO_2 is also utilized as a wear-resistant coating material. In this regard, non-stoichiometric so called Magnéli phases (Ti_nO_{2n-1}) show reduced frictional coefficients under dry sliding conditions, but they tend to transform to the more stable rutile losing their advantageous friction behavior. This can be

avoided by replacing Ti^{4+} cations and possible vacancies, for example, by Cr^{4+} or Cr^{3+} species, respectively, yielding so-called Andersson phases with a broad range of solid solubility. Erne et al. reported on the initial development of SPS parameters for such feedstock material [Erne '09]. However, results of coating experiments are not yet available.

2.2.4. Hydroxyapatite

Hydroxyapatite (HA) is a bioactive ceramic material having a chemical composition ($Ca_5(PO_4)_3OH$) and crystal structure close to human bone [Jaworski '10]. It is therefore particularly appropriate as a coating material for the integration of prostheses into osseous tissue (Sun et al., Lee et al. and Ogiso in [Jaworski '10]). The most widely applied method for manufacturing HA coatings is APS, thanks to its high deposition rate and low cost [d'Haese '10]. The development of SPS enables thinner HA coatings (10-50 µm) to be obtained than with APS, which may thus lead to a reduction in prostheses production costs.

The first developments of SPS-deposited HA coatings were performed at Sherbrooke University (Canada) by using induction plasma (Bouyer et al. in [Jaworski '10]). Current developments in this field are now being carried out in the research group of Pawlowski by using DC arc plasma [Jaworski '10]. The fine HA powder used for the formulation of the suspension is synthesized by a wet method using calcium nitrate and diammonium phosphate in ammoniacal solution as described in [Jaworski '09]. The spray parameters were optimized by analyzing the morphology of the splats obtained after spraying during a few passes of the plasma torch onto aluminum substrate [Kozerski '10a]. The optimized coatings have a so-called *two zones microstructure* (Fig. 9): a dense zone with big well-melted lamellae and a sintered zone with very fine submicrometric grains. The sintered zone is assumed to be formed by the impact of grains, which are only sintered in flight without having reached the molten state, and which continue to sinter after deposition. The formation of the two distinct zones is attributed by the authors to the different trajectories of the droplets formed in the secondary breakup. The droplets remaining in the central area of the plasma jet are properly melted. In contrast, some other droplets may have their

trajectory in the periphery of the jet and therefore receive a heat input sufficient to sinter the grains but not sufficient to be melted.

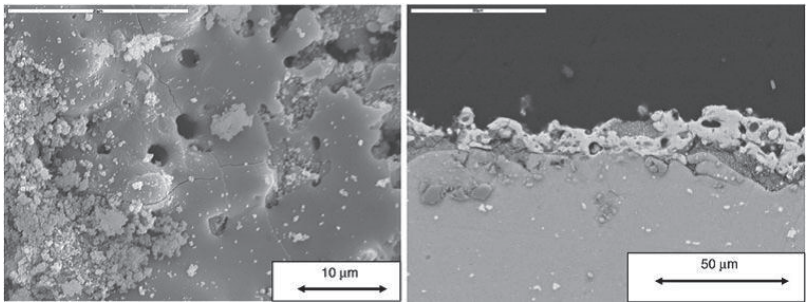

Fig. 9: Scanning electron micrograph (secondary electrons) of suspension-plasma-sprayed HA coating surface (left) and cross-section (right) [Kozerski '10a].

Phase analysis of the deposited coatings by X-ray diffraction (XRD) showed the presence of HA crystals and several phases due to the decomposition of HA due to the high temperature treatment [Jaworski '10]. The authors explain the formation of these phases by the phenomena during the flight of HA particles. The presence of phases from the decomposition of HA and their respective fractions are of great importance since they determine the biological behavior of the coating, such as its dissolution in vivo (Weng et al. in [Jaworski '10]).

Podlesak and al. carried out an advanced microstructural study of these SPS HA coatings [Podlesak '10]. Results show that the first zone (dense zone) contains HA, tetracalcium phosphate (TTCP) and a phase rich in calcium oxide. The second zone (sintered zone) contains only initial HA fine grains. The deposition process was optimized using a statistical design of experiments with two variables: spray distance and electrical power input to the plasma. The phase composition of the obtained deposits was found to be strongly dependent on the spray distance.

These HA coatings were also submitted to corrosion tests in a so-called simulated body fluid (SBF) [d'Haese '10]. The sprayed coatings were soaked in SBF for a period ranging from 3 to 60 days. It was shown that soaking in SBF homogenizes the coating morphology. The so-called sintered zone disappears and the pores are filled by reprecipitated calcium phosphates. The mechanical properties of the soaked samples were also characterized and compared to as-sprayed samples [Łatka '10]. The adhesion of the coatings to the substrate determined by the critical load in a scratch

test shows a slight decrease of about 20% after 60 days of soaking. The Young's modulus of the coatings characterized by depth-sensing indentation test does not change with soaking. Coating hardness measured by a scratch test remains constant during soaking. In contrast, the Martens hardness determined by the indentation test on cross-sections increased with time of soaking. The authors attributed this behavior to the dissolution of fine grains (sintered zone) in the SBF, thus leaving only the hard and dense lamellae.

Furthermore, Huang et al. reported the manufacture of nanostructured HA coatings by SPPS [Huang '10]. The HA liquid precursor prepared by wet chemical synthesis is directly used as feedstock for plasma spraying. The SPPS-deposited HA coatings are characterized and compared to APS-deposited HA coatings. The authors showed that SPPS leads to a lesser degree of decomposition during spraying. This is attributed to the evaporation of the water solvent, which leads to a reduction of temperature during the SPPS process. Moreover, SPPS enables a higher content of OH^- groups to be obtained in the coatings, which may lead to a superior structural integrity than that of APS coatings. According to the authors, these nanostructured HA coatings would achieve better biological properties than conventional APS-deposited ones.

2.2.5. Other materials

Dysprosium-doped yttrium aluminum garnet (Dy^{3+}:YAG, YAG=$Y_3Al_5O_{12}$) can be used as thermographic phosphor to measure surface temperatures by applying a thin coating. Chen et al. reported on the development of an appropriate SPPS process with the objective of higher deposition rates than offered by alternative chemical vapor deposition, spray pyrolysis or pulsed laser deposition processes [Chen '09c]. In addition to the desired photoluminescent properties, the coatings with a thickness of ~60 µm showed a columnar structure with fine splats (0.5-2 µm) and spheres so that a high strain tolerance at elevated temperatures can be expected. More recently, the same authors reported on similar investigations on europium-doped yttrium oxide coatings deposited by SPPS as well for the same application [Chen '11]. Obtained coatings showed a porous structure also enhancing the strain tolerance at high temperature.

Kitamura et al. reported on the deposition of yttrium oxide (Y_2O_3) by SPS for electronic applications [Kitamura '11]. By injecting the suspension axially into the plasma plume of the Axial III™ plasma torch, particle velocity reached 600 m s^{-1}, producing dense (porosity 0.3-0.4%) and uniform coating structures.
Cipri et al. developed a new approach by combining a conventional APS system with a so-called secondary suspension injection system [Cipri '09]. The aim was to manufacture composite coatings consisting of an APS-deposited ceramic matrix containing an SPS-deposited heat-degradable secondary phase. Alumina powder was chosen as feedstock for the APS matrix and flake-like graphite particles dispersed in water were used as the suspension in order to obtain self-lubricating coatings. Optimized deposits showed a uniform distribution of graphite splats or rounded flakes between alumina lamellae, thus demonstrating the feasibility of this combined spraying technique.

2.2.6. Conclusion

The variety of current research and development in plasma spray coatings from liquid feedstock, such as suspensions and solution precursors, is the subject of numerous new scientific articles and conference contributions. At present, it is hardly possible to assess the specific advantages of the different approaches. Thus, developments have to be followed carefully to identify strengths and weaknesses. Although there is still a lack of fundamental understanding of these innovative processes, the evaluation of recent publications since the beginning of 2009 shows great interest and confidence. This is confirmed by the first SPS-related industrial equipment which are now on the market [Cotler '11, Tang '10], thus showing the increasing maturity of SPS developments. However, publications on first commercial applications are still missing. Although the large potential of SPS is generally recognized, its current development situation is characterized by some fundamental uncertainties, particularly concerning its true industrial competitiveness. The following section aims to yield a critical assessment of SPS related to various aspects of the process.

2.3. Study of the industrial competitiveness of SPS

SPS has attracted great and always increasing interest from the thermal spray community and has been subjected to intensive research efforts. Several research groups are working on the development of this process to produce advanced nanostructured coatings with a wide range of materials and applications. These activities are reflected in numerous publications and presentations at conferences, particularly in the recent years, thus showing the rapid development of the technology. This gives evidence of the high interest and confidence with which the community is considering this relatively novel process.

However, the SPS process is not yet established among the other coating technologies. Up to now, there has been no publication on first commercial applications. There are still fundamental uncertainties about the specific advantages of SPS. This study aims to analyze these issues and will focus on the field of thermal barrier coatings (TBCs) as an example of promising application for SPS. A further outlook on functional layers for solid oxide fuel cells (SOFCs) will also be given having in mind that the SOFC technology itself is also not yet established. The competitiveness of SPS compared to conventional coating processes such as APS and physical vapor deposition (PVD) will be investigated. The various strengths and weaknesses of SPS will be critically analyzed. In particular, the similarities and differences with APS will be pointed out and evaluated.

The scope of the study will not be restricted to a simple comparison related to the coating characteristics and properties, but will rather be focused on the processes themselves. Various aspects of the technology will be considered such as among others: processing costs, powder or suspension handling, suspension storage issues, clogging issues in suspension feeding, needs of cleaning the chamber, etc. Several quantitative characteristics will also be evaluated and compared such as: feeding rate, deposition rate, deposition efficiency, spraying distance, etc. The analysis will be based on our own knowledge as well as available data from the literature (scientific articles and patents) and from the industry. A particular emphasis will be laid on the current SPS-related research and development activities in the industry. In this regard, an analysis of the patent situation will be conducted. This investigation aims to

provide a critical assessment of the SPS process and seeks after a better evaluation of its true competitiveness in the field of coating technology.

2.3.1. An overview of the current industry-related activities on SPS provided by an analysis of the patent situation

The analysis of the current patents in the field of SPS provides a good indicator of the SPS-related activities. The patents reflect the interest for this process in the industry. Furthermore, it enables to have an overview of the developments that are already protected by patented inventions and of the further developments that are still to be realized.

Early SPS patent at Sherbrooke University (1997)

The widely-known first patent on SPS was published in March 1997 by Sherbrooke University [Gitzhofer '97] under the title “Suspension plasma spray”. The invention relates to a plasma spray process that replaces the conventional powder feedstock by a suspension comprising small solid particles to produce either a protective coating on a substrate or a near net shape body. The object of the invention is to overcome the drawbacks of the conventional APS process related to the production of the feedstock powders. The SPS process eliminates the long sequence of steps involved in the preparation of the powder from a suspension, which often consist of chemical synthesis using precipitation or co-precipitation processes being costly and time consuming and that can also introduce impurities in the powder. With SPS, the suspension is directly atomized into the plasma, thus representing a significant advantage compared to conventional APS. The invention comprises also the possibility to replace the substrate by a vessel to produce a powder directly from the sprayed suspension. It is often widely known that this early patent on SPS describes a process in which an inductively coupled radio-frequency (RF) plasma torch is used (see Fig. 10), unlike most current plasma spray activities that are realized with direct current (DC) plasma torches. It should be noted that the patent also states that the RF plasma torch could be replaced by a DC plasma torch. Although this remark is written

only in the description of the invention and not in the patent claims, it should affect new patents. It is interesting to note that the spirit of the patented invention is exclusively related to the advantage of overcoming the drawbacks of APS related to the preparation of the powder feedstock. It appears to be not related to the microstructural benefits that arise from using lower particle size in a suspension.

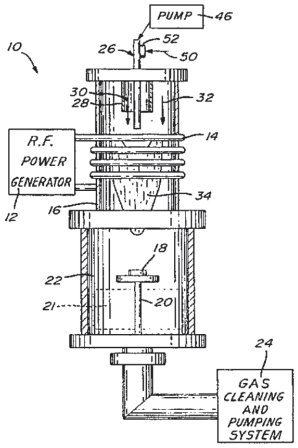

Fig. 10: Schematic diagram of an inductively coupled radio-frequency (RF) plasma torch used for SPS in the early patent by Sherbrooke University [Gitzhofer '97].

Recent SPS-related patents

Since this early patent by Sherbrooke University, several patents and/or patent applications were published in the past years. It is one of the aims of the present study to review the most relevant ones.

The University of Connecticut and the State University of New Jersey have published a U.S. patent in June 2003 entitled “Nanostructured feeds for thermal spray systems, method of manufacture, and coatings formed therefrom” [Strutt '03] (patent already granted). A rather similar version of this patent was published already in August 2001 [Strutt '01]. This invention comprises three separate embodiments for the fabrication of high-quality nanostructured coatings. The first embodiment is worth noticing but does not concern directly the SPS process. It describes a method for “reprocessing as-

synthesized nanoparticles powders to an aggregated form suitable for conventional spray deposition", i.e. for conventional powder APS. The second embodiment is related more directly to SPS. It is a method for "direct injection" of nanoparticles into a plasma stream or a combustion flame by using a liquid medium. Numerous examples of applications are provided in the patent, among them TBCs formed of nanostructured YSZ can be deposited by either the reprocessing method or by the direct injection method. This patent claims also the use of numerous nanostructured materials, being ceramics (e.g. YSZ, Al_2O_3 and hydroxyapatite), cermets and metals.

More recently, General Electric Company has published in October 2006 a U.S. patent application entitled "Method for applying a plasma sprayed coating using liquid injection" [Skoog '06] (patent not yet granted). The described invention covers to a large extent the SPS technology and this patent application is specifically related to the fabrication of TBCs. The method comprises the use of a tank containing the suspension, a pump (preferentially a peristaltic pump) to force the suspension through a conduit and a liquid injector equipped with an atomization nozzle (located outside of the plasma torch), injecting the suspension radially into the plasma jet (see Fig. 11). The employed plasma gun can be for example a 7MB APS gun from Sulzer Metco. The carrier liquid can be water, alcohol or any other organic solvent (that induces the need for safety precautions against explosive conditions in the plasma flame). Solutions may be used instead of suspensions. It is also interestingly stated that one of the advantages of using a liquid injection instead of a conventional powder feeding is that it increases the percentage of particles that enter the plasma jet since the liquid medium "tends to stabilize the fine particles in the plasma stream". This shall increase the process efficiency. A second embodiment of the invention describes a combined SPS and APS process, in which a conventional powder injector is added to the liquid injector in order to inject separately a powder and a suspension. These may be of the same or of different materials. By combining simultaneously SPS with APS, it is expected to increase the deposition rate.

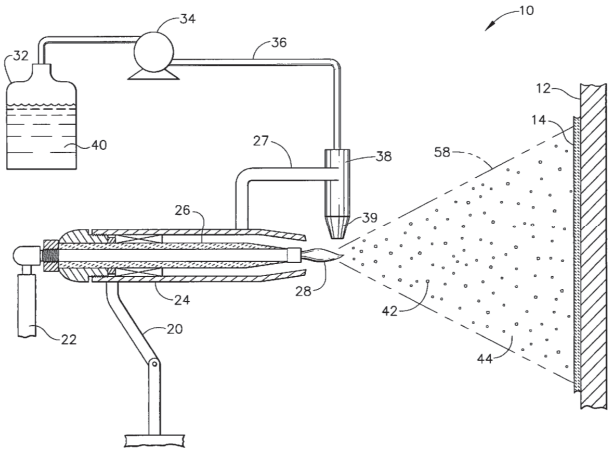

Fig. 11: Schematic diagram of SPS system claimed by General Electric Company [Skoog '06].

Concerning the injection of suspension, the National Research Council of Canada (NRC) has published in December 2006 a U.S. patent application entitled “Method and apparatus for fine particle liquid suspension feed for thermal spray system and coatings formed therefrom” [Oberste-Berghaus '06] (patent not yet granted). The invention is an apparatus providing an axial injection of suspension into the plasma jet (see Fig. 12). The internal configuration of the injector enables to provide “substantially improved protection against obstructions by the solid content in the suspensions”. The advantages of the axial injection are stated to be an improved heat and momentum transfer from the plasma to the liquid suspension feedstock and less sensitivity to size and velocity distributions of the suspension droplets due to their complete entrainment by the plasma stream. The typical plasma torch used with this axial injection system produces three plasma streams converging through a common exit nozzle such as the Axial III™ torch from Northwest Mettech Corp. (North Vancouver, BC, Canada) which was introduced by Z. Tang et al. [Tang '10, Tang '11]. The injector invented by the NRC provides a low flow rate and a high injection velocity. The flow rate is controlled and monitored by a precision flow meter. The coatings deposited by using this apparatus are part of the claims, whereby these coatings can be for a large range of applications such as among others SOFC components (electrolyte and electrodes), TBCs (YSZ and YSZ/Al_2O_3 composites) and

TiO_2 photocatalytic coatings. It is also claimed that this injector can be applied not only for DC plasma spray but also for inductively coupled RF plasma spray, as well as for HVOF among others.

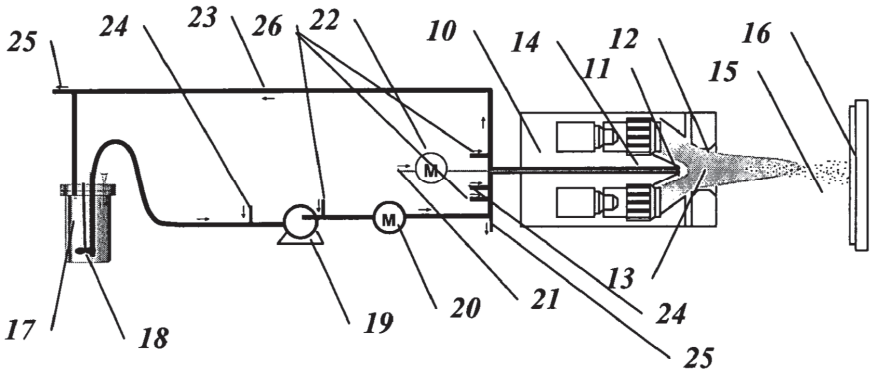

Fig. 12: Schematic diagram of the axial suspension injection system claimed by the National Research Council of Canada (NRC) [Oberste-Berghaus '06].

It should also be noted that the axial suspension injection technique enabled by the Axial III™ torch of Northwest Mettech Corp. is also applied to provide improved TBC microstructures by a further patent application of General Electric Company entitled "Protective coating with high adhesion and articles made herewith" published in November 2009 [Rosenzweig '09] (not yet granted). The coatings feature an elongate material growth or a vertically cracked structure that provides adhesion and strain tolerance being comparable to that of PVD TBCs. This patent does not describe in details the SPS technique used to deposit the coatings but focuses rather on a detailed description of the various coating microstructures that can be obtained.

Sulzer Metco AG has published in August 2011 a U.S. patent entitled "Plasma spraying device and a method for introducing a liquid precursor into a plasma gas stream" [Dorier '11]. This patent is already granted and claims the priority of a European patent application filed in August 2006. Patent applications were also filed in Canada, Japan and South Korea. The invention is related to a new method for introducing a suspension into the plasma jet. It is stated that "the injection of the liquid outside of the torch nozzle known from the prior art has turned out to be

inappropriate to achieve a sufficient penetration of the liquid into the plasma gas stream". Therefore it appeared necessary to develop a technology that enables a liquid injection inside the plasma torch. However, this meets a significant issue arising from the design of the currently available plasma guns. The described invention provides a new plasma spray device that enables to introduce the suspension deeply and completely into the plasma gas stream, inside the plasma torch (see Fig. 13). The plasma gun mentioned as an example is the F4-VB by Sulzer Metco. Two different designs for the suspension injection are described: a direct injection by using a penetration groove on the one hand, and the injection of the suspension with a carrier gas (nebulizing) by using a nebulizer on the other hand. The second design (nebulizer) presents the advantage that the suspension can be injected at high velocity in the form of a mist. The invention comprises also a supply unit constituted of a reservoir for the suspensions and a device for metering the flow of the suspension and/or the carrier gas (see also the recent publication by Sulzer Metco US Inc. on a new suspension feed system [Cotler '11]). The patent claims as well that the liquid must not be a suspension, but also among others a salt solution, an organosilicon, an acid or an alkali fluid. The general term employed throughout the patent is "liquid precursor".

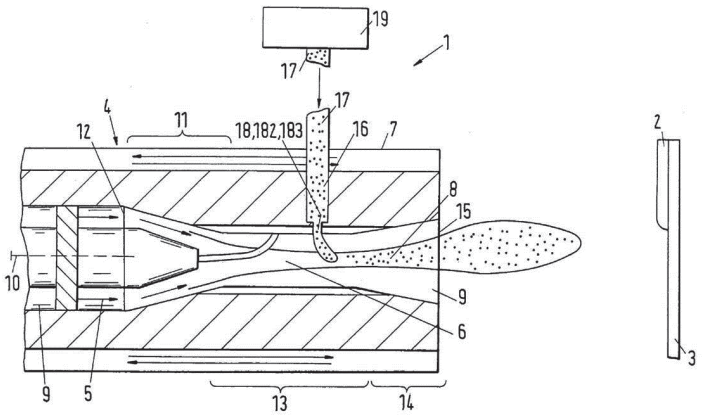

Fig. 13: Schematic diagram of the new plasma spray device patented by Sulzer Metco AG, which enables an injection of the suspension inside the plasma torch [Dorier '11].

The several patents that were introduced above cover together to a large extent the state of the art related to the SPS process. General Electric Company acted early by

applying for a patent which would cover most of the process itself if it would be granted, especially for TBC deposition. In particular, its embodiment related to the simultaneous spraying by APS and SPS is likely to be industrially relevant with regard to increased deposition rate. Nevertheless, this invention from GE comprises a conventional suspension injection, i.e. outside of the plasma torch in a radial manner. Injection-related problematics define the current limitations of the SPS process and are the basis for the patents of the NRC and of Sulzer Metco AG in which an axial injection system and a radial injection inside the plasma torch are presented, respectively. Both techniques present advantages compared to the conventional injection method since they enable to introduce the suspension completely into the plasma stream. It appears clearly to the authors that these two injection techniques are likely to play important roles in future SPS developments.

SPS-related patents at Forschungszentrum Jülich

The Forschungszentrum Jülich GmbH in Germany has published a number of patents related to thermal spraying with liquid feedstocks, for applications in high temperature fuel cells and in TBCs. They are described in the present study in the chronological order of their first filing date.

The earliest of these patents from Jülich is dated back from March 2003 (filing date of German patent application) and was also published as a U.S. patent in September 2009 with the title “Method for producing a layer system comprising a metallic carrier and an anode functional layer” [Vaßen '09b] (already granted). It was also published as a European patent in March 2011 (already granted). The invention relates to the manufacturing of components for high-temperature fuel cells. It describes a method in which thermal spraying is applied not only to produce the individual functional layers but also to deposit the metallic carrier layer. The layer system is subsequently separated from the substrate by using a large range of techniques. This patent appears interesting in the framework of the present study since it claims that suspensions can also be advantageously used instead of powders for the thermal spraying of several ceramic layers, such as a porous YSZ/NiO anode, a dense YSZ electrolyte and a perovskite-based cathode. The use of suspensions leads to a finer porosity in the layers or to a particularly dense deposition in the case of the electrolyte.

A further patent application from the same research group at Jülich entitled “Plasma spraying method, and device that is suitable therefor” was published as an international patent application in January 2005 [Döring '05]. This patent has not yet been granted, but was already granted as a German patent in November 2006. The invention enables to avoid or reduce the deposition of unmolten clusters in the coating (often also referred to as “overspray”) that occurs during spraying. The invention can be applied for any plasma spraying process but is said to be particularly advantageous in the case of SPS since this process often presents the issue of a significant deposition of unmolten clusters, i.e. sprayed particles that diverge from the core of the plasma jet away to the fringes of the jet, or even do not penetrate at all in the core of the jet. These particles are therefore not molten or only partly molten, and tend also to cool down rapidly. They can then either not impact the substrate at all if they significantly diverge from the center of the plasma jet, or they impact the substrate as solidified particles and are embedded in the coating among with molten splats. They represent then microstructural features that lead to an inhomogeneous coating structure and a higher porosity. This provides coatings that show lower adhesion and lower mechanical stability. The aim of the invention is to reduce significantly the problem of unmolten clusters while maintaining the advantages of the SPS process. The patent introduces a device that either redirects the unmolten “overspray” particles into the plasma jet or deflects them completely away from the jet so that they do not impact onto the substrate. In the first case, the said device has e.g. the shape of a funnel that enables to focus the trajectories of these diverging particles back to the center of the plasma jet. In the second case, the device has e.g. the shape of a hollow cylinder that enables to blend out any particles whose trajectory does not go through its opening. Such a device is fabricated by using high melting point materials such as graphite or high-grade steel and can be equipped with an additional cooling system.

The Forschungszentrum Jülich has also published in November 2007 a U.S. patent application entitled “Method for the production of thin dense ceramic layers” [Vaßen '07]. This patent has not yet been granted, but was already granted as a German patent in February 2006. It was also published as an international patent application in March 2006 (not yet granted) and was also filed in Japan. The invention consists mostly of a set of plasma spray parameters that enable to deposit a dense, gas-tight

layer having a thickness below 100 µm in only one single pass of the plasma gun. Parameters are defined to ensure an appropriate melting of the particles and avoid the formation of microcracks. The described method can be applied for the manufacture of dense electrolytic layers for high-temperature fuel cells, membranes for gas separation technologies and oxidation- or corrosion-proof layers. A wide range of ceramic materials can be processed with the said method. Although this invention is mostly related to the APS process, it appears interesting to mention in the framework of the present study since one of its claims comprises the introduction of the feedstock into the plasma flame in the form of a suspension, thus covering also the use of SPS for manufacturing such coatings with the method described in the patent.

A further patent from Forschungszentrum Jülich employing liquid feedstock plasma spraying was applied under the title “Method for producing gas-tight layers and layer systems by means of thermal spraying” as an international patent application published in December 2006 [Siegert '06], along with a German patent application. Both patents have not yet been granted. A method based on SPS is described, in which a layer is deposited by injection of a suspension or a sol into the plasma jet. This layer is subjected to a subsequent thermal treatment by using the same plasma gun used for deposition, without any interruption of the process, simply by switching off the feeding of spray material. The remelting or sintering of the upper layers leads to a sealing of the porosity, thus providing a gas-tight coating. This step can also be favored by increasing the plasma gun power, by reducing the distance between plasma gun and substrate, by reducing the substrate cooling or by reducing the robot speed, or also by a combination of these. The invention comprises also the deposition of layer systems constituted of several individual layers having different microstructures, without interrupting the process. In particular, it is possible to deposit at first a porous layer, followed by a gas-tight layer, and then by another porous layer on top. This interruption-free method can be advantageously applied for the manufacture of complete fuel cell structures constituted of a porous anode, a gas-tight electrolyte and a porous cathode. The transition from a layer deposition to the next layer occurs by varying the spraying parameters and/or the feedstock material. The patent describes how some parameters can be varied to induce changes in the microstructure, such as the suspension injection speed, the feeding rate, and the solid content of the suspension or of the sol. The invention comprises also the production of coatings

advantageously showing segmentation cracks by employing a suspension or a sol as the feedstock. The method consists of increasing the deposition temperature so that an interlamellar grain growth with a high interlamellar bonding occurs. Stress relaxation then leads to the formation of segmentation cracks. The injection speed of the feedstock must also be increased so that the particles are completely molten. The density of the segmentation cracks can be adjusted by varying the solid content of the suspension. Fig. 14 shows an example of such a YSZ segmented coating obtained by SPS. These advantageous segmentation cracks provide a particularly high mechanical stability and these coatings are suited for application as TBCs.

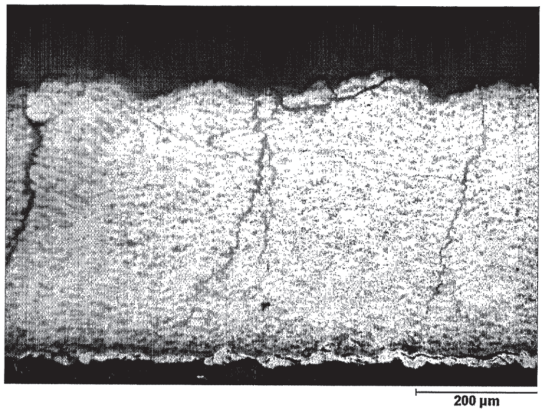

Fig. 14: Cross-section view of a YSZ coating manufactured by SPS and showing a segmentation crack density of approx. 5 cracks/mm, obtained with method described in [Siegert '06].

In the field of TBCs, the Forschungszentrum Jülich GmbH has published in October 2011 a U.S. patent application entitled “Thermal barrier coating system and method for the production thereof” [Meyer '11]. An international patent application and a German patent application were also published in August 2009. None of these three applications have been granted yet. The invention relates to a TBC system that comprises a combination of APS and SPS layers. The advantage of such a system is to increase its reflectivity, particularly in the visible and the near infrared wavelength ranges, thus reducing the thermal radiation penetrating the TBC and heating the component, and also to decrease the thermal conductivity. The aim is to improve the service life of the TBC. The method that is claimed comprises the deposition of at

least one APS coating and one SPS coating. Several variations are claimed such as APS+SPS (SPS coating on top, see Fig. 15) as well as triple-coating system APS+SPS+APS. The SPS coating has a significantly higher porosity and microcrack density than the APS coating. This increases the dispersion of thermal radiation, whereby reflectivity is improved. In addition, the increased porosity leads to a lower thermal conductivity. However, SPS coating shows a lower mechanical stability than APS coating having a comparable thickness. This disadvantage is compensated by using an APS coating exhibiting mechanical and erosive stability. By combining both processes, their advantages are merged, enabling to obtain TBC properties which are not possible with individual single coating. Both SPS and APS coatings are deposited by using a Triplex II burner. Further claims of the patent comprise among others the deposition of at least one graded coating and the application of a large range of ceramic materials (partially or fully stabilized zirconium oxide, aluminum oxide, aluminates, pyrochlores and perovskites). The claims are also extended in general to any bilayer coating system, wherein the top layer has a higher porosity and reflectivity than the bottom layer.

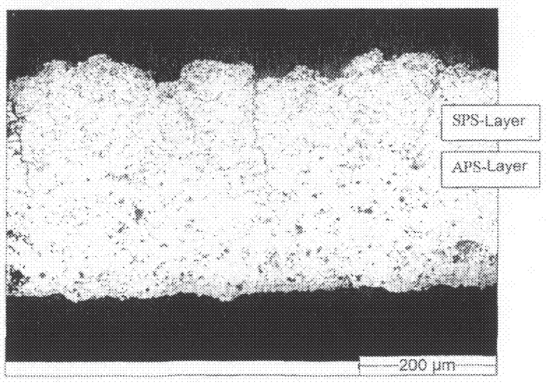

Fig. 15: Cross-section view of a YSZ double layer system manufactured by APS and SPS, obtained with method described in [Meyer '11]. The coating thicknesses of the APS layer and SPS layer are 200 and 150 µm, respectively. The SPS layer has considerably finer pores, and vertical cracks are apparent. The pores of the APS layer are considerably coarser.

The Forschungszentrum Jülich has also published in August 2007 an international patent application entitled “Thermal spraying method using a colloidal suspension”

[Siegert '07]. The invention relates to the deposition of a conductor or semiconductor coating (especially TiO_2 in its anatase phase) on a glass substrate. This is one of the components of so-called dye-sensitized solar cells (also called "Grätzel cells"). The coating deposition is carried out by a SPS or SPPS process, in which the TiO_2 particles are in the nanometer range. This patent application has been abandoned.
Another abandoned patent application from Forschungszentrum Jülich had the focus on the manufacture of mullite coatings by SPPS for application as thermal and environmental barrier coatings. It was published in August 2008 as a U.S. patent application entitled "Production of a gas-tight, crystalline mullite layer by using a thermal spraying method" [Siegert '08].

2.3.2. Considerations on suspension storage and choice of the solvent

It is clear that processing suspensions instead of powders induce additional requirements when applied at the industry scale. One of these considerations is that the presence of the solvent requires additional storage space (see Fig. 16). For instance, a YSZ suspension in ethanol with a 20 wt.% solid content leads to a necessary storage volume being approx. 13 times higher than if the mere powder would be stored for APS, for the same amount of solid. Using water instead of ethanol reduces slightly the volume of storage. Increasing the solid content of suspensions used in SPS leads to a much reduced volume and hence to a reduction in storage costs. Besides, an increased suspension solid content induces also increased feedstock feeding rates and increased deposition rates. These characteristics are determining for economical success at the industrial scale. Further considerations on these aspects, particularly when comparing SPS with APS, are presented in section 2.3.5.
An even more significant consideration is the safety-related aspect of such storage of solvent. Most of the current research studies on SPS are carried out with ethanol-based suspensions. Ethanol presents the advantage of easily stabilized suspensions. However, the use of ethanol requires particular safety precautions, such as storing in a segregated and approved area for flammable liquids, protected from potential ignition sources. Besides, ethanol requires also the use of personal protective equipment since it is irritating to skin and presents the risk of serious damage to eyes. When scaled up to the industrial scale, the storage and transport of such flammable suspensions would

thus lead to additional costs related to these safety precautions. One possibility to solve this issue could be to replace ethanol-based suspensions by water-based ones. However, the injection of ethanol into the plasma jet is known to provide higher enthalpy because its combustion enthalpy is higher than its vaporization enthalpy [Mauer '10]. On the contrary, the injection of water leads to a significant cooling of the plasma jet. Therefore, replacing ethanol by water leads to lower particle temperatures, which in turns lead to different coating microstructures than obtained when processing ethanol-based suspensions. Therefore, replacing organic solvent by water will require further developments to adjust the existing optimized spray parameters. This can be realized by increasing the enthalpy of the plasma jet in order to compensate the cooling effect of water injection. These adjustments can be monitored by using process diagnostic tools such as an enthalpy probe to measure the plasma characteristics and a particle diagnostic system (e.g. Accuraspray-g3 from Tecnar Automation Ltd, St. Bruno, QC, Canada, whose ensemble measurement method is more appropriate for SPS [Mauer '10]) to measure the in-flight particle properties (i.e. particle temperature and velocity). The aim is e.g. to quantify the loss in particle temperature when replacing ethanol by water in given conditions. When already quantified, this temperature loss can be compensated by e.g. increasing the plasma current in a given range. The time and money invested in these additional developments are likely to be compensated by the reduction of costs related to transportation and storage-induced safety precautions that are less significant with water than with flammable solvents.

Besides, it should also be noted that replacing ethanol by water can have detrimental effects on suspension stability and viscosity. A different viscosity leads to changes in the suspension feeding conditions during spraying operations and has also significant effects on the droplet size distribution upon atomization [Rampon '08a]. An increase of viscosity tends to hinder the atomization. It is important to perform viscosity measurements with a rheometer in order to verify suspension properties before processing. This plays a role in guaranteeing the reproducibility of SPS.

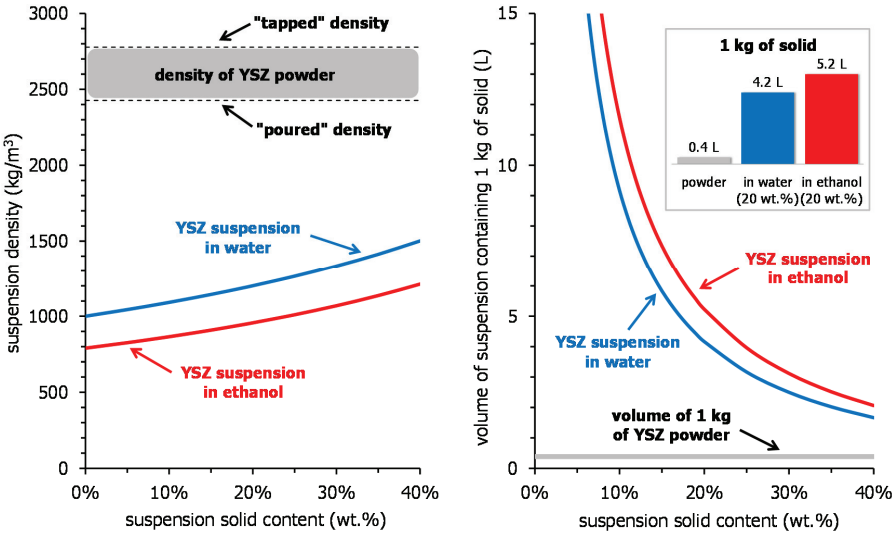

Fig. 16: Graphs showing storage-related problematic.

Left: suspension density vs. solid content. The following density values in kg/m^3 are considered for calculation, water: 1000, ethanol: 790, 5YSZ: 6070. The density of a common thermal spray YSZ powder (204 NS from Sulzer Metco) is showed for comparison purpose. Its value is considered to be situated between its "poured" density (2427 kg/m^3) and "tapped" density (2778 kg/m^3) depending on how the powder is handled upon storage.

Right: volume of a suspension batch containing 1 kg of solid vs. suspension solid content. The volume of 1 kg of 204 NS powder is showed for comparison purpose. Its "poured" volume (0.41 L) and "tapped" volume (0.36 L) are very similar and therefore cannot be distinguished from each other on the graph. The inset shows in particular the volume of suspensions with 20 wt.% solid content compared to the volume of powder.

Another point that arises when replacing ethanol by water is that its surface tension is different (38 mN.m^{-1} for water; 25 mN.m^{-1} for ethanol [Marchand '11]). When working for example with a two-phase atomizer, the average size of suspension atomized droplets is larger with water than with ethanol in identical atomization conditions since an increase of surface tension tends to hinder atomization [Rampon '08b]. Droplet size has a significant effect on its interactions with the plasma jet. Smaller droplets tend to be more easily conveyed by the plasma jet [Marchand '07]. It

is also commonly accepted that the size of droplets injected into the plasma jet has a direct influence on the size of agglomerates that are being melted in the plasma. Therefore, a mere change of the surface tension of the liquid used as carrier is likely to have a significant influence on the coating build-up mechanisms and the obtained microstructure. It is therefore necessary to investigate thoroughly all changes induced by the replacement of ethanol by water and to adjust correspondingly the process parameters in order to obtain similar coating microstructures and properties that were achieved with previous ethanol-based suspensions.

2.3.3. Suspension stability and suspension transportation issues

For any suspension the question of its long-term stability is an important point. Even when using a dispersant, it is recommended to stir or to rotate the suspension in order to avoid undesired sedimentation and agglomeration. This could be problematic at the industrial scale when dealing with large amount of suspensions since it would require a large number of facilities such as e.g. roller benches or “turbula” mixers for suspension batches that have been delivered and that are waiting to be sprayed. One approach to tackle this issue is to store the powder and the solvent separately and to formulate and homogenize the suspensions on site prior to spraying. The opinion of the author is that this method will turn out to be more reliable and more economical for supplying industrial spray shops for SPS. It presents the advantage of avoiding agglomeration and sedimentation of suspension during transportation. In the experience of the author, an intercontinental transportation of such liquid feedstocks involves safety precautions and the related additional costs. This transportation can last for more than one week and thus lead to important agglomeration and sedimentation of the suspension upon arrival at the spray shop. Although an appropriate mixing enables to re-obtain a suspended state, it is observed that the behavior of the suspension and especially its sedimentation tendency is critically changed compared to what was claimed on the as-prepared state. In other words, it is challenging to turn an aged suspension into a fresh one. By opting for an on-site formulation of the suspensions, the properties of fresh suspensions are guaranteed. This can definitely contribute to the improvement of the reliability and reproducibility of SPS. Besides, separate transportations of powder and solvent can be carried out in

the same way that spray shops are currently and regularly supplied in powder feedstocks and that any chemical lab is supplied in solvent, e.g. ethanol. The ceramic powders being selected for an on-site suspension formulation are recommended to be spray-dried powders being constituted of spherical granules that are easy to break. If the granules have not been subjected to any consolidating heat treatment, they present the advantage of being easily broken by simple ball milling operations after the formulation of the suspension. This ball milling step combines homogenization of the suspension and breaking the granules into their constituents, i.e. the primary particles. By doing so, the granules can have a size being in the range of several tenths of micrometers for easy handling, while the primary particles that constitute the granules are in the sub-micrometer range or even nano-sized. Hence the "ball milling" step after the formulation does not have the aim of actually breaking particles and reducing further their size but rather to separate the bonded primary particles. In this case, the powder being supplied is not in the nano-sized range and thus does not induce more safety precautions than when transporting conventional powder feedstocks for APS operations. This powder constituted of easy-to-break granules is not a powder that is claimed to be developed for thermal spray processes. Instead, it is necessary to consider how the powder was fabricated and especially to select powders being granule-shaped without having been sintered after spray drying operations in order to guarantee that it will be easy to break. These kinds of ceramic powders are appropriate for SPS and are widely known for pressing processes.

2.3.4. Cleaning requirements

The conventional APS process involves already needs of cleaning at the spraying facility. Most notably is the cleaning of powder feeders that requires to be carried out thoroughly to avoid any powder contamination when changing the content of a feeder for another powder. Working with suspensions involves the same precautions. Nevertheless it can be noted that the pressurized vessels that are commonly used to contain and feed suspensions are somewhat easier to clean than conventional powder feeders, due to their particular shape. A powder feeder features often complex shapes that lead to a higher amount of surfaces on which powder has to be removed. This has to be realized within a hood for the removal of powder fumes and compressed air is

commonly used. On the contrary, a suspension vessel has often a much simpler shape than a powder feeder and its cleaning process can thus be realized faster. It often features simply a lid and a stirrer that need to be cleaned as well. Besides, the presence of a liquid ensures that the cleaning process is dust-free. This is an important consideration since it enables to proceed to the cleaning without employing an exhaust hood. This in turn leads to a gain in facility utilizations and costs and in cleaning time as well, which is an advantage for the application at an industrial scale. However, it should also be noted that the deposition of dust in the chamber often takes place to a larger extent with SPS operations than with APS. This may induce additional needs of cleaning the chamber.

Besides, processing suspensions for plasma spray commonly involves the utilization of injection nozzles for the liquid feedstocks. These nozzles can be of different natures. The most commonly employed techniques are either the mechanical injection of a full liquid jet or the use of a two-phase atomizer to obtain a fragmentation of the suspension into fine droplets before penetration into the plasma jet. Both types of injection involve the use of nozzles or needles with small inner diameter that can be in the range of approx. 0.1 mm to 1 mm. These parts regularly need to be cleaned in order to ensure a clogging-free process and to guarantee the reliability of the spraying process. It is common use to flush the feeding pipes and the nozzle immediately after spraying operations with a solvent contained in an additional vessel in order to avoid any unwished drying of suspensions especially in these parts with small dimensions. In the author's experience, it is also recommended to perform a complete cleaning of the injection nozzle regularly. This requires unmounting the nozzle from its support off the plasma gun, disassembling the nozzle and performing a thorough cleaning of each individual part constituting the nozzle by using a solvent and eventually an ultra-sonic bath. It is recommended to perform this precaution cleaning e.g. after approx. 2 to 10 spraying operations or after approx. 30 to 60 min of spraying (this is very depending on the nature of the suspension, its viscosity and its tendency to leave dried particles in the inside of the nozzle). Besides, it is absolutely necessary to realize this cleaning before spraying another material with the same nozzle.

Another remark concerns the use of exhaust hood inside of the spraying booth. This is commonly used when performing APS in order to evacuate powder fumes that would sustain in the atmosphere of the spray booth and lead to hazards for the operators being in contact with the process. When dealing with SPS, the presence of a well-

functioning exhaust hood during spraying operations is even more necessary since feedstock particle size is in the sub-micrometer range and presents therefore a higher hazard when entering the human body. Nano-particles can reach parts of the biological system which are normally not accessible for larger particles [Fauchais '09]. Since the current knowledge on the toxicity of nanopowders is not yet fully developed, it is necessary to apply specific precautions such as employing filters with very high efficiency that are capable of stopping nano-particles as well.

2.3.5. Feeding rates and deposition rates

It is interesting to compare common quantitative values for APS and SPS such as feeding rates, deposition rates and deposition efficiencies since these characteristics are determining for economical success at the industrial scale. In the industry, it is common to work with the APS process at powder feeding rates being in the range of 50-60 g/min or even higher. When judging from the current SPS developments, feeding rates are rather of e.g. approx. 60 g/min of liquid (with a 20 wt.%-concentrated suspension), i.e. approx. 12 g/min of solid content. Deposition efficiencies are also somewhat lower for SPS than for APS, since in the experience of the author SPS can provide approx. 40-45% of deposition efficiency (calculated from the sample gain of weight) while common APS values are of approx. 50-60%. This can be critical in terms of cost efficiency of the process. Nevertheless, better coating characteristics obtained by SPS compared to APS coatings can justify accepting lower deposition efficiencies. Besides, in some specific applications such as high temperature fuel cells components, a low deposition rate might not be critical if thin coatings are sufficient to achieve the function.

2.3.6. Spraying distance

The SPS process involves usually a shorter spraying distance than APS. This is due to the lower inertia of the fine particles, which are cooled down faster at large spraying distance, leading to re-solidified particles, poor coating deposition and heterogeneous microstructure. It is common in the literature to describe SPS experiments performed

with spraying distance in the range of approx. 40 to 70 mm, while common spraying distance for APS with e.g. Triplex II plasma gun is rather in the range of approx. 100 to 200 mm. The short spraying distance of SPS induces the necessity of an appropriate backside cooling to avoid substrate overheating. Moreover, with regard to applications of the SPS process in the industry, this short spraying distance is expected to be an issue. It is a problem particularly for coating deposition on components being sensitive to overheating and/or which cannot be cooled properly from the backside during spraying operations. Besides, components having complex shapes cannot be sprayed at such a short distance from the surface. Therefore, it is important to be able to develop the SPS process at larger spraying distance as well in order to better meet the industrial requirements. A spraying distance of e.g. 100 mm would be valuable for the development of the process and for its acceptance in the industrial field. In order to obtain similar microstructure and properties at larger spraying distance, an approach is e.g. to increase the plasma enthalpy in order to compensate the larger spraying distance, so that the particle state (temperature and velocity) at e.g. 100 mm is similar as it is usually at shorter spraying distance. This approach may involve increasing the plasma torch current and/or increasing the fraction of helium in the plasma gas mixture.
On the other hand, for some niche applications, it might be possible to take advantage of the short spraying distance of SPS, such as for the deposition of inner diameter coatings.

2.3.7. Conclusion

It appears that the use of liquid feedstocks tends to make the plasma spraying process more demanding than it is with powders. As it was presented in this study, storage and transportation of suspensions are likely to be challenging. Beyond the higher requirements in terms of volume when dealing with suspensions instead of powders, particular safety precautions for flammable liquids will raise additional costs. It is therefore recommended to favor the use of water as a solvent instead of ethanol. Besides, the question of the long-term stability of suspensions might lead to a preference for an on-site formulation of the suspensions. This approach will likely turn out to be more economical. Further efforts are required in order to increase the

performances of the SPS process in terms of feeding rates and deposition rates, in order to improve it cost efficiency. Although it might be challenging to reach the current industrial efficiency of the established APS process, the better coating properties that SPS can provide are likely to be attractive enough to justify higher costs. Finally, short spraying distances are also an issue to meet industrial requirements. Further developments will be necessary to be able to obtain the desired coating microstructures and properties at longer spraying distance.

The development of SPS into a reliable, reproducible and robust process might require new appropriate equipment being specifically developed for liquid feedstocks. Reliable suspension feed systems are already commercially available. The developments of appropriate diagnostic tools for SPS could also contribute significantly to a better understanding of the more complex phenomena that occur when a liquid is used instead of a powder. The analysis of current patents showed that the trend goes towards modifying significantly the suspension injection techniques in order to reach better process reliability that conventional injection methods did not permit. It appears clearly that plasma torches have probably to be re-designed in order to match the requirements of SPS. Therefore it is likely that plasma torches being specifically conceived for liquid feedstocks can lead to a breakthrough in SPS developments and finally to commercial applications.

3. Materials and methods

3.1. Suspensions

Various suspensions were used as feedstocks for SPS experiments (Table 3). For the manufacture of YSZ TBCs, a suspension was prepared by dispersing a commercially available ZrO_2-5 mol.% Y_2O_3 powder (TZ-5Y product from Tosoh Corporation, Tokyo, Japan) in ethanol with the addition of 1.5 wt.% of polyethylenimine (PEI) as a dispersant (Polysciences, Inc., Warrington, PA, USA). PEI is a cationic polymer [Fengqiu '00] that is constituted of highly-branched molecules and is frequently used to stabilize ceramic suspensions [Wang '99]. The formulated suspension was then subjected to a subsequent ball-milling for 24 h on a roller bank at 120 rotations per minute. The used powder is constituted of large spray-dried granules having diameters typically of about 30-50 µm. Fig. 17 (left) shows that the granules are full. They are so-called soft granules and can thus be easily broken to return the individual primary particles such as shown on Fig. 17 (right) that presents the particles of the prepared suspension after the ball milling step. For all suspensions, the characterization of the particle size by means of scanning electron microscopy (SEM, Ultra55, Carl Zeiss NTS GmbH, Oberkochen, Germany) turned out to be more precise and reliable than measurement techniques based on static light scattering and dynamic light scattering, due to the very fine sizes of the particles. Besides, SEM images enabled also to reveal the shape of the particles. It is observed on Fig. 17 (right) that particle sizes in the prepared suspension are in the range of approx. 30-200 nm (estimated from an analysis on SEM micrographs). The viscosity of the suspensions was measured with the rheometer Physica MCR 301 (Anton Paar, Graz, Austria). The YSZ suspension has a dynamic viscosity of 2.0 mPa.s at a shear rate of 10 s^{-1}. This low viscosity enables to avoid clogging issues during SPS operations.

As a new promising material for TBCs, an in-house lanthanum zirconate suspension ($La_2Zr_2O_7$) was also used for the manufacture of SPS coatings. The suspension was produced with initial compounds being La_2O_3 and ZrO_2 in stoichiometric proportions. Fig. 18 shows the particles of the suspension and details are presented in Table 3.

Table 3: Details on the various suspensions used as feedstocks for SPS

Material	Solvent	Solid content (wt.%)	Range of particle diameter (nm)
YSZ	Ethanol	20	30-200
$La_2Zr_2O_7$	Ethanol	20	30-600
TiO_2 + 5 mol.% TiN	Water	5	50-200

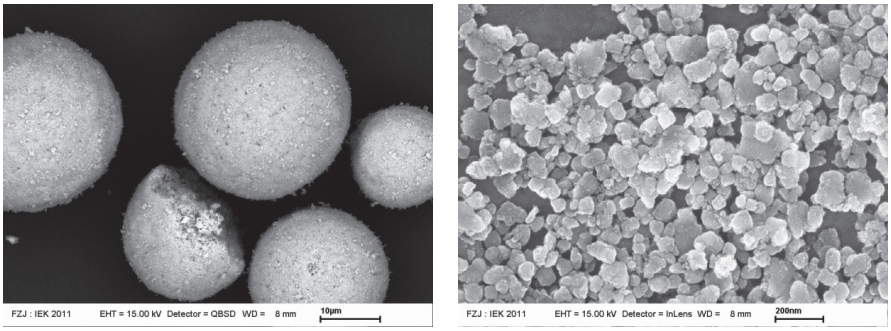

Fig. 17: SEM images showing the 5YSZ powder from Tosoh Corporation used for the formulation of the YSZ suspension (left) and the particles in the YSZ suspension after formulation and milling (right).

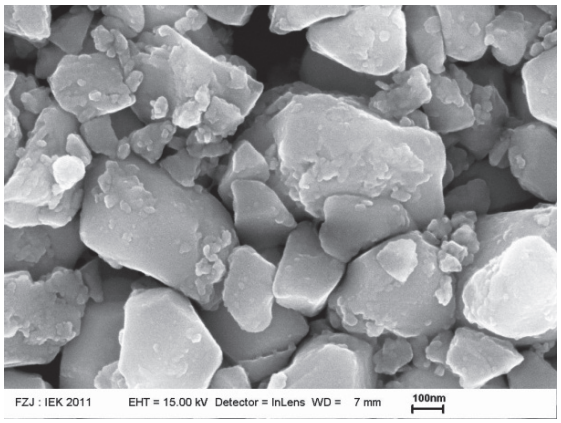

Fig. 18: SEM image showing the particles in the $La_2Zr_2O_7$ suspension.

With regard to application as photocatalytic coatings, SPS experiments were conducted with a TiO_2 suspension (99.9% anatase phase) that was formulated by

dispersing a commercial TiO_2 powder (nanopowder from Inframat, USA) in deionized water with the addition of 0.3 wt.% of a dispersant (PEI from the company Sigma Aldrich) and a subsequent ball-milling for 24 h on a roller bank at 120 rotations per minute. A doping of the suspension was obtained by adding 5 mol.% of TiN. Fig. 19 shows the particles of this suspension and details are presented in Table 3.

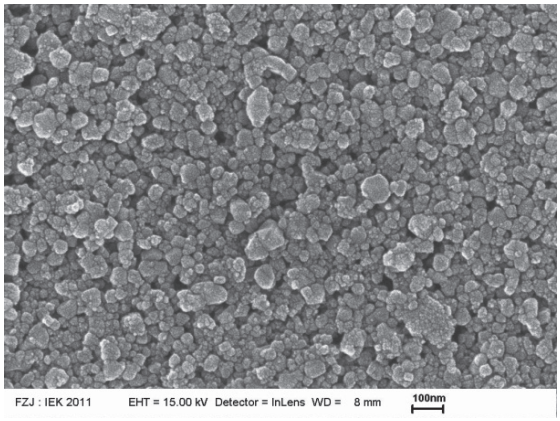

Fig. 19: SEM image showing the particles in the TiO_2 + 5 mol.% TiN suspension.

3.2. Suspension plasma spraying operations

The SPS coatings presented in this study were sprayed in an A-3000 atmospheric plasma spray facility (Sulzer Metco, Wohlen, Switzerland) with a Triplex II plasma gun (Sulzer Metco, Wohlen, Switzerland) mounted on a six-axis robot. The feeding of the suspension is enabled by a delivery system developed at Forschungszentrum Jülich, Germany and shown in Fig. 20a. It comprises a pressurized vessel containing the suspension to inject and an additional vessel containing ethanol for the cleaning of the lines after spraying. The injection of the suspension into the plasma jet is carried out radially (Fig. 20b) by a two-phase atomizer also developed by Forschungszentrum Jülich, Germany, using air as atomizing gas, which enables a pre-fragmentation of the droplets before they enter the plasma. Suspensions were agitated during the spray process by using a stirring apparatus integrated in the pressurized vessel.

The plasma spray parameters for each SPS coating are presented in detail in the corresponding sections. Therefore, the following description constitutes only general

indications on the parameters in plasma spraying that are also accompanied with some typical values that were employed for SPS. The employed plasma gases were argon and helium. A typical composition was 40 slpm Ar + 10 slpm He (slpm: standard liters per minute). Plasma current was typically 500 A, but can be increased or reduced in order to vary the power accordingly to the specific requirements of coatings. Spraying distance is typically shorter for SPS than for the conventional APS process and a typical value was 65 mm. The feeding rate of suspension was in the range of about 50-60 $g.min^{-1}$. The robot kinematics is a meander-shaped motion in a plane parallel to the substrate surface. The robot motion in front of the substrate is horizontal and the vertical meander is 2 mm. Robot speed is typically 700 $mm.s^{-1}$. The substrate is typically cooled from the front side by compressed air nozzles. An additional cooling from the back side of the substrate must also be realized in most cases. The temperature of the substrate was monitored during spraying operations by a pyrometer.

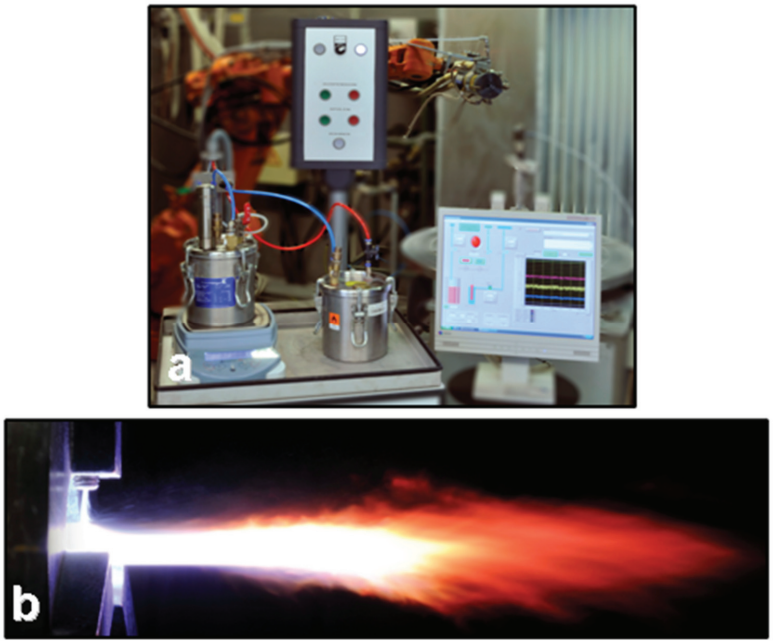

Fig. 20: (a) Suspension feeding facility developed at Forschungszentrum Jülich, showing also the monitoring and control unit; (b) injection of suspension into the plasma jet by using a two-phase atomizer.

SPS coatings were sprayed on sand-blasted rectangular steel or stainless steel substrates with typical dimensions being 40 mm by 30 mm or alternatively 24 mm by 24 mm. Other specific substrates were also employed for the realization of thermal cycling tests. In this case, specimens are constituted of a disc-shaped Ni-based alloy substrate (Inconel™ 738) having 30 mm in diameter, 3 mm in thickness and a curvature radius at the outer edge of 1.5 mm. These substrates are first coated with a 150 µm-thick NiCoCrAlY bondcoat layer manufactured by low pressure plasma spraying (LPPS) using Ni 192-8 powder by Praxair Surface Technologies Inc., Biebesheim, Germany. The thickness of the ceramic topcoat layer was typically in the range 400-500 µm.

3.3. Characterization of SPS-deposited coatings

3.3.1. Characterization of coatings microstructures and properties

In order to study the coating microstructure, the samples were embedded in an epoxy resin to prepare metallographic sections. Embedding was always realized before cutting, thus limiting the risks of damage in the specimens. The metallographic polished cross-sections were investigated by using a confocal laser microscope (VK-9700, Keyence Corporation, Osaka, Japan) and a scanning electron microscope (SEM, Ultra55, Carl Zeiss NTS GmbH, Oberkochen, Germany). Segmentation crack densities were determined on images from confocal laser microscopy by counting the cracks over a large area of coating cross-section (on three different areas of the sample representing above 12 mm cumulated), covering a high amount of individual vertical cracks (in the range of approx. 80-100 cracks). This enables to obtain a reliable value of the segmentation crack density. It should be noted that only the vertical cracks having a length higher than half of the coating thickness are counted as real segmentation cracks.

Hardness measurements were performed on polished cross-sections by using a Vickers micro-indentation apparatus with a load of 0.5 kg.

Coatings deposited on steel substrates were removed from the substrates by using a solution of hydrochloric acid. These free-standing coatings were used to characterize the as-sprayed condition. The porosity was measured by mercury porosimetry. This intrusion technique enables to determine the pore size distribution and is based on the pressure dependence [Ilavsky '10]. Two complementary devices from Fisons Instruments were employed (Pascal 140 for low pressures in the range 0.01 to 400 kPa and Pascal 440 for high pressures in the range up to 400 MPa). Specific surface area was determined by the adsorption method based on the "Brunauer-Emmett-Teller" theory (BET) with the device Areameter II from Ströhlein Instruments.

Phase analysis by X-ray diffraction (XRD) was performed with a D4 Endeavor diffractometer (Bruker AXS GmbH, Karlsruhe, Germany). The measurement conditions were Cu-Kα radiation, acceleration voltage 40 kV, and beam current 40 mA. The step increment was 0.02° and the count time 5 s or 2 s per step.

Young's modulus at room temperature was determined by three-point bending tests on freestanding coatings (apparatus Setsys TMA-18, Setaram, Caluire, France). The load is applied on the coating by a wedge ended alumina rod. The span d is 12 mm. The sample dimensions were the following: width b = 3.4 mm; thickness h = 500 µm. Coatings were loaded three times consecutively (three different loads: 5 g, 10 g, 15 g, leading to stresses σ = approx. 1 MPa, 2 MPa and 3 MPa respectively). Each load was applied for one minute. The unloading period between each loading lasts one minute as well. Applying different load values enables to achieve a better accuracy of the Young's modulus calculation. The freestanding coatings kept their full integrity during the bending tests but presented a slight bending afterwards.

3.3.2. Isothermal annealing tests

SPS free-standing coatings were tested in isothermal annealing in furnace. For all tests, the temperature of the annealing was 1400°C and duration of the dwell was 10 h and 55 h. Annealed coatings were then characterized further by microscopy, mercury porosimetry and bending tests.

3.3.3. Three-point bending tests realized in-situ at high temperature

Measurements of the elastic modulus of free-standing coatings were also performed in-situ during annealing at 1400°C in order to investigate the sintering-related stiffening in more detail. The measurement is carried out by successive three-point bending tests. The setup for bending test is enclosed in a thermomechanical analysis (TMA) facility (Setsys TMA-18, Setaram, Caluire, France). The apparatus and sample dimensions were identical to the tests performed at room temperature. The samples were first heated up to 1400°C at 5 K/min. This temperature is kept constant during the whole duration of the measurement (about 12 hours). Samples are loaded hourly (except for the beginning of the experiment in which they are loaded every 30 min) with two different loads consecutively: 1 g during 2 min and 2 g during 4 min respectively (leading to stresses $\sigma = 0.22$ MPa and 0.43 MPa respectively). The presented data are average values obtained from calculated Young's moduli at each load. The unloading time between these two loadings is set to 3 min. Data for standard APS coatings were employed as reference for comparison purpose. These bending tests data were acquired by the identical method and apparatus [Ahrens '04].

3.3.4. Thermal cycling tests

Thermal cycling tests were performed by using gas burner rigs (Fig. 21 left). The sample is heated from the front by the burner to the desired surface temperature and cooled from the back by compressed air to induce a temperature gradient. It is subsequently cooled down at the front side to almost room temperature. The heating phase and the cooling phase last respectively 5 min and 2 min (Fig. 21 right). The surface temperature of the ceramic top-coat and the substrate temperature (backside) are continuously measured and controlled by using respectively a pyrometer and a thermocouple. In the presented experiments, the nominal temperature of the top-coat surface is 1400°C while the nominal substrate temperature is 1050°C, which represents a severe thermal load of the TBCs. The thermal cycling tests are performed until spallation of at least 30% of the coating total surface area. The lifetime is the number of cycles that the coating has undergone before failure. The temperature at the interface topcoat/bondcoat is of high relevance for the growth of the TGO. This

temperature is estimated by using the thermal conductivities of the topcoat (about 0.9 $W.m^{-1}.K^{-1}$ for SPS coating [Kaßner '09a] and about 1.0 $W.m^{-1}.K^{-1}$ for APS coatings), of the bondcoat (about 31 $W.m^{-1}.K^{-1}$) and of the substrate (about 26 $W.m^{-1}.K^{-1}$). The thickness of the TGO layer was investigated after thermal cycling tests by confocal laser microscopy. The bondcoat temperature data correlated to the TGO thickness data enabled to put the results in perspectives and to perform an appropriate comparison of the cycled specimens.

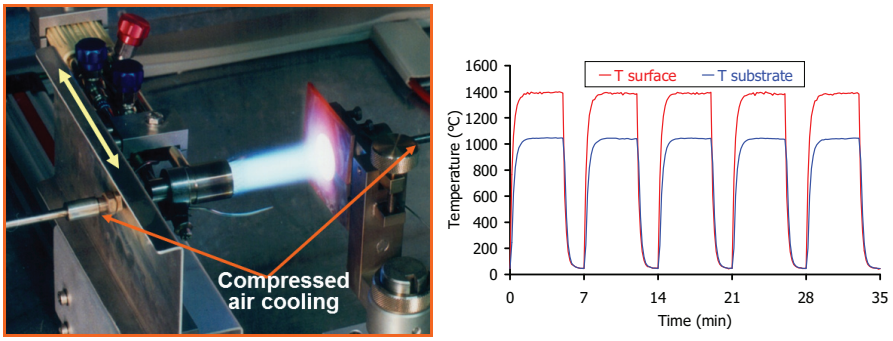

Fig. 21: Burner rig used for thermal cycling tests on TBCs (left), and pattern of the thermal cycles applied on TBCs at the burner rig facility (right).

4. Results and discussion

4.1. Developments on SPS YSZ TBCs

4.1.1. Motivation

The developments of submicrometer-structured YSZ coatings by SPS are subjected currently to active research efforts. Recent investigations on several aspects of the process, such as the injection of the suspension and its interaction with the plasma jet [Marchand '11, Meillot '11], the sintering during coating growth [Łatka '11] and the challenging characterization of the nanometer-scaled porosity of SPS coatings [Bacciochini '10, Montavon '11], enable a better understanding of SPS. The environmental impacts of liquid feedstock plasma spraying were also recently investigated [Moign '10]. The SPS process is currently being investigated for the field of TBCs in several working groups [Ben-Ettouil '09, Kaßner '08a, Tang '11, VanEvery '11]. SPS-manufactured TBCs already showed benefits compared to APS-deposited ones. They present a higher density of vertical segmentation cracks than APS coatings, providing high strain tolerance and low Young's modulus, with still relatively high porosity for good thermal insulation [Kaßner '08a]. Most of the pores are in the submicrometer range. The higher density of segmentation cracks than that of APS coatings is related to the different relaxation processes during spraying [Vaßen '10b]. Previous studies demonstrated advantages in terms of coating properties, such as reduced thermal conductivity, improved optical properties [Kaßner '08b] and enhanced thermal cycling lifetime at moderate surface conditions [Kaßner '09a]. On the other hand, investigations of the sintering behavior of such coatings at moderate temperature (1200°C) showed that SPS coatings have a higher sintering rate than APS ones [Kaßner '09a, Kaßner '09b]. This is related to their very fine microstructure and particularly to the large fraction of submicrometer pores and the high amount of unmolten clusters.

Since the requirements in gas turbines are constantly increasing and demand higher inlet temperatures, the present investigations focus on the evolution of the YSZ coating microstructure during exposure to very high temperature (1400°C) both in thermal cycling in a temperature gradient and in isothermal annealing. The effects of sintering phenomenon on the coating properties such as Young's modulus are pointed

out. A large part of the author's work in sections 4.1.2, 4.1.3 and 4.1.4 was already published in a journal article in 2012 [Guignard '12].

4.1.2. Microstructural investigations on as-sprayed SPS coating

The spraying parameters are detailed in Table 4. The obtained coating exhibits a porous microstructure as well as a large amount of vertical segmentation cracks (perpendicular to the coating surface) as shown in Fig. 22a and Fig. 22b. They provide strain tolerance, which is an important characteristic for the TBC application [Guo '06, Karger '11, Vaßen '05]. The segmentation crack density is equal to approx. 6.5 cracks/mm.

Table 4: Spraying parameters for SPS of YSZ suspension for TBCs (slpm = standard liters per minute) (sample number A-10-020-T2)

spraying distance	65 mm
plasma current	500 A
plasma gas	40 slpm Ar, 10 slpm He
plasma power	56 kW
robot speed	700 mm/s
robot meander height	2 mm
YSZ suspension solid content	20 wt.%
suspension feeding pressure	2 bar
air pressure for atomization	0.5 bar
suspension feeding rate	approx. 60 g/min
substrate cooling	front side and back side
deposition rate	12 µm per deposition cycle
deposition efficiency	approx. 40%
YSZ coating thickness	approx. 500 µm

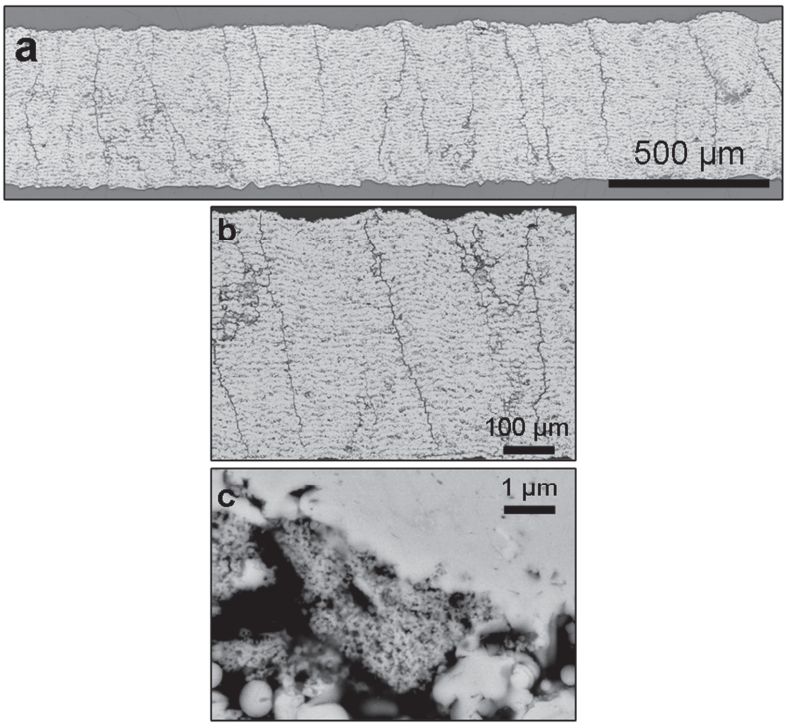

Fig. 22: Images of the microstructure of as-sprayed SPS free–standing coating on polished cross-sections (sample number A-10-020-T2). (a) Confocal laser microscope image consisting of a stitching of five individual pictures providing an overview of the coating, (b) SEM image (BSE mode) showing porous structure and segmentation cracks, (c) SEM image (BSE mode) at higher magnification showing an example of unmolten cluster.

SEM observations at higher magnification reveal the presence of unmolten clusters (Fig. 22c). It consists of very fine particles situated in the fringes of the plasma jet during flight. They are therefore not properly thermally treated and embedded in the microstructure as fine solid particles forming kind of nests. Although the relative volume of unmolten clusters embedded in the coating is typically low (below 15% estimated by image analysis techniques), it contributes to a large extent to the coating properties. Such weakly-bonded fine particles might be detrimental to the coating mechanical properties.

The pore size distribution in Fig. 23 shows that the SPS coating has finer pores than the standard APS one. Particularly, the fraction of pores having a radius below 0.3 µm is significantly different (66% for SPS and 28% for APS). These very fine pores were reported to act as scattering centers, thus providing an enhanced shielding against near-infrared radiation [Kaßner '08b, Stuke '07]. Previous investigations showed also that thermal conductivity of SPS coatings can be very low (in the range of approximately 0.5 to 1 $W.m^{-1}.K^{-1}$ depending on porosity level). When featuring similar porosity levels, SPS and APS coatings have comparable thermal conductivities, but SPS coatings can also be manufactured with much higher total porosity leading to reduced thermal conductivity [Kaßner '09b].

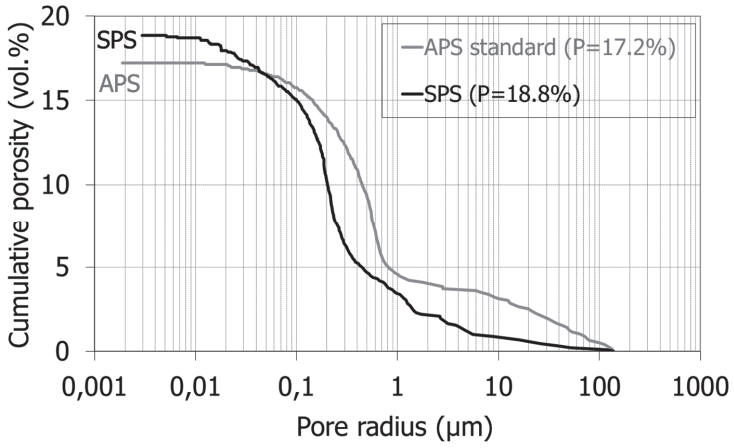

Fig. 23: Pore size distribution of as-sprayed SPS coating measured by mercury porosimetry (sample number A-10-020-T2). For comparison purpose, a standard APS coating having a similar total porosity was selected (sample number M-08-632-T2).

The large fraction of very fine pores and the presence of unmolten clusters in the coating induce a high specific surface area. The coating BET specific surface area is 0.57 m²/g and is therefore higher than typical values of conventional APS-deposited TBCs (from 0.2 to 0.4 m^2/g). Further properties of as-sprayed coatings were measured. The average hardness is 634 $HV_{0.5}$ ± 92. Young's modulus measured by the three-point bending test is about 3.3 GPa, thus being much lower than that of APS

TBCs (in the range of about 15-20 GPa, measured by identical method and apparatus [Ahrens '04]).

4.1.3. Thermal cycling tests at surface temperature of 1400°C

With respect to the TBC application, it is of high interest to investigate the sintering of SPS coatings within a complete TBC system (i.e. YSZ topcoat + bondcoat + substrate) in a thermal gradient as can be performed in burner rigs. These severe testing conditions enable to simulate the real operating conditions in a gas turbine. SPS TBCs proved in previous investigations [Kaßner '09a] to have high lifetime in thermal cycling tests at moderate surface temperature ($T_{surface}$ ~ 1240°C; $T_{substrate}$ ~ 1030°C; lifetime in the range of 1000-2500 cycles depending on feedstock and microstructures). Since TBC systems in gas turbines are expected to be subjected to higher surface temperatures in the future, the scope of the present investigation is on microstructure sintering at these conditions (thermal cycling tests at $T_{surface}$ ~ 1400°C and $T_{substrate}$ ~ 1050°C).

The failure of the TBC during thermal cycling tests occurs as a partial spallation of the top-coat (Fig. 24a). Under these extreme temperature conditions, the coatings reach an average lifetime of 660 cycles. Lifetime at this very high temperature is lower than at moderate temperature. For these tests at 1400°C, the lifetime of SPS TBCs is still approximately 50% lower than that of standard established APS TBCs.

The diffusion of oxygen through the porous top-coat during thermal cycling leads to oxidation of the bond-coat at the interface and to the formation of the so-called thermally-grown oxide layer (TGO), which grows between the bond-coat and the top-coat. The TGO layer is in the range of approx. 3-6 µm in thickness (Fig. 24b). The aluminum-depletion zone in the upper region of the bond-coat is in the range of 8-12 µm in thickness. The horizontal delamination is located within the YSZ top-coat, close to the interface with the TGO. Delamination cracks occur parallel to the interface, propagate, join each other and lead eventually to the spallation of the YSZ top-coat.

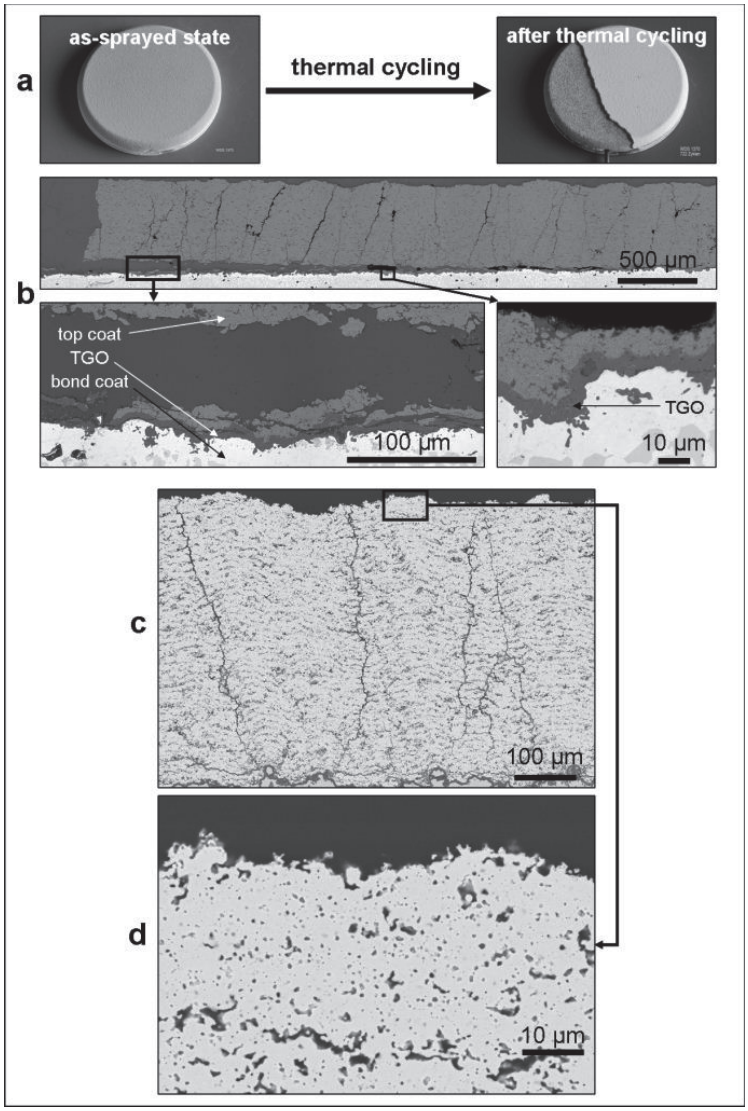

Fig. 24: Images of SPS TBC subjected to thermal cycling test (sample WDS 1370 having deposition number A-10-019-T2 with identical spraying parameters as A-10-020-T2). (a) Photographs of the specimen in the as-sprayed state and after thermal cycling; (b) confocal laser microscope images of polished cross-section after thermal cycling showing coating spallation and TGO layer; (c) SEM image (BSE mode) after thermal cycling showing segmentation cracks that survived; (d) SEM image (BSE mode) at higher magnification after thermal cycling pointing out beginning of sintering.

Further observations showed that delamination cracks may propagate preferentially through unmolten clusters (Fig. 25). Since these microstructural features consist of embedded weakly-bonded fine particles, they are assumed to be weak points in the coating in terms of mechanical properties and may promote the propagation of delamination cracks from an unmolten cluster to another at the bottom of the top-coat and eventually lead to the coating spallation. Although they may have also a positive effect on the coating porosity via the finest pores that they contain, the main effect of the unmolten clusters is considered to be their detrimental influence on the coating mechanical stability. Therefore, efforts on reducing the presence of unmolten clusters embedded in the microstructure in order to improve the coating performances are presented in section 4.1.5.

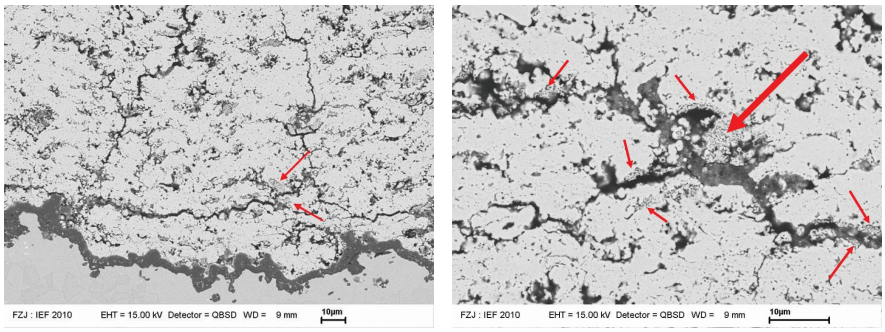

Fig. 25: SEM images of polished cross-section of SPS TBC sample (sample WDS 1370 having deposition number A-10-019-T2 with identical spraying parameters as A-10-020-T2) after thermal cycling test, showing evidences of delamination cracks propagating through unmolten clusters (indicated by arrows).

The evolution of the coating microstructure due to thermal cycling was investigated. It is found that the segmentation cracks are not closed during thermal cycling in spite of such high temperatures (Fig. 24c). Segmentation crack density after thermal cycling is 6.2 ± 0.5 cracks/mm compared to 6.5 ± 0.7 in the as-sprayed state. This may play an important role in maintaining partly the coating strain tolerance during thermal cycling.

Further microscopical observations showed that most of the unmolten clusters sintered during thermal cycling. Due to their very small particle size, the particles in

the unmolten clusters have a particularly high sintering activity and, therefore, neck formation and coarsening take place when exposed to thermal treatment.

At higher magnification, the particular, rather spherical shape of the pores reveals that the coating started to sinter during the thermal cycling test as shown in Fig. 24d (as an example located close to the coating surface). This phenomenon occurs along the whole thickness of the coating. Sintering is known to increase the intersplat contact area and to heal the intrasplat microcracks in plasma sprayed TBCs. These phenomena increase the coating hardness: average hardness after thermal cycling is 816 $HV_{0.5}$ ± 82 compared to 634 $HV_{0.5}$ ± 92 in the as-sprayed state.

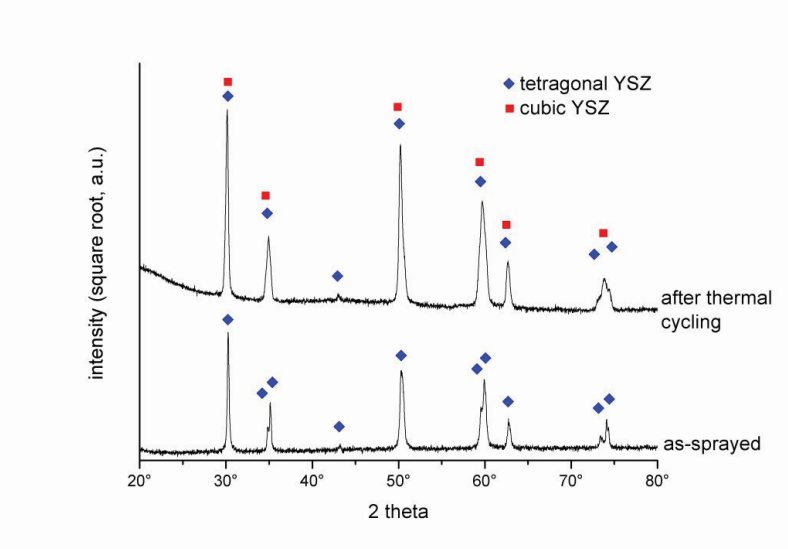

Fig. 26: Diffractogram of SPS YSZ coating after thermal cycling compared to the as-sprayed state. A phase transformation occurs from the initial tetragonal prime phase to cubic and tetragonal phases (as-sprayed state: sample number A-10-020-T2; after thermal cycling: sample WDS 1370 having deposition number A-10-019-T2 with identical spraying parameters as A-10-020-T2).

It is known that an exposure of YSZ to such high temperature (1400°C) may induce phase transformations in this material. Particularly, if a phase transformation from the initial tetragonal prime phase to the cubic and tetragonal phases and further during cooling to the monoclinic phase would occur, it would be accompanied by a dramatic volume change, leading to the spallation of the coating. Therefore, it is important to perform XRD phase analysis on the coating after the thermal cycling test in order to

determine if such a phase transformation would have been the reason for the coating spallation. Results showed that, although no indication of monoclinic phase was found, the transformation from tetragonal prime to cubic and tetragonal started at the high cycling temperatures (Fig. 26). As it was found in the literature, the development of monoclinic phase is often retarded, maybe due to the fine crystallite size of the tetragonal grains.

4.1.4. Sintering behavior under isothermal annealing at 1400°C

In order to investigate the sintering behavior of SPS TBCs in more detail, the evolutions of the pore size distribution and of the Young's modulus during exposure to high temperature are of high interest. Working with free-standing coatings enables to perform mercury porosimetry measurements as well as three-point bending tests. Therefore, as-sprayed reference SPS coatings sprayed on stainless steel substrates were stripped off by using hydrochloric acid. These coatings in the as-sprayed state were subjected to isothermal annealing in a furnace at 1400°C for 10 h and 55 h respectively. The coatings subjected to thermal cycling tests and presented in the previous section underwent a total exposure at 1400°C equal to 55 h until failure (660 cycles x 5 min = 55 h). It is therefore interesting to investigate coatings subjected to isothermal annealing during this same duration. This experiment provides valuable information on the sintering behavior of SPS TBCs despite the fact that it is not as close to the real gas turbine operating conditions as thermal cycling tests. Fig. 27 shows cross-section images of coatings annealed at 1400°C. It can be seen that isothermal annealing for 10 h already leads to a beginning of sintering. It is recognizable especially at the shape of the pores compared to the as-sprayed state. It is observed that a pore coarsening takes place. Besides, the unmolten clusters tend also to sinter rapidly. The sintering goes further as it can be seen on the microstructure of the coating annealed during 55 h.

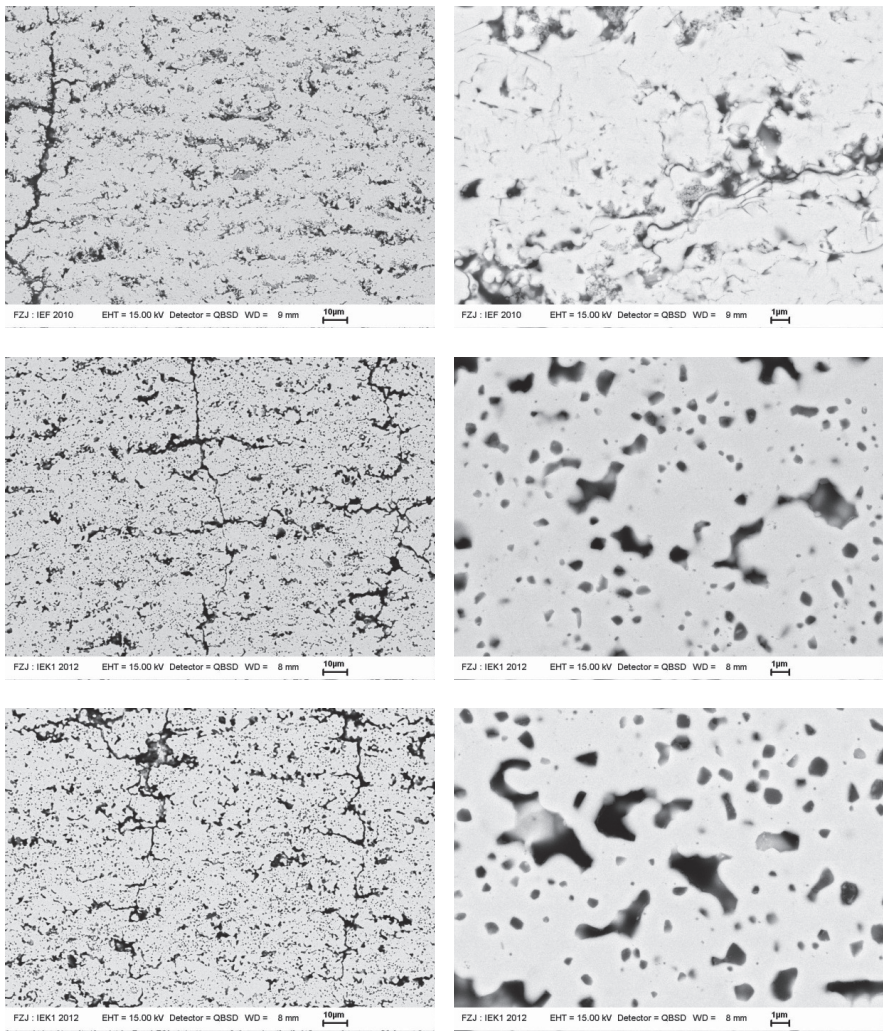

Fig. 27: Sintering-related evolution of the microstructure showed by SEM images of polished cross-sections in the as-sprayed state (top), after isothermal annealing at 1400°C for 10 h (middle) and after 55 h (bottom) (all images from sample number A-10-020-T2).

In order to investigate the phenomenon of sintering-related pore coarsening, mercury porosimetry measurements were carried out. The measured total porosities did not show a significant trend. It is considered that the coating total porosity does not decrease during sintering (total porosity volume of about 18-19%). The significant effect of thermal treatment is rather on the size of pores. The presentation in

normalized cumulative curves in Fig. 28 enables to show the evolution of the pore size distribution, which is shifted in the direction of coarser pores during annealing, thus revealing a pore coarsening. The pore size distribution is constituted of several types of porosity, comprising microcracks, micropores, vertical segmentation cracks and coarse globular pores. The fraction of the porosity with pore radius below 0.3 µm (corresponding to microcracks and micropores) is significantly reduced during isothermal annealing (66% in the as-sprayed state; 17% after 10 h annealing; 7% after 55 h) while the fraction above 0.3 µm increases. Reduction of fine porosity occurs due to diffusion-related phenomena such as sintering of unmolten clusters, healing of microcracks and pore agglomeration. Pore coarsening may play a role in the evolution of the coating properties during high temperature exposure. For example, a change of the elongated microcrack-like pores to globular pores might be detrimental for the thermal insulation property of the TBC.

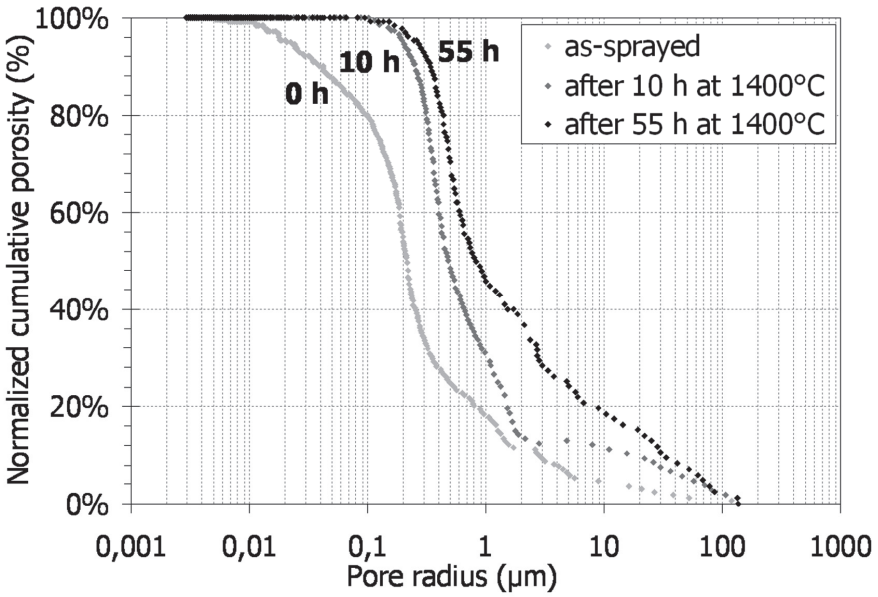

Fig. 28: Normalized pore size distribution of SPS free-standing TBC measured by mercury porosimetry after isothermal annealing at 1400°C for 10 h and 55 h compared to the as-sprayed state, showing pore coarsening (sample number A-10-020-T2).

Since sintering is also expected to increase the coating stiffness, measurements of Young's modulus K_I by means of three-point bending tests on free-standing coatings were performed. The coatings were subjected to isothermal annealing at 1400°C for 10 h and 55 h. The Young's modulus is then measured at room temperature after thermal treatment is completed. Fig. 29 shows that the Young's modulus significantly increases during isothermal annealing when compared to the as-sprayed state (i.e. 0 h annealing). The increase of Young's modulus is higher during the first 10 hours than during the following 45 hours, thus showing that sintering occurs rather quickly during the first hours of annealing. After 55 h at 1400°C, the Young's modulus reaches the high value of 51.6 GPa. This strong stiffening probably promotes coating failure in the thermal cycling operation, although segmentation cracks continue to play a significant role in maintaining partly the strain tolerance by reducing the formation of in-plane tensile stresses during thermal cycling.

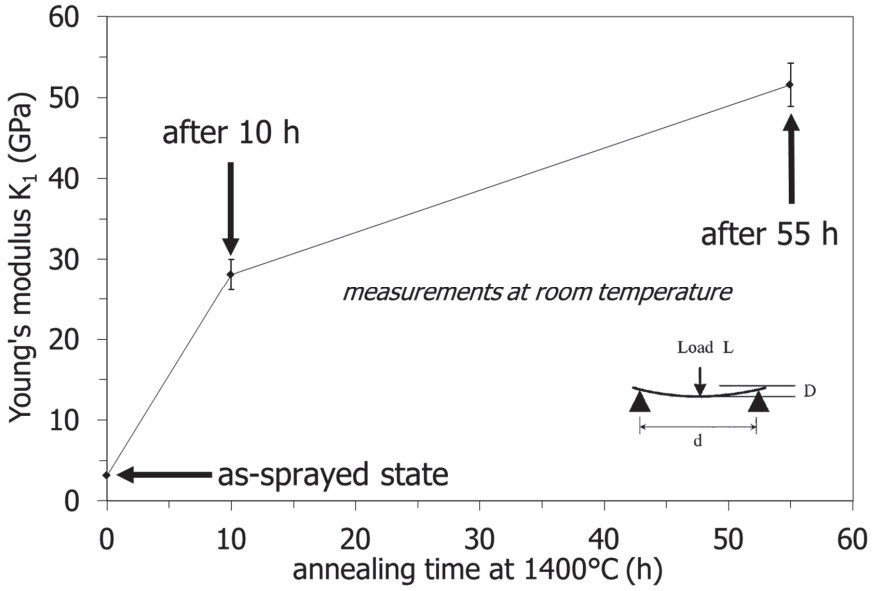

Fig. 29: Young's modulus K_I measured by three-point bending tests at room temperature on free-standing SPS YSZ coatings which were subjected to isothermal annealing at 1400°C during 10 h and 55 h compared to the as-sprayed state (sample number A-10-020-T2).

In order to investigate the sintering-related stiffening in more detail, measurements were also performed in-situ during annealing at 1400°C by successive three-point bending tests on a free-standing as-sprayed coating. The evolution of the total elastic modulus K_{eff} is plotted as a function of time in Fig. 30. The time t = 0 min corresponds to the beginning of the dwell after reaching 1400°C. The measurements were realized at 1400°C and the values of elastic modulus are therefore lower than values obtained at room temperature. Reference data from [Ahrens '04] for standard APS TBC are also presented for comparison purpose (data acquired by identical method and apparatus). It is interesting to notice that the measured elastic modulus of standard APS TBC at 1400°C is significantly lower than the modulus at room temperature (about 3 GPa at 1400°C for t = 0 min, and about 20 GPa at room temperature according to [Ahrens '04]). This strong temperature dependence of the elastic modulus of APS coatings contrasts with the commonly known data for bulk YSZ such as from [Adams '97], which reports values of about 220 GPa at room temperature and about 170 GPa at 1350°C (decrease of only approximately 20%). The particular microstructure of plasma sprayed coatings with pores and cracks leads to much lower elastic modulus than the bulk material and seems also to amplify strongly its temperature dependence. It might also be related to a strong creep effect (viscoplasticity) that takes place at such very high temperature [Ahrens '04], which would affect the measured value that might therefore represent not solely the elastic modulus. Nevertheless, Fig. 30 shows through an in-situ measurement how the elastic modulus increases during annealing and confirms the high tendency to sinter at such high temperature. Besides it should be noted that sintering is likely to begin already during the temperature increase of the facility (heating rate 5 K/min) before reaching the dwell temperature of 1400°C. Therefore, the first data point does not exactly correspond to the as-sprayed state. The sintering-related stiffening takes place due to the increase of the intersplat contact area and the healing of the intrasplat microcracks that are occurring during annealing at such high temperature. Furthermore, the fine porous microstructure of SPS coating and the presence of unmolten clusters promote the tendency to sinter during high temperature exposure.

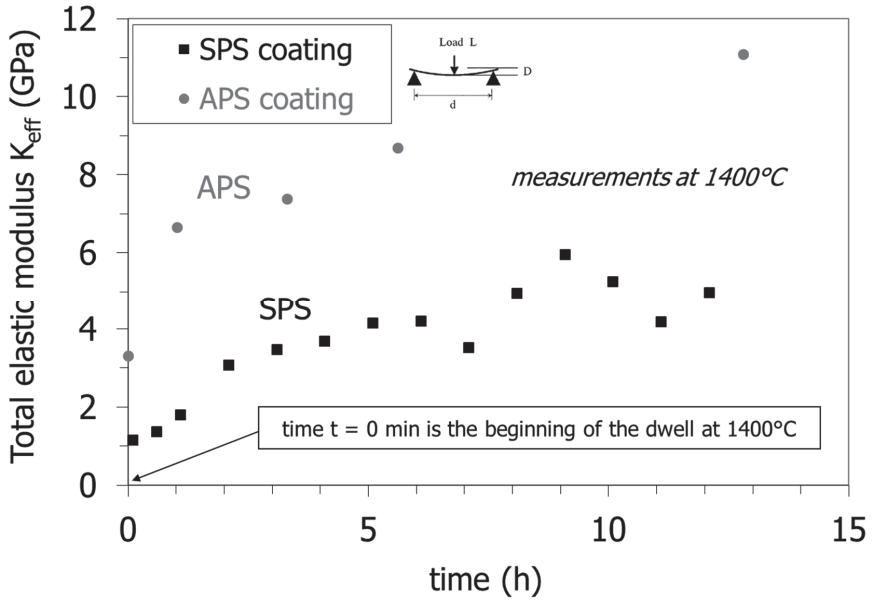

Fig. 30: Evolution of the total elastic modulus K_{eff} measured by successive three-point bending tests at 1400°C in-situ during annealing on free-standing as-sprayed SPS YSZ coating (sample number A-10-020-T2). Reference data from [Ahrens '04] for standard APS TBC are also presented for comparison purpose (data acquired by identical method and apparatus).

4.1.5. Improvement of YSZ TBC coating microstructure

It was shown in section 4.1.2 that the SPS coating contains a non-negligible fraction of unmolten clusters. These are constituted of very fine primary particles which were not properly thermal treated in the plasma jet and are therefore embedded in the microstructure as very fine solid unmolten particles, weakly-bonded to each other, forming kind of bulk "nests". One can recognize unmolten clusters on cross-sections with their gray color, darker than the rest of the coatings. In terms of mechanical properties, they represent weak points in the microstructure. Evidences were presented in section 4.1.3 showing that the formation and the propagation of delamination cracks are likely to be enhanced by the presence of these weak areas in the coating. Moreover, due to their very small size, these fine unmolten particles have a high sintering activity and might therefore lead to higher sintering rate of the whole coating, thus yielding undesirable effects in high temperature operations such as reduction of the strain tolerance and increase of the thermal conductivity. Indeed, section 4.1.4 showed that the sintering-related stiffening occurs rather quickly during thermal treatment, thus yielding high Young's modulus values compared to as-sprayed coatings. This may play a significant role in the failure of the coating in thermal cycling test. Therefore, the driving force for the improvement of the YSZ microstructure is the reduction of the total fraction of embedded unmolten clusters.

Since the particles responsible for the deposition of unmolten clusters are located in the colder fringes of the plasma jet during flight, one hypothesis is that these particles are related to the most external droplets upon atomization of the suspension by the atomizing nozzle. It is thought that the fraction of droplets being atomized at a wide angle are projected next to the plasma jet or penetrate into the colder plasma fringes, while the fraction of droplets that are closed to the centerline of the cone-shaped atomization are likely to penetrate directly into the center of the plasma jet and further into the hot plasma core. It appears therefore to be a valuable approach to optimize the suspension injection to reduce the angle of the atomization. This angle can be influenced by the gas and suspension pressure. However these parameters have also a significant effect on the droplet size and velocity. For this reason, the internal geometry of the atomizing nozzle must be modified in order to reduce the angle of the

cone-shaped atomization without modifying the pressure parameters. Fig. 31 is a schematic of the head of the two-phase atomizer showing its inner geometry. The chamber where the mixture of suspension with air occurs has a width *a* that is fixed. The zone situated before the outlet has a width *b* that is fixed and a length *L* in the millimeter range that was varied in the presented experiments. An increase of *L* is expected to provide a narrower angle of the generated atomization. The previous standard atomization conditions with which previous SPS coatings were manufactured featured a ratio $L/a = 0.5$.

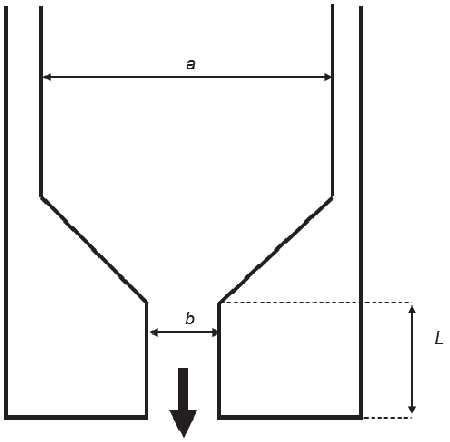

Fig. 31: Schematic of the head of the two-phase atomizer. The chamber where the mixture of suspension with air occurs has a width *a* that is fixed. The zone situated before the outlet has a width *b* that is also fixed and a length *L* that was varied in the presented experiments ($L/a = 0.5$ in previous standard conditions).

Fig. 32 shows photographs of the suspension atomization by two-phase atomizers with a varying ratio L/a in the range 0.25-1.0 with a step of 0.25. It shows clearly the influence of the internal geometry on the angle of the cone-shaped atomization. In spite of their very short exposure time (24 µs), these photographs do not permit to estimate properly droplet sizes and droplet velocities due to a too strong overlapping of droplets on the images. Nevertheless, the provided information on the atomization angle enable to define $L/a = 1$ as new optimal conditions in terms of nozzle internal geometry with the aim of reducing the fraction of unmolten clusters in the coating.

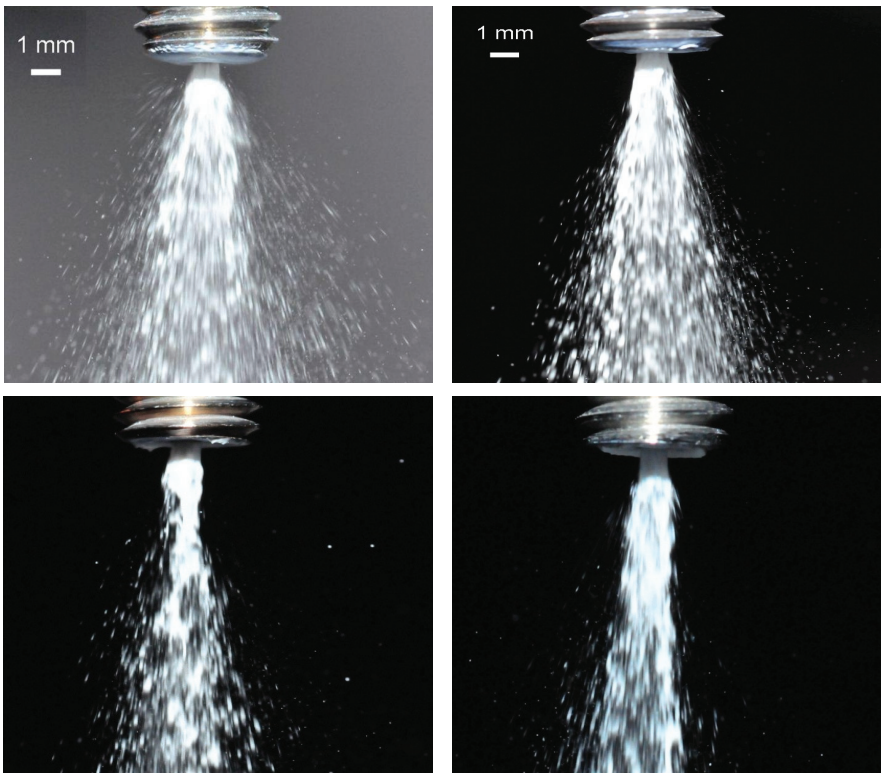

Fig. 32: Photographs of the suspension atomization by two-phase atomizers with varying internal geometry: $L/a = 0.25$ (upper left), $L/a = 0.5$ (upper right), $L/a = 0.75$ (bottom left), $L/a = 1$ (bottom right), showing the influence on the angle of the cone-shaped atomization. Suspension and pressure parameters are kept identical. Exposure time is 24 µs (short flash duration in dark room).

SPS experiments were realized with a new nozzle featuring $L/a = 1$ in order to estimate the effect on the presence of embedded unmolten clusters. All other process parameters are kept constant. Fig. 33 shows SEM micrographs of the reference coating (with $L/a = 0.5$) while Fig. 34 shows SEM micrographs of the new coating (with $L/a = 1$). Results show clearly the positive influence of the new nozzle geometry on the microstructure. It is observed that the coating sprayed with the improved nozzle contains significantly less unmolten clusters, compared to the reference coating.

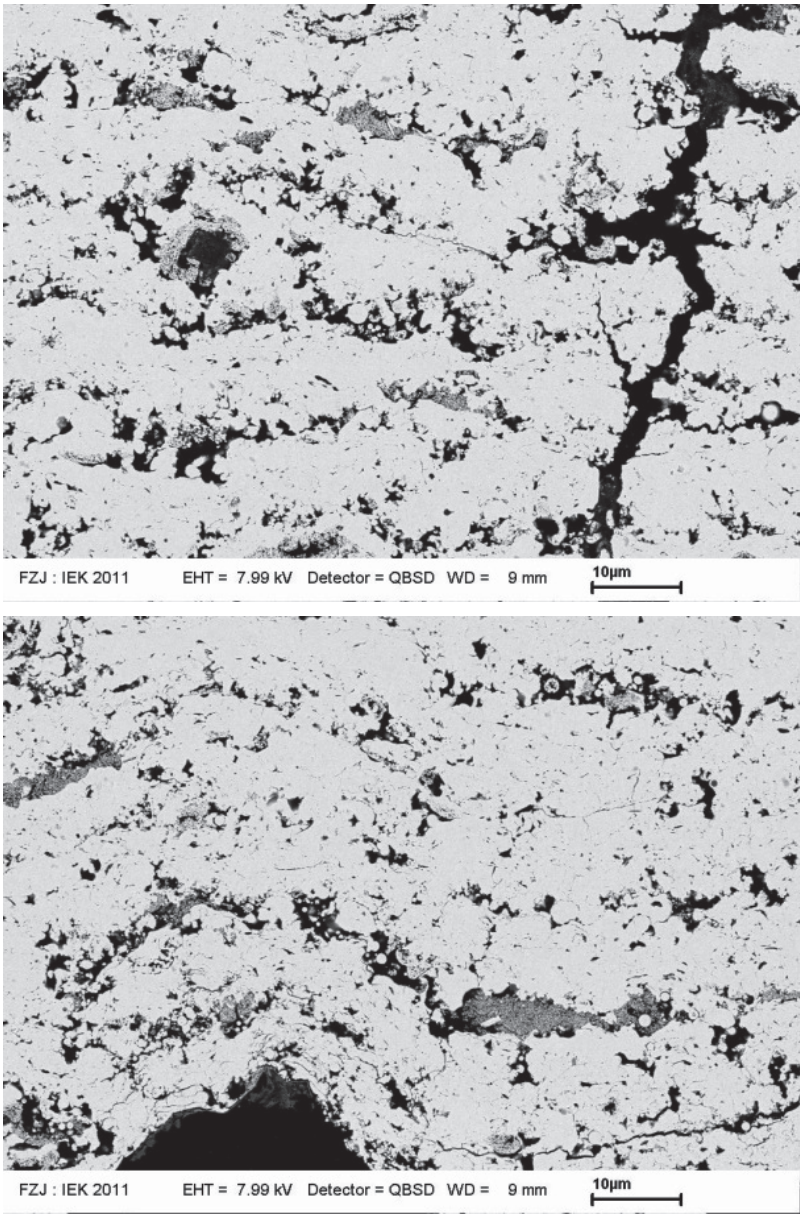

Fig. 33: SEM micrographs of the SPS reference coating (with nozzle having $L/a = 0.5$) (sample number A-10-020-T2).

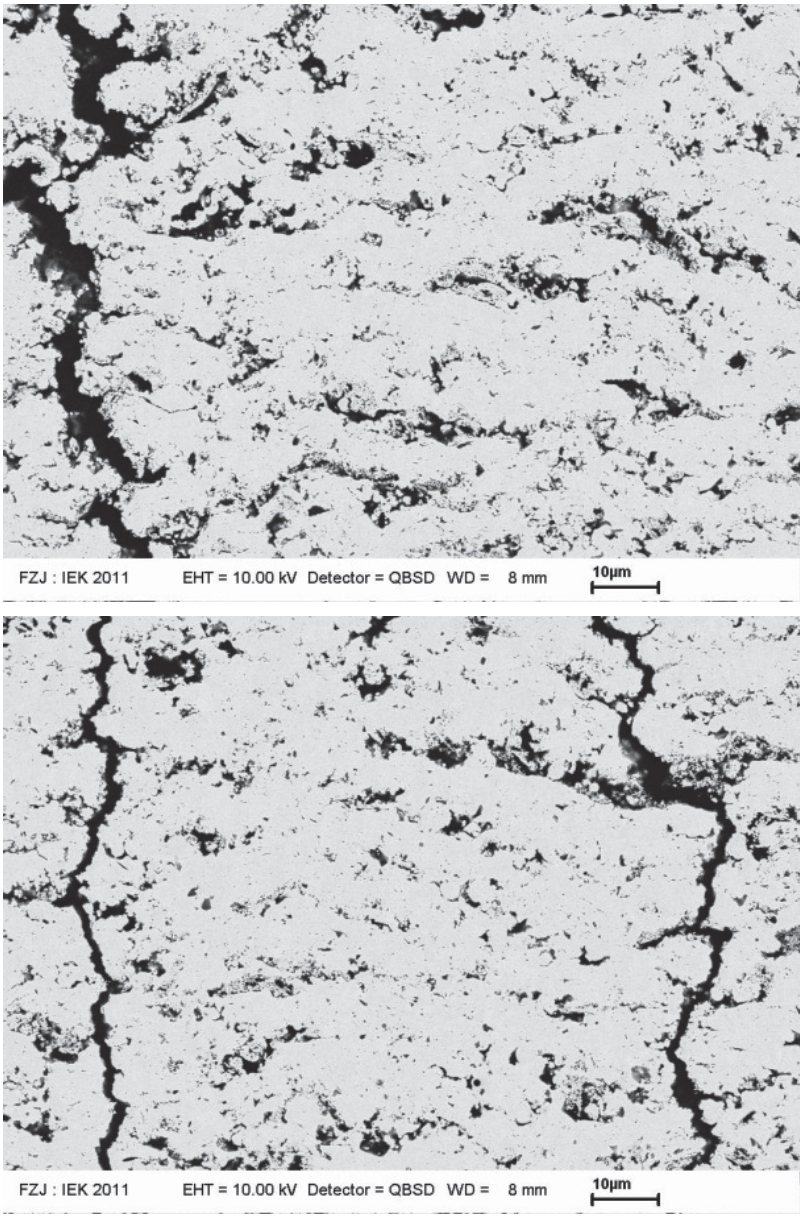

Fig. 34: SEM micrographs of the SPS new coating (with new nozzle having $L/a = 1$) (sample number A-11-173-T2).

A further observation on the micrographs indicates that the coating sprayed with the improved nozzle does not exhibit much other variation in terms of microstructure when compared to the reference coating. Both coatings are fairly porous and contain a

large amount of vertical segmentation cracks. These two microstructural characteristics were evaluated quantitatively in order to verify that the microstructure modification induced by the new atomization nozzle significantly affects only the presence of unmolten clusters and do not has a detrimental influence on the total porosity and the segmentation crack density. For the purpose of mercury porosimetry measurements, a further coating was sprayed by using also the new improved nozzle ($L/a = 1$) with a sufficient coating thickness to permit reliable mercury porosimetry (sample number A-11-301-T2). Results showed a total porosity of 17.2%. This is rather similar to the reference coating, on which two values of total porosity were generated (by two distinct measurements on the same sample): 18.1 and 18.8%. This very slight decrease of the total porosity might be related to the reduced fraction of unmolten clusters since these clusters contain also very fine pores. Nevertheless, total porosity is not decreased dramatically. Further microstructural investigations reveal a segmentation crack density of approx. 6 cracks/mm, being therefore similar with the reference coating in terms of strain tolerance. Therefore, the positive effect of the new optimized internal geometry of the atomization nozzle is demonstrated since it enables to deposit coatings with a significantly reduced fraction of unmolten clusters while total porosity and segmentation crack density are not decreased dramatically.

In an effort to test the potential performances of this improved microstructure, thermal cycling tests were carried out on two TBC specimens (YSZ topcoat + NiCoCrAlY bondcoat + Inconel substrate) in which the YSZ topcoats were manufactured with the improved microstructure sprayed with the new nozzle. Other parameters were kept constant. Thermal cycling tests were performed on the same burner rig as previous tests presented in section 4.1.3 and the nominal surface and substrate temperatures were similar ($T_{surface} \sim 1400°C$ and $T_{substrate} \sim 1050°C$, nominal values). Fig. 35 shows the photographs of the specimens after thermal cycling tests showing the spallation and Fig. 36 shows the cross-section of one of them. Failure of the TBCs occurred after approx. 200 cycles for both samples. This experimental result does not constitute an improvement of the lifetime since the previous coatings reached an average lifetime of approx. 660 cycles (section 4.1.3). For a better comparison of these results, further analysis were conducted by considering the TGO thickness after failure and the calculated bondcoat temperature during thermal cycling at which the TGO grows. This permits to draw more precise and adapted conclusions when comparing the performances of TBCs under thermal cycling [Vaßen '09a]. Average TGO thicknesses

at the center of the specimen for the two tested samples with the new improved YSZ microstructure is 4.8 and 5.1 µm respectively (samples number WDS 1993 and WDS 1994). An example is shown on Fig. 37. The two reference TBC samples deposited by SPS with the previous YSZ microstructure (former standard atomization nozzle featuring $L/a = 0.5$) show average TGO thicknesses at the center of the specimen of 3.8 and 3.7 respectively (samples number WDS 1370 and WDS 1371). An example is shown on Fig. 38. TGO growth is directly related to the temperature at the topcoat/bondcoat interface. Calculations of the average value of this temperature during thermal cycling for each sample enable to interpret variations in TGO thickness at failure. TGO thicknesses, temperatures at interface and lifetime are plotted in Fig. 39 and Fig. 40 to illustrate the comparisons between all samples. In addition, the data for four standard TBC specimens deposited by APS and cycled at the same burner rig are plotted for comparison purpose. Two additional SPS samples that were sprayed with another type of YSZ suspension are also added to complete data (samples number WDS 1481 and WDS 1482) but are not directly taken into account in comparisons and interpretations. On Fig. 39, the theoretical TGO growth patterns at various interface temperatures are plotted as a guide. These data were calculated by using the TGO growth model described by Vaßen et al. [Vaßen '09a]. The results of these analyses show that the two tested samples with the new improved YSZ microstructure do not show thinner TGO layers than the two previous TBC samples deposited by SPS with the previous YSZ microstructure, in spite of their shorter number of cycles. Further observations show even that their aluminum-depleted zones are thicker. It appears that the thermal cycling conditions for these two new samples induced slightly higher temperatures at the TGO, as shown on Fig. 39 and Fig. 40. This has led to an accelerated TGO growth when compared to the two previous TBC samples and has eventually led to an early failure of the TBC. It is commonly known that the temperature at the TGO plays a predominant role in the lifetime of TBCs [Vaßen '09a]. This is particularly reflected on Fig. 40 showing that lifetime drops rapidly with increasing TGO temperature especially above 1090°C. These observations lead to the conclusion that the two tested samples with the new improved YSZ microstructure do not show lower performances in spite of their apparent lower number of cycles. As a whole, TBC performances of these SPS samples are rather comparable. In fact, the significant improvement of the YSZ microstructure yielded by the optimized suspension atomization nozzle is not

reflected in TBC performances. This shows that other mechanisms might also play a role. It is also thought that the fraction of unmolten clusters might need to be further reduced to increase coating performances.

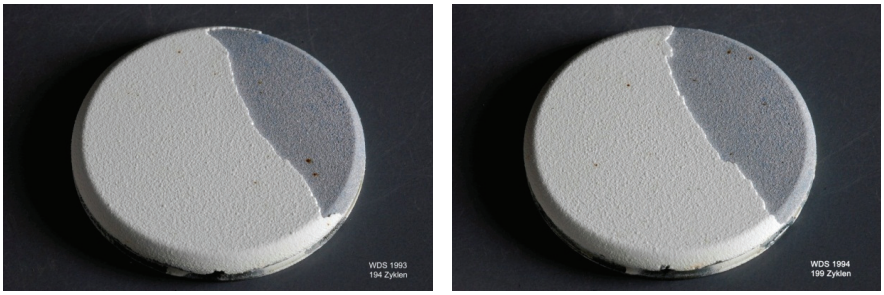

Fig. 35: Photographs of the two SPS TBCs specimens deposited with the new improved microstructure (new atomization nozzle) after thermal cycling tests (samples number WDS 1993 and WDS 1994 having deposition number A-11-301-T2) showing the spallation.

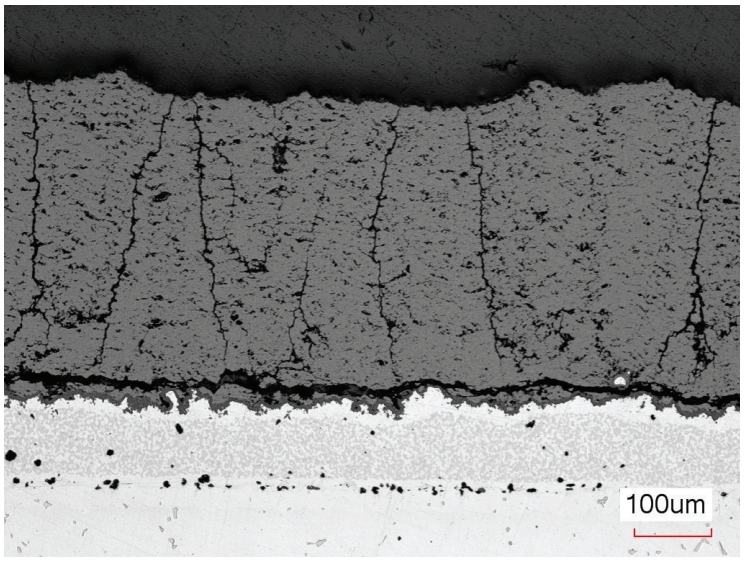

Fig. 36: Confocal laser microscope image of polished cross-section after thermal cycling showing coating spallation (sample number WDS 1994 having deposition number A-11-301-T2).

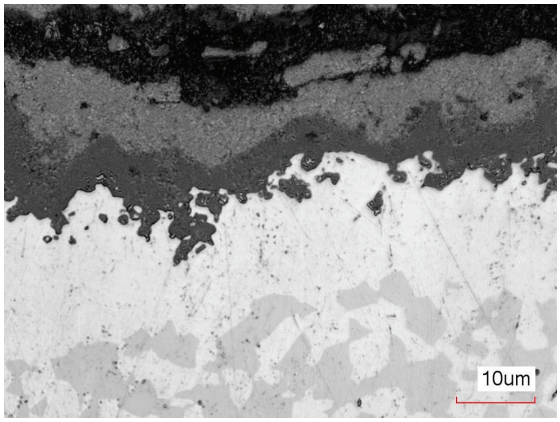

Fig. 37: Confocal laser microscope image of polished cross-section of TBC sample deposited by SPS with the new improved YSZ microstructure (new atomization nozzle featuring $L/a = 1$) after thermal cycling showing TGO layer (sample number WDS 1994 having deposition number A-11-301-T2). Average TGO thickness at the center of the specimen is 5.1 µm.

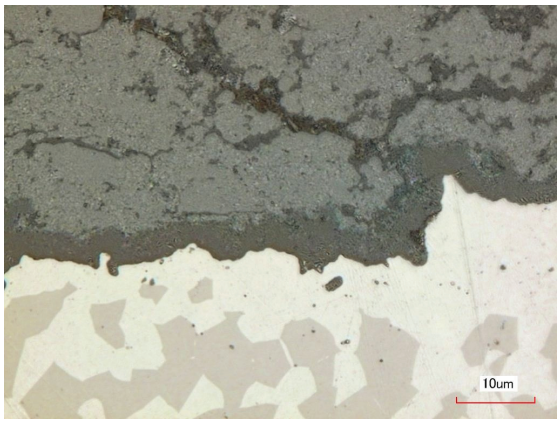

Fig. 38: Confocal laser microscope image of polished cross-section of TBC sample deposited by SPS with the previous reference YSZ microstructure (former standard atomization nozzle featuring $L/a = 0.5$) after thermal cycling showing TGO layer (sample number WDS 1371 having deposition number A-10-019-T2 with identical spraying parameters as A-10-020-T2). Average TGO thickness at the center of the specimen is 3.7 µm.

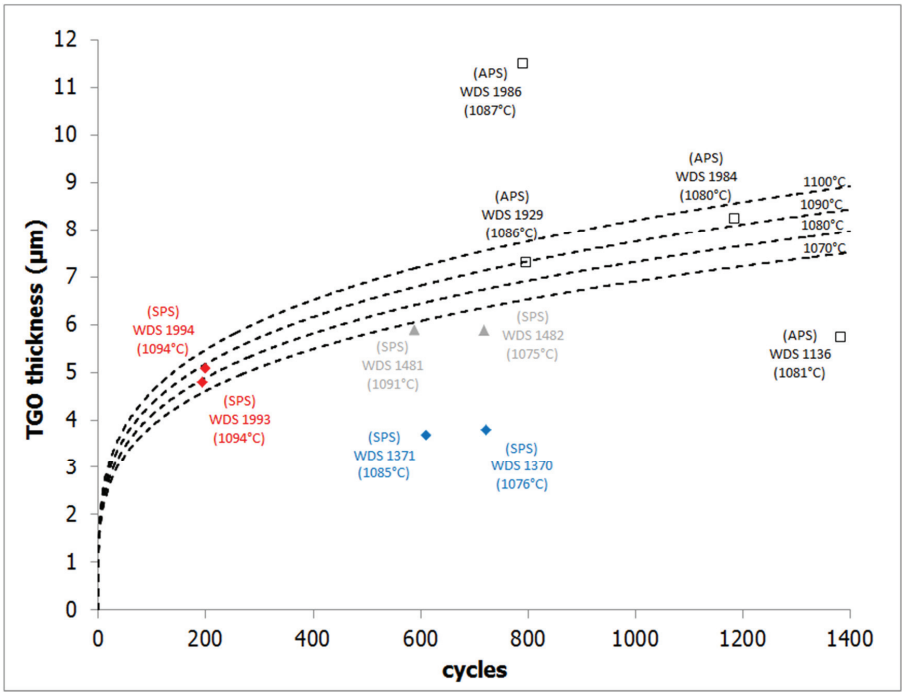

Fig. 39: Thickness of TGO of several TBC samples cycled in burner rig as a function of the number of cycles. In addition, the temperatures at the topcoat/bondcoat interface are indicated. The theoretical TGO growth patterns at various interface temperatures are also plotted as a guide. These data were calculated by using the TGO growth model described by Vaßen et al. [Vaßen '09a].

Fig. 40: Cycles to failure in burner rig for several TBC samples as a function of the temperature at the topcoat/bondcoat interface.

4.1.6. New developments of SPS-deposited YSZ coatings with columnar microstructure

Columnar microstructures such as produced by EB-PVD are particularly advantageous in terms of TBC lifetime since the voids between the columns promote strain tolerance. The voids can open and close and therefore reduce in-plane stresses during thermal cycling [Schulz '00]. However, the high costs and the low deposition rates that are correlated with this technique tend to limit its application to the most critical components in a gas turbine. The recent developments in the thin film low pressure plasma spraying (LPPS-TF) enable to obtain EB-PVD-like structures while keeping the costs at the relatively low level of plasma spray [Hospach '11].

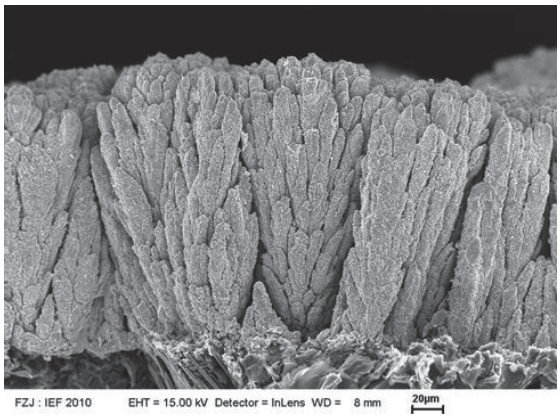

Fig. 41: Columnar-structured YSZ coating deposited by LPPS-TF through vapor deposition mechanisms [Hospach '11].

Besides, there is a growing interest in the thermal spray community in the possibility of producing columnar YSZ TBCs at atmospheric pressure conditions, in order to eliminate the costs associated with the vacuum chamber employed in the LPPS-TF process. Some experimental investigations have proved the feasibility of manufacturing such columnar structures by spraying YSZ suspensions with the SPS process [Kaßner '09a, Tang '11, VanEvery '11] such as shown on Fig. 42 and Fig. 43. This constitutes the motivation for the new experiments presented below, that were conducted with the SPS process with YSZ suspension.

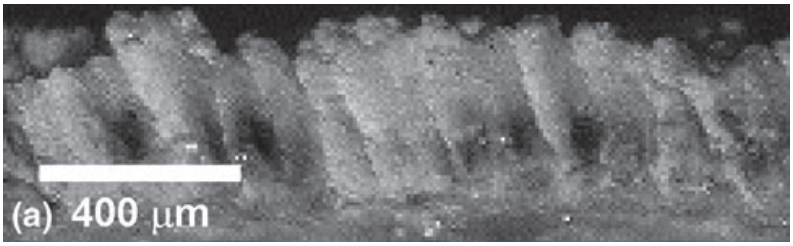

Fig. 42: Columnar-structured YSZ coating deposited by VanEvery et al. with the SPS process [VanEvery '11].

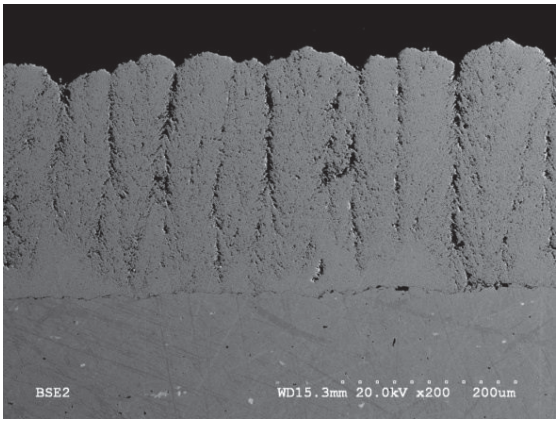

Fig. 43: Columnar-structured YSZ coating deposited by Tang et al. with the SPS process by using an axial injection of the suspension [Tang '11].

A SPS YSZ columnar coating was deposited by spraying a diluted YSZ suspension (solid content was 5 wt.% instead of 20 wt.%; dynamic viscosity was 1.5 mPa.s at a shear rate of 10 s^{-1}), by employing a shorter spraying distance (50 mm instead of 65 mm) while increasing significantly the plasma gas flow (56.2 slpm Ar + 13.8 slpm He instead of 40 slpm Ar + 10 slpm He) and the robot velocity (1400 m/s instead of 700 m/s). These modified spraying parameters compared to those listed in Table 4 enable to deposit the new coating shown on Fig. 44. It can be observed that a columnar microstructure is evidenced, being comparable to the structure shown on Fig. 42. The coating was deposited on a NiCoCrAlY bondcoat. The monitoring of the substrate temperature during deposition turned out to be not reliable in these conditions due to the shorter spraying distance that hindered the measurement by the

pyrometer. Therefore, no reliable data on substrate temperature could be acquired for this experiment.

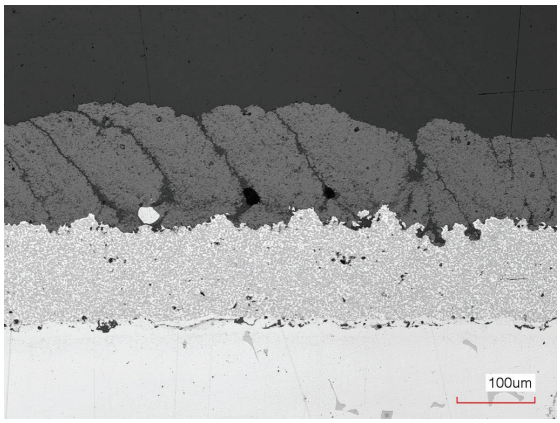

Fig. 44: Confocal laser microscope image of polished cross-section showing YSZ columnar microstructure obtained by SPS at atmospheric pressure with YSZ suspension having a lower solid content (5 wt.% instead of 20 wt.%), a shorter spraying distance (50 mm instead of 65 mm), an increased plasma gas flow (56.2 slpm Ar + 13.8 slpm He instead of 40 slpm Ar + 10 slpm He) and an increased robot velocity (1400 m/s instead of 700 m/s), (sample A-11-204-T2).

An analysis of the cross-section reveals that the positions of the columns coincide with the asperities at the bondcoat surface. This indicates that the deposition mechanisms of such coating involve interactions of the sprayed particles with the surface roughness. VanEvery et al. reported in their recent findings that this kind of microstructure is obtained when the plasma drag forces occurring very close to the substrate surface dominate the inertia of the arriving molten YSZ droplets and thus tend to modify strongly their angular directions, eventually leading to impacts on the sides of surface asperities [VanEvery '11]. Fig. 45 and Fig. 46 illustrate these deposition mechanisms.

In the case of the SPS-deposited coating shown on Fig. 44, the modified spraying parameters tend to particularly favor this type of deposition mechanism. The plasma flow conditions very close to the substrate surface play an important role. The plasma impinges on the surface, which acts here as a barrier to the plasma flow. Therefore the plasma jet is forced to turn along the surface and the plasma flow is redirected locally

from a normal direction to a direction parallel to the surface. This phenomenon generates drag forces that apply to the arriving molten YSZ droplets very close to the substrate surface. As indicated above, the modifications of the spraying parameters include a higher plasma gas flow of 70 slpm instead of the previous standard value of 50 slpm (56.2 slpm Ar + 13.8 slpm He instead of 40 slpm Ar + 10 slpm He). This tends to increase the drag forces from the impinging plasma close to the substrate surface. Besides, the shorter spraying distance that was applied (50 mm instead of 65 mm) tends to have a positive influence on the drag forces as well.

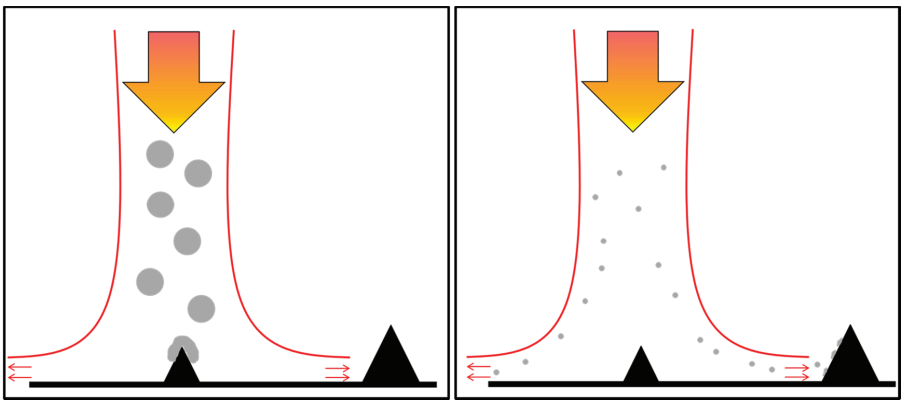

Fig. 45: Schematics illustrating the mechanisms where plasma drag forces dominate the inertia of small molten YSZ droplets, thus modifying strongly their angular directions (right), compared with the conventional mechanisms where large massive droplets with a high inertia follow a path normal to the substrate and impact without significant modification of their directions (left).

Fig. 46: Schematics illustrating the mechanisms for the deposition of columnar microstructure by interactions of splats with surface asperities [VanEvery '11].

The drag forces from the plasma impingement tend to modify the angular directions of the arriving molten YSZ droplets. The drag forces compete with the inertial forces of the droplets. Large massive droplets with a high inertia follow a path normal to the substrate and impact on the substrate without significant modification of their directions. On the other hand, small droplets with a low inertia are more sensitive to changes in the plasma flow and follow easily the plasma movements. Therefore, when arriving very close to the substrate where drag forces are dominant, their angular direction is redirected along the substrate surface. Their velocity component perpendicular to the substrate tends to be decreased while their velocity component parallel to the substrate is increased. As already reported by VanEvery et al., calculations made by Oberste-Berghaus et al. demonstrated the influence of the diameter of the YSZ molten droplets [Oberste-Berghaus '05]. It was shown that drag forces have already a slight deviation effect on 5-µm diameter droplets and that they strongly dominate inertial forces particularly for droplet diameters below approx. 2 µm. For such small droplets, the substrate parallel velocity component tends to dominate the substrate normal component and the droplets impact mostly on the sides of surface asperities.

In the present investigations, the diameters of the YSZ molten droplets arriving to the substrate surface were estimated by realizing spraying experiments into water and collecting the sprayed particles. SEM observations of these particles revealed their spherical shape. They correspond to the YSZ agglomerates that form upon evaporation of ethanol and subsequently melt during flight, thus forming spherical molten YSZ droplets. The results of this experiment were also presented in section 2.1.3 and were originally realized with a YSZ suspension having a 20 wt.% solid content. The diameters of the collected particles were estimated from a series of micrographs. Fig. 47 shows an example. Droplet diameters are in the range of 0.5-4 µm, with an average value being of approx. 2 µm. In the case of the SPS-deposited coating shown on Fig. 44, the modified spraying parameters include a lower solid content of the suspension (5 wt.% instead of 20 wt.%). Dynamic viscosity was approx. 1.5 mPa.s at a shear rate of 10 s^{-1}, therefore it can be assumed that the atomized droplets have a similar average diameter as with the standard 20 wt.% solid content (dynamic viscosity: 2.0 mPa.s). It is also assumed that the secondary fragmentation of the droplets by the plasma shear effects is similar. Since the suspension solid content is decreased by a factor 4, the average mass of zirconia

contained in each fragmented droplets is 4 times lower than with the standard conditions. Upon evaporation of ethanol, the YSZ agglomerates in each droplet are melted during flight to form spherical molten YSZ droplets with an average volume being also 4 times smaller than with the standard conditions and therefore an average diameter 1.6 times smaller, i.e. approx. 1.25 µm in average instead of 2.0 µm, as shown by calculation results on Fig. 48.

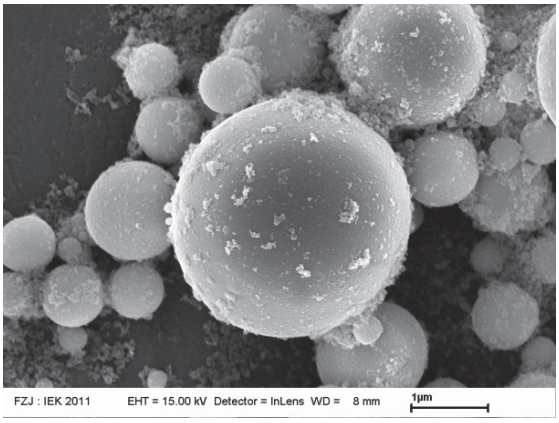

Fig. 47: SEM image showing typical diameters of the YSZ molten droplets that impact on the substrate. The diameters were estimated from a series of micrographs like this image and are in the range of 0.5-4 µm, with an average value being of approx. 2 µm. These spherical particles were collected by spraying into water (spraying distance = 500 mm; plasma current = 500 A; plasma gas composition = 40 slpm Ar + 10 slpm He; a specific funnel-shaped equipment was employed to collect the particles). They correspond to the YSZ agglomerates that form upon evaporation of ethanol and subsequently melt during flight, thus forming spherical molten YSZ droplets that impact on the substrate.

Therefore, the modified solid content used for the deposition of the coating shown in Fig. 44 favored the formation of smaller YSZ molten droplets and reduced their inertia. They are therefore more sensitive to the drag forces from the impinging plasma and their substrate parallel velocity component dominates their substrate normal component. As a result, in these specific conditions, the molten droplets impact mostly on the sides of surface asperities. Moreover, the higher plasma gas flow applied for this spraying experiment can tend to enhance the secondary fragmentation

of the entering suspension droplets by the plasma shear effects, leading to even smaller suspension droplets in the plasma jet and eventually to smaller agglomerates and smaller YSZ molten droplets impacting the substrate. Besides, their reduced diameter promotes their complete melting during flight in the plasma jet. This leads to a better sticking of the splats on the sides of surface asperities. A good sticking of the splats plays an important role in these coating deposition mechanisms since it guarantees that the asperities are not progressively smoothed by droplet impacts. Surface roughness plays also an important role. The surface asperity heights must be significantly larger than the average diameter of the YSZ molten droplets. It is considerably the case in the realized experiment shown on Fig. 44 since the bondcoat roughness was $R_a = 7.5$ µm and $R_t = 58.6$ µm. As a whole, this hypothesis on deposition mechanisms is supported by a given quantitative consistency with the findings of VanEvery et al.

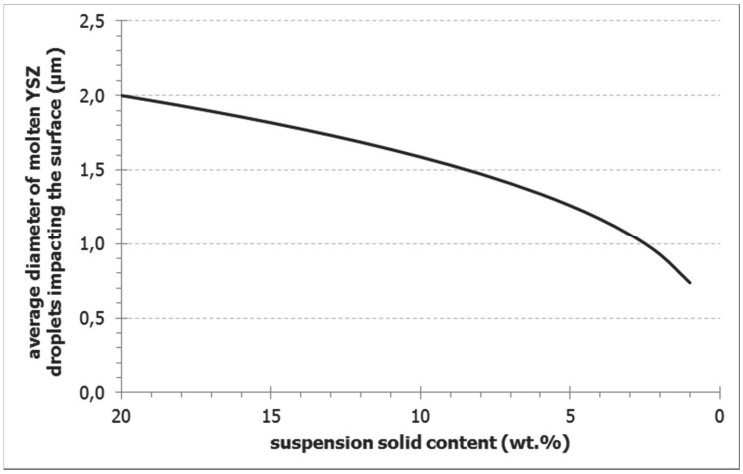

Fig. 48: Calculation results showing how a decrease in the suspension solid content influences the average diameter of the molten YSZ droplets impacting the substrate. A reference value of 2 µm was considered for 20 wt.% solid content from the observations illustrated on Fig. 47.

The splat depositions on the sides of surface asperities lead progressively to both lateral and vertical growth starting from each asperity. The spacing between two neighboring asperities tends to decrease until it forms a narrow gap. According to VanEvery et al. [VanEvery '11], the impinging plasma moving along the coating

surface ceases to flow between the two neighboring growing deposits when the interdeposit gap reaches a critical minimum width. Therefore, no more particles penetrate into this gap and lateral growth stop. Vertical growth continues, leading to columns separated by the interdeposit gaps. A complete coating is formed, featuring eventually a columnar structure as shown on Fig. 44.

4.1.7. Summary on SPS YSZ TBCs

The SPS YSZ TBCs presented in this section show benefits compared to APS deposited coatings, such as very fine porosity, high segmentation crack density and low Young's modulus. The segmentation cracks survive during thermal cycling test. These investigations showed that sintering occurs quickly during the first hours of exposure at 1400°C, leading to pore coarsening and stiffening of the coating. High Young's modulus is reached after 55 h of exposure. This may play a significant role in reducing the coating strain tolerance and promoting failure in thermal cycling operations. The advantages of the improved microstructure provided by SPS tend to be sensitive to very high temperatures (1400°C) when YSZ is chosen as coating material.

It was shown that SPS coatings contain a rather large fraction of unmolten clusters being detrimental to the coating mechanical stability. They stem from very fine particles that do not penetrate into the core of the plasma jet and are therefore located in the colder fringes of the plasma during flight. They do not reach the molten state and are embedded as unmolten clusters. It is thought also that their very small size tends to increase the sintering tendency of the coating. Therefore, the driving force for the improvement of the YSZ microstructure was the reduction of the total fraction of embedded unmolten clusters. The approach was to optimize the internal geometry of the atomization nozzle in order to generate a narrower angle of the cone-shaped suspension atomization, since droplets being atomized with a wide angle tend to penetrate into the colder plasma fringes and eventually lead to unmolten clusters. This optimization of the nozzle yielded coatings with a significantly reduced presence of the unmolten clusters. The positive effect of the new nozzle was demonstrated since unmolten clusters are reduced while total porosity and segmentation crack density are nearly kept constant. In an effort to test the potential performances of this new improved microstructure, thermal cycling tests were realized with this new coating. Although the number of cycles until failure was not improved, a more thorough comparison of the results was performed by analyzing TGO thicknesses and bondcoat temperatures. This showed that the new coatings were cycled with slightly higher bondcoat temperatures, thus yielding thicker TGOs and aluminum-depletion zones.

As a result, real performances are rather comparable with previous coatings. The significant improvement of the YSZ microstructure yielded by the optimized atomization nozzle was not reflected in TBC performances. This implies that other mechanisms might also play a role. It is also thought that the fraction of unmolten clusters might need to be further reduced to increase coating performances.

New developments were also carried out in order to achieve a YSZ coating with columnar structure. The driving force is to enable the manufacture of YSZ coatings having a microstructure similar to that obtained by LPPS-TF and inspired by that of EB-PVD while keeping the relatively low costs of plasma spray at atmospheric pressure conditions. Promising properties are related to this type of structure since intercolumnar voids can considerably comply with in-plane stresses during thermal cycling. A successful columnar YSZ coating was deposited by SPS with modified spraying parameters featuring a decreased suspension solid content, a shorter spraying distance and an increased plasma gas flow. Based on recent findings by VanEvery et al. [VanEvery '11], the deposition mechanisms of this type of structure were described. In given conditions, the plasma drag forces occurring very close to the substrate surface dominate the inertia of the arriving molten YSZ droplets and thus tend to modify strongly their angular directions, eventually leading to impacts on the sides of surface asperities. These deposits continue to grow starting from asperities. Lateral growth stops eventually and vertical growth goes on, leading to columns separated by narrow interdeposit gaps. It was demonstrated that the modified parameters that were used to manufacture the columnar coating tend to increase the impinging plasma drag forces and to decrease the average diameter of the arriving YSZ molten droplets and hence their inertia. The sticking of these droplets is also favored by these conditions. As a result, the modified spraying parameters promote significantly the deposition of such columnar structures that are very promising in terms of TBC performances and might yield better lifetimes in thermal cycling at surface temperature of 1400°C than the previously presented SPS YSZ coatings.

Since YSZ is known to present shortcomings at such temperatures, another valuable approach is to combine the microstructural benefits of SPS with new TBC materials such as zirconate pyrochlores which have lower sintering tendency than YSZ. This is the object of the following section.

4.2. Investigations on SPS TBCs with an alternative material: lanthanum zirconate

4.2.1. Motivation

In order to circumvent the limitations of YSZ at temperatures above 1200°C, investigations on new TBC materials are of particular interest in the thermal spray community. Among them, lanthanum zirconate ($La_2Zr_2O_7$, pyrochlore structure) is a promising ceramic material for TBCs [Vaßen '00]. It has attractive properties such as low thermal conductivity (1.56 $W.m^{-1}.K^{-1}$), high thermal stability and lower sintering tendency compared to YSZ. On the other hand, its low fracture toughness is a considerable weakness. Therefore it is better to apply it in a double-layer TBC system comprising a first layer of YSZ and a second layer of $La_2Zr_2O_7$ [Stöver '04, Stöver '11, Vaßen '04a, Vaßen '04c]. At stoichiometric composition, $La_2Zr_2O_7$ solidifies in its stable pyrochlore phase below its melting temperature of 2280°C, according to phase diagram. In plasma spraying operations, however, the metastable fluorite phase can be formed at high cooling rate upon deposition, when the composition is not stoichiometric. The defect fluorite phase is less ordered than the pyrochlore phase. It transforms to pyrochlore when heated above 1000°C, without volume change.

At atmospheric plasma spraying (APS) of $La_2Zr_2O_7$, the main issue is that this compound is prone to evaporation of lanthania (La_2O_3) in the plasma jet due its high vapor pressure, thus yielding non-stoichiometric coatings [Cao '01]. This is eventually detrimental for TBC performances since it leads eventually to the formation of unstabilized zirconia. Therefore, the evaporation of La_2O_3 needs to be prevented as much as possible during spraying in order to manufacture stoichiometric coatings to obtain the advantages of this material as TBC. Recent investigations at Forschungszentrum Jülich [Mauer '12a] on APS $La_2Zr_2O_7$ coatings sprayed with TriplexPro^{TM}-200 gun were carried out by applying different torch input power levels in order to attain different degrees of La_2O_3 evaporation and different levels of stoichiometry. At high power level (51 kW), the La_2O_3 content was 27.0 mol.%, thus showing a significant loss compared to the stoichiometric feedstock (33.3 mol.% La_2O_3). These investigations showed that the torch input power needs to be low to obtain stoichiometric coatings by APS. It appears that a maximum torch input power of about 22 kW is necessary to limit the La_2O_3 loss and obtaining a La_2O_3 content of

about 32.5 mol.% being still acceptable. However, such low power spraying conditions present also the disadvantage of increasing the fraction of unmolten material deposited in the coating, which is detrimental to coating mechanical properties.

4.2.2. SPS experimental series conducted for $La_2Zr_2O_7$ coatings

In order to improve these characteristics, $La_2Zr_2O_7$ coatings were sprayed by employing the SPS process. An experimental series was conducted by varying the plasma current in a large range from 200 A up to 500 A, thus yielding different torch input powers. The plasma gas composition was 40 slpm Ar and 10 slpm He and the spraying distance was 65 mm. Details on the ethanol-based $La_2Zr_2O_7$ feedstock suspension are given in section 3.1. Table 5 presents an overview of the conducted experimental series. Further details are given on Fig. 49 and Fig. 50 concerning the substrate temperature during deposition and the deposition rate respectively. Fig. 50 shows clearly how the deposition rate is strongly reduced for low plasma currents at 300 A and 250 A. This tends to show that a large fraction of the particles is unmolten upon impact at such low currents. The coating sprayed at 200 A provides an extreme case for which the deposition rate is extremely low thus showing that most of the particles probably consist of unmolten material leading to very poor deposition. On the other end of the experimental series, the deposition rate slightly drops for high plasma current at 450A and above. This might indicate that a given fraction of the sprayed particles are vaporized at such high currents or that splat fragmentation occurs at impact. Besides, an hypothesis would be that the substrate parallel velocity component of the particles dominates so strongly the substrate normal component when the particles approach very close to the substrate (due to the plasma drag forces related to the impingement of the plasma onto the surface) that a non-negligible fraction of the arriving particles “miss” the substrate.

Table 5: Overview of the experimental series conducted for $La_2Zr_2O_7$ coatings by SPS

Sample number	**plasma current (A)**	power (kW)	substrate temperature during deposition (°C)	deposition rate (µm/cycle)	photograph of coating
A-11-149-T2	**500**	56,6	440	15,4	
A-11-150-T2	**450**	48,4	438	16,7	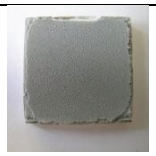
A-11-151-T2	**400**	41,0	383	17,9	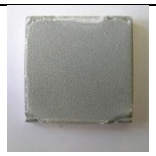
A-11-152-T2	**350**	34,3	324	17,6	
A-11-153-T2	**300**	27,8	290	15,9	
A-11-154-T2	**250**	22,1	258	12,3	
A-11-155-T2	**200**	16,9	154	3,2	

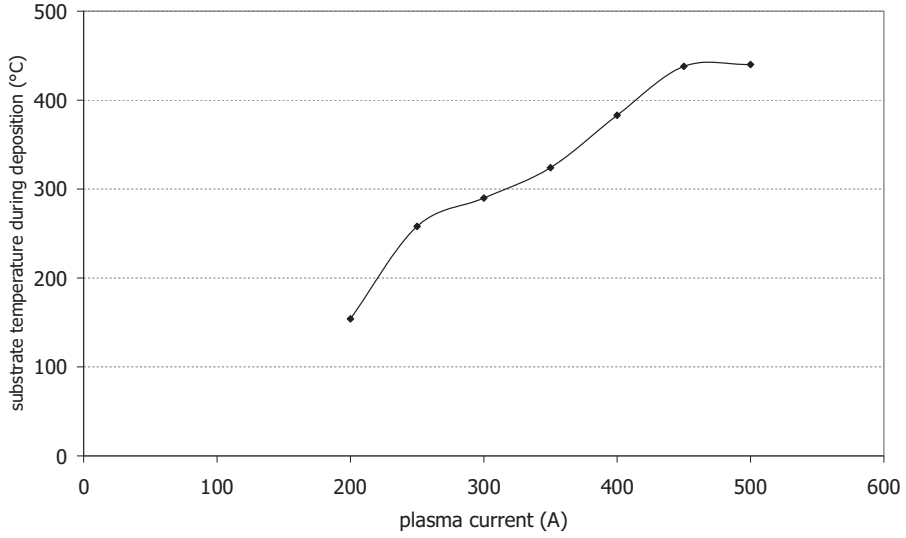

Fig. 49: Substrate temperature during deposition (measured by a pyrometer) vs. plasma current.

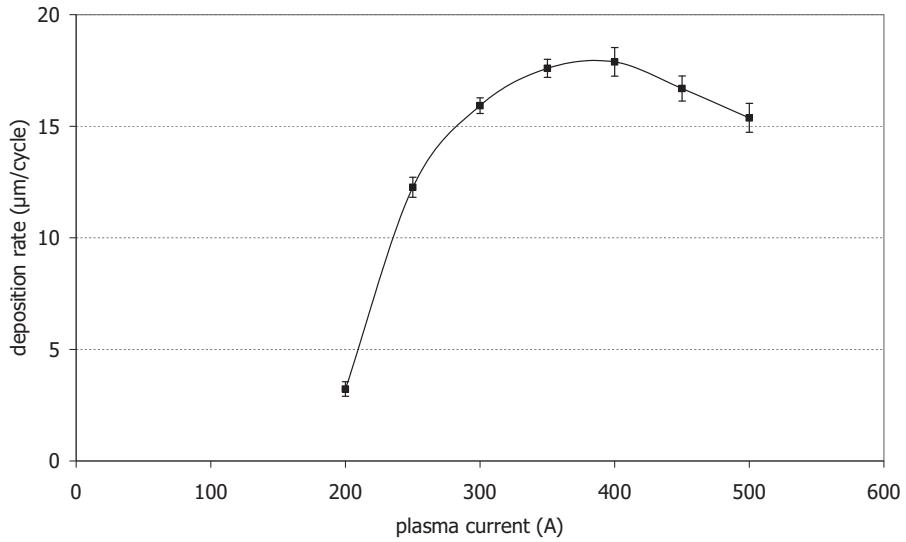

Fig. 50: Deposition rate vs. plasma current.

4.2.3. $La_2Zr_2O_7$ coatings microstructures

The microstructures of the deposited coatings are shown on Fig. 51 to Fig. 57 made by confocal laser microscope. One can see that coatings sprayed with low plasma currents feature a large fraction of a darker phase which is supposed to be unmolten or partly unmolten material. There is a clear trend for the amount of this unmolten material that increases strongly with decreasing plasma current. Coatings sprayed at 250 A and 200 A are constituted of a large fraction of this unmolten material. At 200 A it is observed that the deposition is quite poor leading to large irregularities in coating thickness. At 250 A, the coating is uniform in thickness but does not contain vertical segmentation cracks. Starting from 300 A and above, coatings contain less unmolten material and show interesting microstructures featuring vertical segmentation cracks. Moreover, one can see that the coatings tend to partly show a columnar structure with tree-like features. Some vertical segmentation cracks show a distinct propagation path that can be clearly identified. Some other vertical segmentation cracks might not be real cracks that occur within coating and propagate but rather inter-columnar gaps, i.e. voids between individual columns that grew vertically. At 500 A, the amount of unmolten material is strongly reduced and can hardly be seen on confocal laser microscope images. The columnar growth that is observed for coatings in the range 300 – 500 A is similar to the columnar YSZ microstructure presented in section 4.1.6. The same deposition mechanisms occur here as well for the $La_2Zr_2O_7$ coatings. It is thought that the low melting point of $La_2Zr_2O_7$ when compared to YSZ might promote further this type of deposition through a better sticking of the splats on the sides of surface asperities, which plays an important role in this deposition mechanism, as reported in section 4.1.6. This aspect is likely to counterbalance the high solid content of the $La_2Zr_2O_7$ suspension (20 wt.%) and its rather large primary particle size (reported in section 3.1).

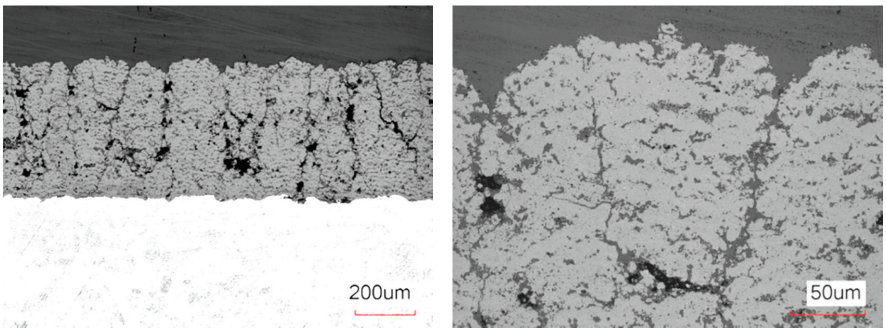

Fig. 51: Microstructure of coating A-11-149-T2 (500 A) (confocal laser microscope images).

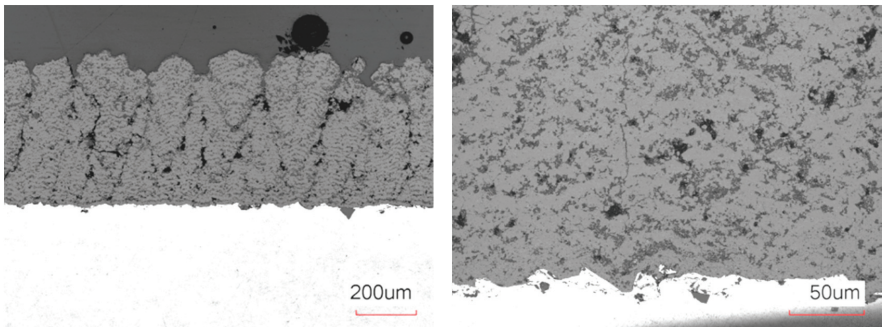

Fig. 52: Microstructure of coating A-11-150-T2 (450 A) (confocal laser microscope images).

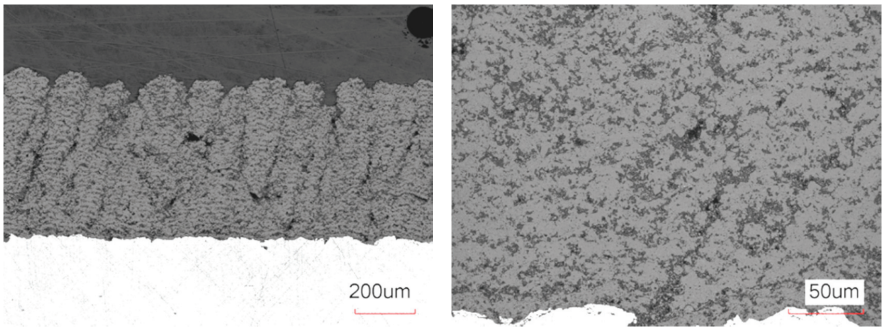

Fig. 53: Microstructure of coating A-11-151-T2 (400 A) (confocal laser microscope images).

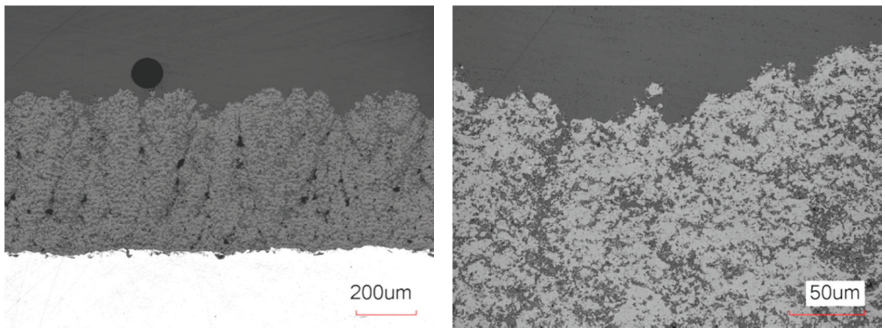

Fig. 54: Microstructure of coating A-11-152-T2 (350 A) (confocal laser microscope images).

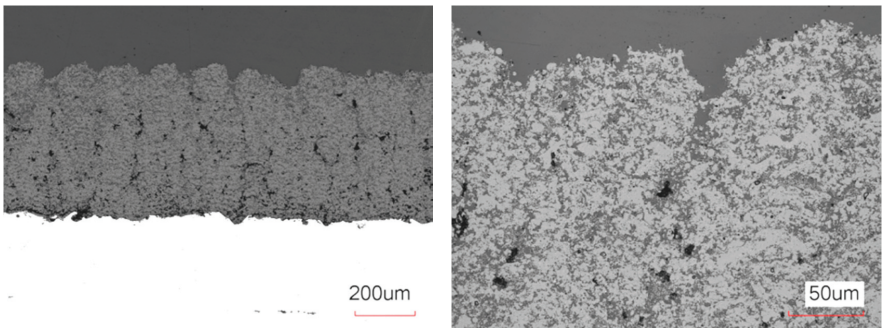

Fig. 55: Microstructure of coating A-11-153-T2 (300 A) (confocal laser microscope images).

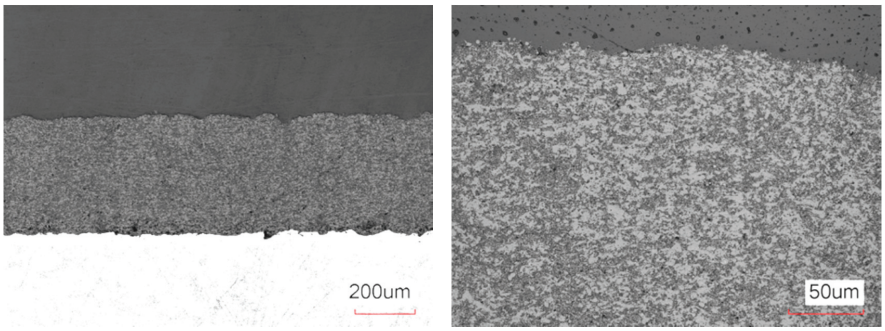

Fig. 56: Microstructure of coating A-11-154-T2 (250 A) (confocal laser microscope images).

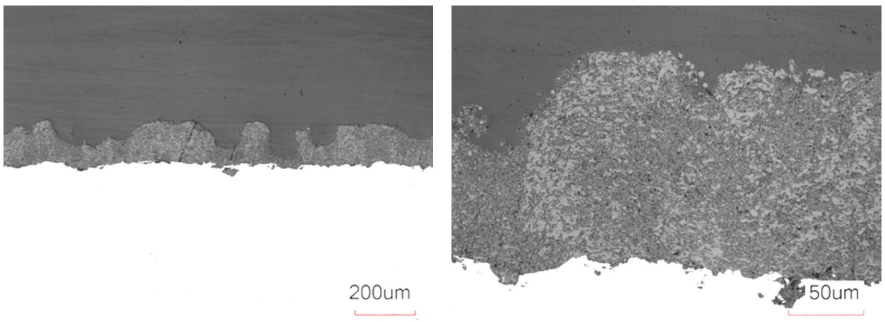

Fig. 57: Microstructure of coating A-11-155-T2 (200 A) (confocal laser microscope images).

These screening microstructural investigations by confocal laser microscopy are completed by SEM analyses in order to improve the characterization of these coatings. Polished cross-sections and top views of coating surface were investigated. Two samples considered as typical for the complete series were chosen for these further analyses: coating number A-11-149-T2 sprayed at 500 A (Fig. 58 and Fig. 59) and coating number A-11-154-T2 sprayed at 250 A (Fig. 60 and Fig. 61). The porous columnar structure obtained at 500 A is confirmed on Fig. 58 (left) and Fig. 59 (left). Especially the surface top view reveals a cauliflower-like coating surface where the tips of the vertical columns can be observed. On the other hand, the coating sprayed at 250 A is characterized by a rather smooth and uniform surface as it can be seen on Fig. 61 (left). Cross-section micrographs at higher magnification enable to demonstrate more precisely the degree of melting of the material constituting the coatings. On Fig. 58 (right), the coating sprayed at 500 A is constituted almost exclusively of well molten splats. Only very few re-solidified particles can be observed. On the contrary, Fig. 60 (right) shows that a large fraction of re-solidified particles are embedded in the coating sprayed at 250 A. These findings are confirmed by top view micrographs at high magnification where on the one hand molten flattened splats can be clearly observed on the surface in Fig. 59 (right) while on the other hand a large amount of small re-solidified particles are detected in Fig. 61 (right). Interestingly, the micrograph in Fig. 59 (right) shows also an inter-columnar gap seen from the top for the coating sprayed at 500 A.

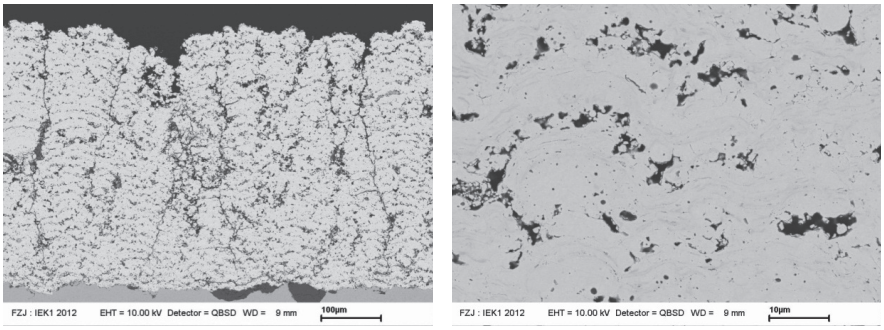

Fig. 58: SEM polished cross-section micrographs (BSE mode) of coating A-11-149-T2 (500 A).

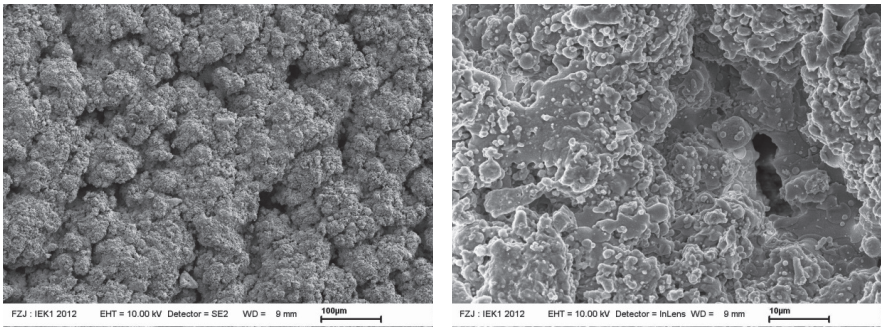

Fig. 59: SEM surface top view micrographs (SE mode) of coating A-11-149-T2 (500 A).

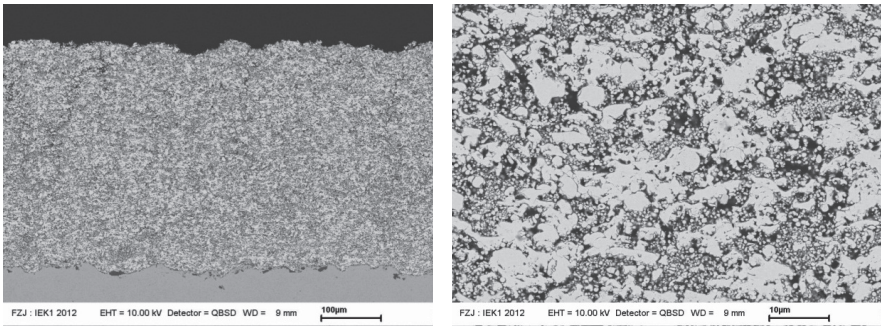

Fig. 60: SEM polished cross-section micrographs (BSE mode) of coating A-11-154-T2 (250 A).

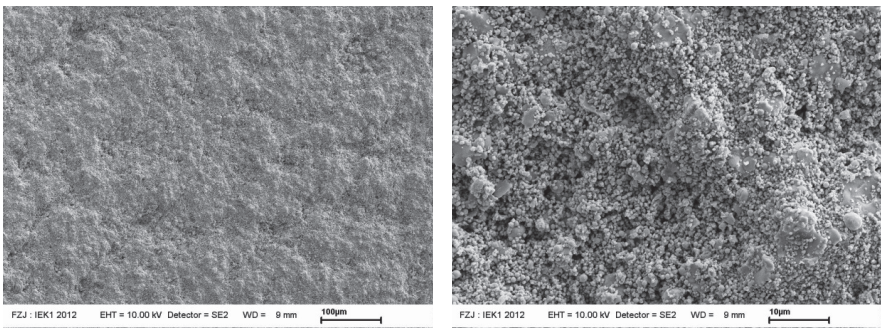

Fig. 61: SEM surface top view micrographs (SE mode) of coating A-11-154-T2 (250 A).

4.2.4. $La_2Zr_2O_7$ coatings stoichiometry

Chemical analysis yields results on lanthania contents for the coatings sprayed at 250, 350, 450 and 500 A (see Fig. 62). Lanthania content at low torch input power (22.1 kW, i.e. 250 A) already shows a slight drop (33.0 mol.%) compared to the stoichiometric suspension feedstock (33.3 mol.%). At 34.3 kW (350 A) lanthania content is still very acceptable with a value of 32.6 mol.%. This corresponds to a La/Zr atomic ratio of 0.97. This constitutes a remarkable result that is very promising for the manufacture of $La_2Zr_2O_7$ coatings being almost stoichiometric at relatively high torch input power, when compared with previous results obtained with APS [Mauer '12a]. The reasons for this advantage yielded by SPS over APS in limiting the lanthania evaporation during spraying might be related to the shorter spraying distance applied in the case of SPS (65 mm here). This leads to a reduced time of flight of the particles until impact on the substrate, which might limit the evaporation of lanthania. Besides, the presence of a liquid carrier at injection of the feedstock (ethanol here) might also retard the loss of lanthania. The ethanol is vaporized in the plasma jet upon injection of the suspension droplets, thus forming a vapor around $La_2Zr_2O_7$ particles that may play the role of a shroud gas until this vapor is consumed by combustion. The possibility to apply such level of torch input power enables at the same time to keep the fraction of unmolten material rather low in the deposited coating. This corresponds to the sample shown on Fig. 54 which exhibits a promising tree-like columnar structure. Coatings sprayed at higher torch input powers show

larger lanthania losses that are too significant to be acceptable in spite of constituting relative good results compared to APS coatings. The coating sprayed at torch input power of 34.3 kW (350 A) constitutes the most interesting result and these plasma parameters are expected to generate high TBC performances in burner rig tests at 1400°C when combined in a double-layer system with an APS or SPS-deposited YSZ coating exhibiting a good bonding and a high fracture toughness.

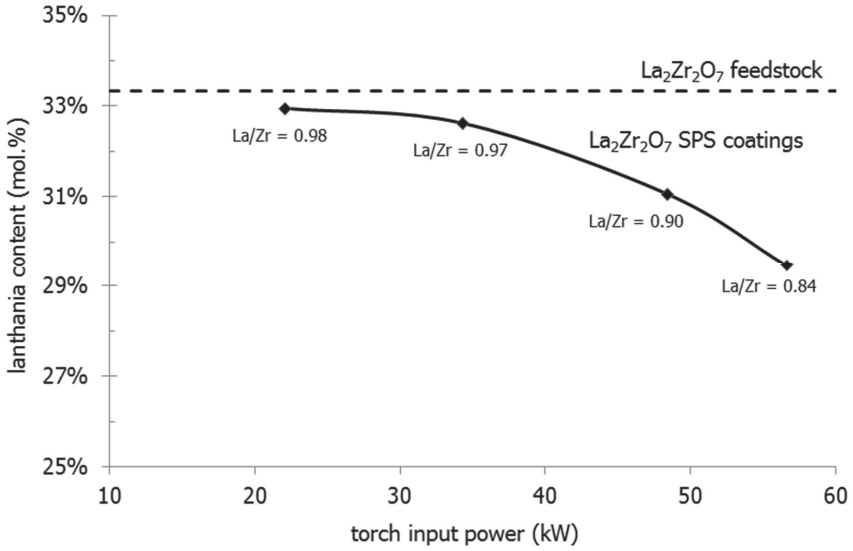

Fig. 62: Lanthania content in SPS coatings determined by chemical analysis vs. torch input power. The data points correspond to the plasma currents 250, 350, 450 and 500 A (see Table 5). La/Zr atomic ratios are also added.

4.2.5. $La_2Zr_2O_7$ coatings phase composition

All 7 coatings of the experimental series were investigated by X-ray diffraction. Only the extreme cases (coatings sprayed at 200 A and at 500 A) are presented below on Fig. 64 and Fig. 65 respectively, while the results for the feedstock suspension, being solely pyrochlore phase, can be seen on Fig. 63. One can see that both extreme coatings sprayed at 200 A and 500 A present the same peaks of the pyrochlore phase at nearly the same peak positions as the feedstock suspension. When a significant loss

of La_2O_3 by evaporation occurs in the case of APS, it is common to see that the peak positions are shifted due to a modification of the lattice parameters. This phenomenon occurs for non-stoichiometric coatings since the ionic radius of Zr^{4+} is smaller than that of La^{3+}. These considerations tend to indicate that the SPS coatings presented here have close-to-stoichiometric compositions since no such shifts of the peak positions are observed, thus confirming the results of the chemical analysis.

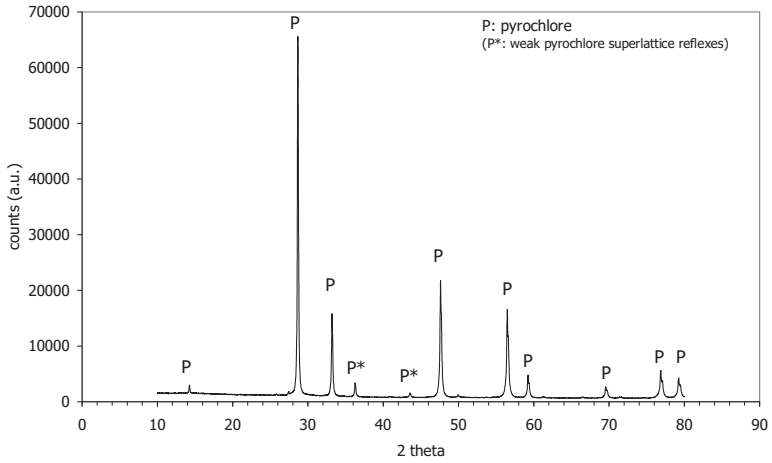

Fig. 63: Diffractogram of the $La_2Zr_2O_7$ feedstock suspension.

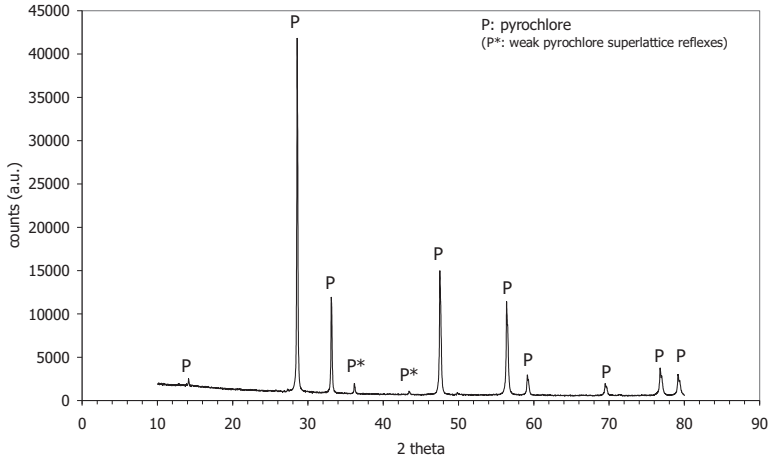

Fig. 64: Diffractogram of $La_2Zr_2O_7$ coating number A-11-155-T2 (200 A).

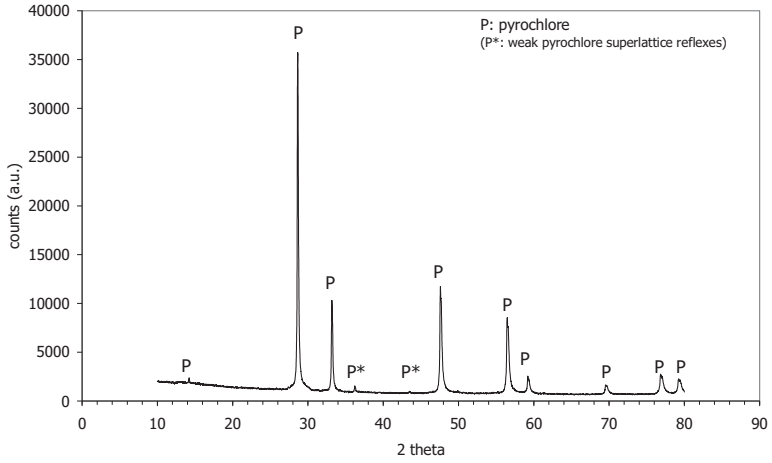

Fig. 65: Diffractogram of $La_2Zr_2O_7$ coating number A-11-149-T2 (500 A).

4.2.6. Summary on SPS $La_2Zr_2O_7$ coatings

Lanthanum zirconate ($La_2Zr_2O_7$), a promising new TBC material, was formulated in suspension to perform SPS experiments in a large experimental series with varying plasma currents. Results indicate that coatings sprayed at low currents contain a large amount of unmolten material, thus leading to lower deposition rates and poor microstructure. At high plasma currents, columnar microstructure is observed, which is promising for TBC performances.

Chemical analyses demonstrate that lanthania loss during spraying can be mostly prevented up to torch input power of about 34 kW (plasma current of about 350 A), thus yielding an almost stoichiometric coating, that still shows a remarkable columnar microstructure with low fraction of unmolten material. These promising results are thought to be related to the shorter spraying distance employed with SPS compared to APS and/or to the positive effect of the suspension solvent in the plasma plume.

4.3. Further application of the SPS process: manufacture of photoactive TiO_2 coatings

4.3.1. Motivation

Thanks to their photocatalytic effect, TiO_2 coatings represent an interesting area of investigation for a wide range of applications such as the destruction of organic compounds in polluted air and waste waters [Linsebigler '95], and also potentially for dye-sensitized solar cells [Vaßen '09d]. It is commonly accepted that a mixture of both anatase and rutile phases generates the highest photoactivity (typically 70-80% of anatase and 20-30% of rutile) [Berry '94, Nazeeruddin '93]. Besides, a high specific surface area is an important property to enhance the photoactivity.

Previous APS experiments with a fused and crushed powder (particle size in the range of 5-20 µm) generated a too dense microstructure and hence a low surface area [Mauer '12b]. Since this type of microstructure does not enhance the photoactivity, a valuable approach is to employ the SPS process with submicrometer-sized feedstock particles. The focus is especially on the possibility to fabricate coatings with a tree-like columnar microstructure in order to enhance the surface area. The suspension employed for the SPS experiments is presented in section 3.1.

4.3.2. SPS screening experimental series

First experiments were carried out to realize a screening in order to estimate the effect of the main process parameters on the microstructure and the phase composition. These experiments cover a large range of various deposition conditions. Varying parameters were plasma current (in the range 300-500 A) and spraying distance (in the range 65-95 mm). The plasma gas composition was kept constant to 40 slpm Ar + 10 slpm He. Substrate cooling was performed during spraying operations only at the front side. Table 6 presents the performed experiments and shows photographs of the coated samples. Fig. 66 shows an overview of the results of the screening experiments by presenting the microstructures and the anatase contents. It can be observed that a wide range of microstructures can be achieved from a very dense and smooth coating to tree-like columnar microstructures that exhibit a large surface area. The phase

compositions estimated by Rietveld analysis on XRD patterns of the deposited coatings span also over a large range from an almost exclusively anatase phase to an almost exclusively rutile phase. Coatings sprayed at low substrate temperatures are mostly constituted of anatase phase, thus showing no significant transformation compared with the suspension feedstock that is constituted of 99% of anatase. On the other hand, coatings sprayed at high substrate temperatures are mostly constituted of rutile phase.

Table 6: Overview of the screening experimental series consisting of 9 spray experiments with varying plasma currents and spraying distance

		Spraying distance		
		95 mm	80 mm	65 mm
Plasma current	300 A	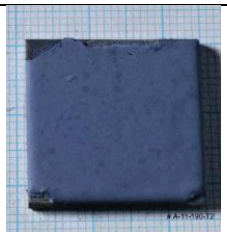 A-11-190-T2	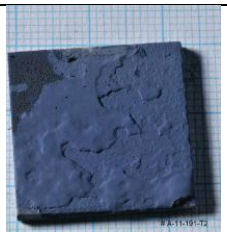 A-11-191-T2	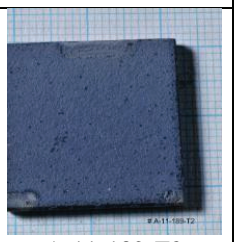 A-11-189-T2
	400 A	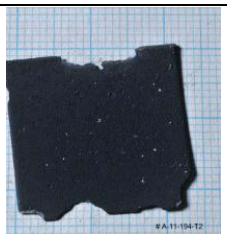 A-11-194-T2	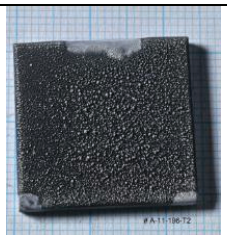 A-11-196-T2	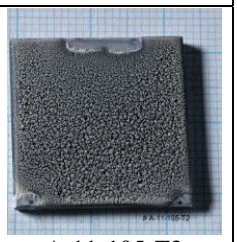 A-11-195-T2
	500 A	 A-11-188-T2	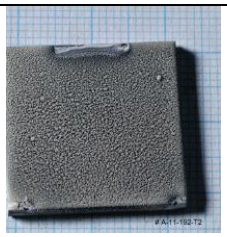 A-11-192-T2	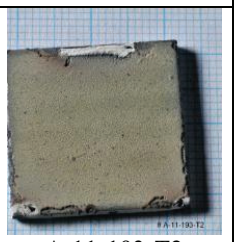 A-11-193-T2

These results demonstrate that the partial transformation from anatase to rutile can be controlled by adjusting plasma current and spray distance in order to obtain a specific phase composition. This potential to tailor the anatase content is particularly valuable with regard to enhanced photoactivities that are commonly obtained with an anatase content of about 70-80%.

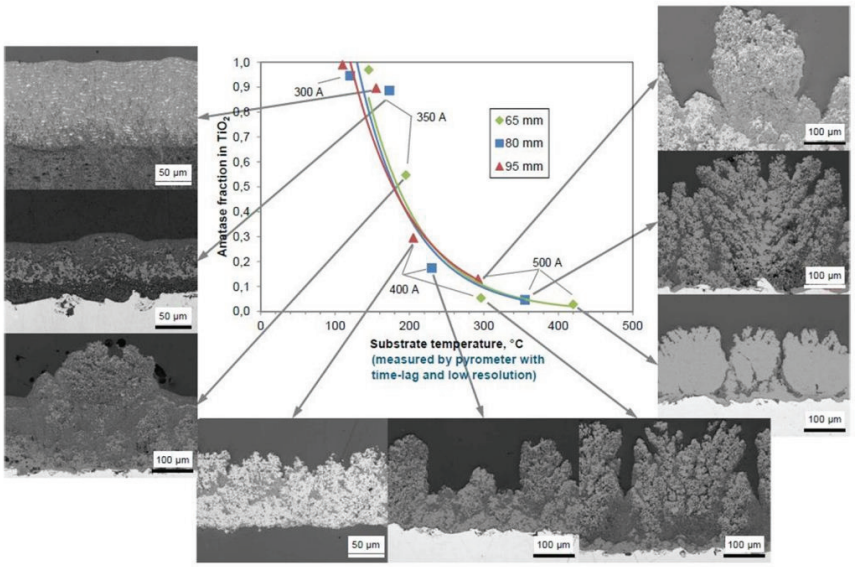

Fig. 66: Overview of the results of the screening experiments presenting the microstructures and the anatase contents (confocal laser microscope images).

4.3.3. Further microstructural investigations and phase analyses on coatings deposited with selected conditions

Based on the results of the screening experimental series, two different conditions were selected: cold deposition conditions on the one hand with a plasma current of 350 A and a spraying distance of 70 mm and hot deposition conditions on the other hand with a plasma current of 500 A and a spraying distance of 80 mm. A new set of coatings were manufactured with these parameters and SEM investigations were conducted. These microstructural analyses enable to estimate the degree of melting in the coating. Fig. 67 shows that the coating deposited with the cold conditions contains a large fraction of unmolten material (appearing as dark grey on the SEM images).

Fig. 68 (left) shows at higher magnification the very fine unmolten particles in the coating. It is observed that their sizes are similar to that of the primary particles contained in the suspension as shown on Fig. 68 (right). On the other hand, Fig. 69 shows that the coating deposited with the hot conditions is almost exclusively constituted of molten material. Anatase contents are 40% and 4% at the cold and hot conditions respectively.

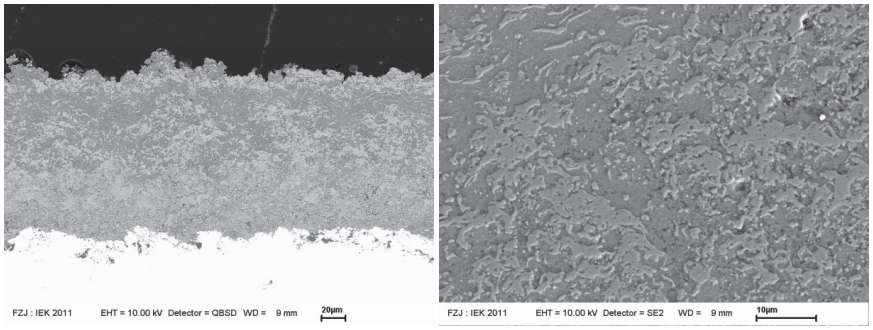

Fig. 67: SEM images of the coating deposited with the cold conditions (BSE mode at low magnification on the left; SE mode at high magnification on the right) (sample number A-11-260-T2).

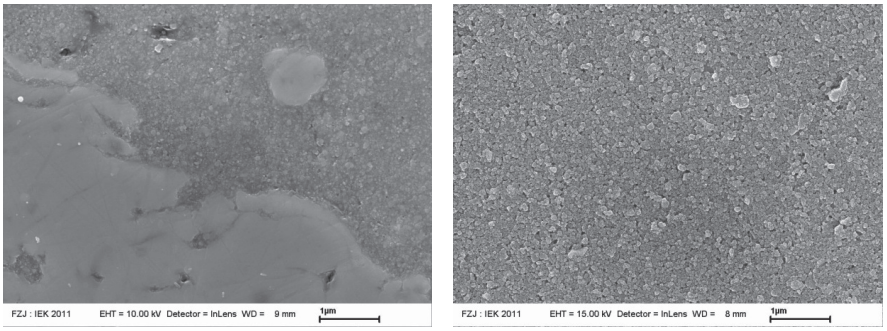

Fig. 68: SEM images (SE mode) of the coating deposited with the cold conditions showing at high magnification the very fine unmolten particles in the coating (sample number A-11-260-T2) (left) compared with the primary particles contained in the suspension (right).

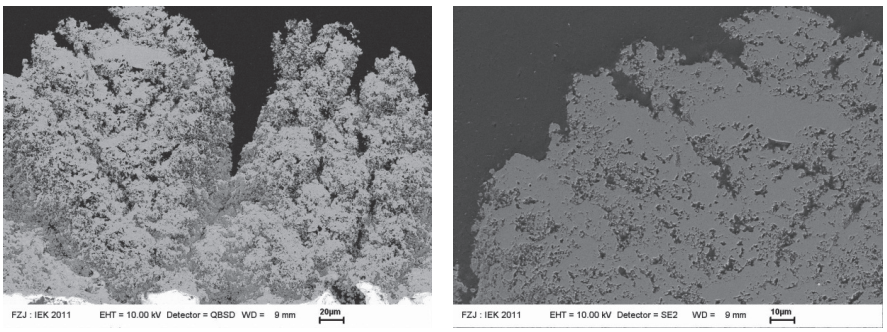

Fig. 69: SEM images of the coating deposited with the hot conditions (BSE mode at low magnification on the left; SE mode at high magnification on the right) (sample number A-11-258-T2).

4.3.4. Summary on SPS TiO_2 coatings

With regard to the photocatalytic application field, SPS experiments with TiO_2 suspension were performed. An experimental series provided a large range of coating microstructures. Porous coatings featuring tree-like columnar structures with large surface area can be achieved when employing hot spraying conditions. These findings can be related to the YSZ and $La_2Zr_2O_7$ columnar microstructures that are presented in sections 4.1.6 and 4.2 respectively. However, these hot spraying conditions tend to provide low anatase content. On the other hand, very high anatase contents are obtained at cold spraying conditions. This potential of the SPS process to manufacture coatings with tailored microstructures and phase compositions is particularly promising to generate TiO_2 coatings with enhanced photoactivity.

5. General summary

Submicrometer-structured YSZ TBCs deposited by SPS show several benefits compared to conventional APS coatings, such as very fine porosity, high segmentation crack density and low Young's modulus. Although segmentation cracks survive during thermal cycling at 1400°C, it was shown that the sintering tendency is high at such temperature exposure. An improvement of the SPS YSZ microstructure was realized by reducing significantly the fraction of unmolten clusters. This was enabled by an optimization of the suspension injection into the plasma jet. However, this improvement was not reflected in thermal cycling performances in burner rig tests. Further experimental investigations were conducted on SPS YSZ coatings with the aim of manufacturing columnar-structured coatings at atmospheric pressure conditions. Modified spraying parameters yielded such a columnar microstructure, which is related to interactions of the angular direction of the impinging particles with surface asperities of the substrate. This type of microstructure is promising for TBC applications since intercolumnar voids can comply with in-plane stresses during thermal cycling, similarly to EB-PVD deposited TBCs.

Lanthanum zirconate ($La_2Zr_2O_7$) is a promising material for TBCs showing higher thermal stability and lower sintering tendency than YSZ. The main issue when spraying $La_2Zr_2O_7$ is that it is prone to evaporation of La_2O_3, yielding non-stoichiometry being eventually detrimental to TBC lifetime. Experimental investigations showed that the SPS process enables to mostly prevent La_2O_3 loss up to torch input power of 34.3 kW, yielding at the same time a columnar microstructure being promising in terms of compliance for in-plane stresses. The advantage of SPS over APS in limiting La_2O_3 loss is thought to be related to the shorter spraying distance or to the positive effect of the solvent in the plasma plume.

TiO_2 coatings were manufactured by SPS with regard to photocatalytic applications. It was demonstrated that a large range of various microstructures can be deposited and that a specific phase composition can be tailored. Tree-like columnar structures obtained with hot spraying conditions are particularly attractive for their large surface area that promotes photoactivity. On the other hand, colder conditions are necessary

to yield anatase contents being sufficient for this field of applications. The potential of the SPS process to tailor both aspects is particularly promising.

6. References

Adams J.W., Ruh R., and Mazdiyasni K.S., Young's modulus, flexural strength, and fracture of yttria-stabilized zirconia versus temperature, *Journal of the American Ceramic Society*, 1997, **80**(4), p. 903-908

Ahrens M., Lampenscherf S., Vaßen R., and Stöver D., Sintering and creep processes in plasma-sprayed thermal barrier coatings, *Journal of Thermal Spray Technology*, 2004, **13**(3), p. 432-442

Bacciochini A., Montavon G., Ilavsky J., Denoirjean A., and Fauchais P., Porous architecture of SPS thick YSZ coatings structured at the nanometer scale (~50 nm), *Journal of Thermal Spray Technology*, 2010, **19**(1), p. 198-206

Ben-Ettouil F., Denoirjean A., Grimaud A., Montavon G., and Fauchais P., Sub-micrometer-sized Y-PSZ thermal barrier coatings manufactured by suspension plasma spraying: process, structure and some functional properties, *Thermal Spray 2009: Expanding Thermal Spray Performance to New Markets and Applications*, editors Marple B.R., Hyland M.M., Lau Y.-C., Li C.-J., Lima R.S., and Montavon G., May 4-7, 2009 (Las Vegas, Nevada, USA), ASM International, Materials Park, Ohio, USA, 2009, p. 193-199

Berry R.J., and Mueller M.R., Photocatalytic decomposition of crude oil slicks using TiO_2 on a floating substrate, *Microchemical Journal*, 1994, **50**(1), p. 28-32

Brousse E., Montavon G., Denoirjean A., Fauchais P., and Wittmann-Teneze K., Gastight yttria-partially stabilized zirconia layers manufactured by suspension plasma spraying for SOFC electrolyte functional layers, *Thermal Spray 2009: Expanding Thermal Spray Performance to New Markets and Applications*, editors Marple B.R., Hyland M.M., Lau Y.-C., Li C.-J., Lima R.S., and Montavon G., May 4-7, 2009 (Las Vegas, Nevada, USA), ASM International, Materials Park, Ohio, USA, 2009, p. 120-125

Cao X.Q., Vaßen R., Jungen W., Schwartz S., Tietz F., and Stöver D., Thermal stability of lanthanum zirconate plasma-sprayed coating, *Journal of the American Ceramic Society*, 2001, **84**(9), p. 2086-2090

Chen D., Jordan E.H., and Gell M., Microstructure of suspension plasma spray and air plasma spray Al_2O_3-ZrO_2 composite coatings, *Journal of Thermal Spray Technology*, 2009a, **18**(3), p. 421-426

Chen D., Jordan E.H., and Gell M., Suspension plasma sprayed composite coating using amorphous powder feedstock, *Applied Surface Science*, 2009b, **255**(11), p. 5935-5938

Chen D., Jordan E.H., Renfro M.W., and Gell M., Dy:YAG phosphor coating using the solution precursor plasma spray process, *Journal of the American Ceramic Society*, 2009c, **92**(1), p. 268-271

Chen D., Jordan E.H., Renfro M.W., and Gell M., Solution precursor plasma spray Eu: Y_2O_3 phosphor coating, *International Journal of Applied Ceramic Technology*, 2011, (in press, published online 21 October 2011, DOI: 10.1111/j.1744-7402.2011.00681.x)

Cipri F., Marra F., Pulci G., Tirillò J., Bartuli C., and Valente T., Plasma sprayed composite coatings obtained by liquid injection of secondary phases, *Surface and Coatings Technology*, 2009, **203**(15), p. 2116-2124

Clarke D.R., and Levi C.G., Materials design for the next generation thermal barrier coatings, *Annual Review of Materials Research*, 2003, **33**(1), p. 383-417

Clarke D.R., and Phillpot S.R., Thermal barrier coating materials, *Materials Today*, 2005, **8**(6), p. 22-29

Cotler E.M., Chen D., and Molz R.J., Pressure-based liquid feed system for suspension plasma spray coatings, *Journal of Thermal Spray Technology*, 2011, **20**(4), p. 967-973

d'Haese R., Pawlowski L., Bigan M., Jaworski R., and Martel M., Phase evolution of hydroxapatite coatings suspension plasma sprayed using variable parameters in simulated body fluid, *Surface and Coatings Technology*, 2010, **204**(8), p. 1236-1246

Darut G., Ben-Ettouil F., Denoirjean A., Montavon G., Ageorges H., and Fauchais P., Dry sliding behavior of sub-micrometer-sized suspension plasma sprayed ceramic oxide coatings, *Journal of Thermal Spray Technology*, 2010a, **19**(1-2), p. 275-285

Darut G., Valette S., Montavon G., Ageorges H., Denoirjean A., Fauchais P., Klyatskina E., Segova F., and Salvador M.D., Comparison of Al_2O_3 and Al_2O_3-TiO_2 coatings manufactured by aqueous and alcoholic suspension plasma spraying, *Thermal Spray 2010: Global Solutions for Future Applications*, editors Marple B.R., Agarwal A., Hyland M.M., Lau Y.-C., Li C.-J., Lima R.S., and Montavon G., May 3-5, 2010 (Singapore), DVS Media GmbH, Düsseldorf, Germany, 2010b, DVS-Berichte vol. 264, p. 197-202

Delbos C., Fazilleau J., Rat V., Coudert J.-F., Fauchais P., and Pateyron B., Phenomena involved in suspension plasma spraying part 2: zirconia particle treatment and coating formation, *Plasma Chemistry and Plasma Processing*, 2006, **26**(4), p. 393-414

Dorier J.-L., Hollenstein C., Barbezat G., and Refke A., Plasma spraying device and a method for introducing a liquid precursor into a plasma gas stream, U.S. Patent, US 8,001,927, issued 2011

Döring J.-E., Siegert R., Vaßen R., and Stöver D., Plasma spraying method, and device that is suitable therefor, International Patent Application, WO 2005/007921, issued 2005, in German

Erne M., Bach F.-W., Möhwald K., and Kolar D., Basic principles to obtain oxide ceramic coating systems with reduced sliding wear by suspension plasma spraying, *Thermal Spray 2009: Expanding Thermal Spray Performance to New Markets and Applications*, editors Marple B.R., Hyland M.M., Lau Y.-C., Li C.-J., Lima R.S., and Montavon G., May 4-7, 2009 (Las Vegas, Nevada, USA), ASM International, Materials Park, Ohio, USA, 2009, p. 200-206

Evans A.G., Mumm D.R., Hutchinson J.W., Meier G.H., and Pettit F.S., Mechanisms controlling the durability of thermal barrier coatings, *Progress in Materials Science*, 2001, **46**(5), p. 505-553

Fauchais P., and Vardelle A., Heat, mass and momentum transfer in coating formation by plasma spraying, *International Journal of Thermal Sciences*, 2000, **39**(9-11), p. 852-870

Fauchais P., Vardelle A., and Dussoubs B., Quo vadis thermal spraying?, *Journal of Thermal Spray Technology*, 2001, **10**(1), p. 44-66

Fauchais P., Coudert J.F., and Vardelle M., Diagnostics of plasma spray process and derived on-line control, *High Temperature Material Processes*, 2002, **6**(2), p. 247-265

Fauchais P., Understanding plasma spraying, *Journal of Physics D: Applied Physics*, 2004a, **37**(9), p. R86-R108

Fauchais P., Fukumoto M., Vardelle A., and Vardelle M., Knowledge concerning splat formation: an invited review, *Journal of Thermal Spray Technology*, 2004b, **13**(3), p. 337-360

Fauchais P., Etchart-Salas R., Rat V., Coudert J.-F., Caron N., and Wittmann-Ténèze K., Parameters controlling liquid plasma spraying: solutions, sols, or suspensions, *Journal of Thermal Spray Technology*, 2008a, **17**(1), p. 31-59

Fauchais P., Rat V., Coudert J.-F., Etchart-Salas R., and Montavon G., Operating parameters for suspension and solution plasma-spray coatings, *Surface and Coatings Technology*, 2008b, **202**(18), p. 4309-4317

Fauchais P., Montavon G., and Bertrand G., Influence of powders on thermal spray coating structures: recent developments in nano or finely structured coatings and some safety issues, *Thermal Spray 2009: Expanding Thermal Spray Performance to New Markets and Applications*, editors Marple B.R., Hyland M.M., Lau Y.-C., Li C.-J., Lima R.S., and Montavon G., May 4-7, 2009 (Las Vegas, Nevada, USA), ASM International, Materials Park, Ohio, USA, 2009, p. 799-817

Fauchais P., and Montavon G., Latest developments in suspension and liquid precursor thermal spraying, *Journal of Thermal Spray Technology*, 2010a, **19**(1-2), p. 226-239

Fauchais P., Montavon G., and Bertrand G., From powders to thermally sprayed coatings, *Journal of Thermal Spray Technology*, 2010b, **19**(1), p. 56-80

Fauchais P., Montavon G., Lima R.S., and Marple B.R., Engineering a new class of thermal spray nano-based microstructures from agglomerated nanostructured particles, suspensions and solutions: an invited review, *Journal of Physics D: Applied Physics*, 2011a, **44**(9), p. 093001

Fauchais P., and Vardelle A., Innovative and emerging processes in plasma spraying: from micro- to nano-structured coatings, *Journal of Physics D: Applied Physics*, 2011b, **44**(19), p. 194011

Fazilleau J., Delbos C., Rat V., Coudert J.-F., Fauchais P., and Pateyron B., Phenomena involved in suspension plasma spraying part 1: suspension injection and behavior, *Plasma Chemistry and Plasma Processing*, 2006, **26**(4), p. 371-391

Fengqiu T., Xiaoxian H., Yufeng Z., and Jingkun G., Effect of dispersants on surface chemical properties of nano-zirconia suspensions, *Ceramics International*, 2000, **26**(1), p. 93-97

Feuerstein A., Knapp J., Taylor T., Ashary A., Bolcavage A., and Hitchman N., Technical and economical aspects of current thermal barrier coating systems for gas turbine engines by thermal spray and EBPVD: a review, *Journal of Thermal Spray Technology*, 2008, **17**(2), p. 199-213

Gitzhofer F., Bouyer E., and Boulos M.I., Suspension plasma spray, U.S. Patent, US 5,609,921, issued 1997

Guignard A., Mauer G., Vaßen R., and Stöver D., Deposition and characteristics of submicrometer-structured thermal barrier coatings by suspension plasma spraying, *Journal of Thermal Spray Technology*, 2012, **21**(3-4), p. 416-424

Guo H.B., Kuroda S., and Murakami H., Microstructures and properties of plasma-sprayed segmented thermal barrier coatings, *Journal of the American Ceramic Society*, 2006, **89**(4), p. 1432-1439

Hospach A., Mauer G., Vaßen R., and Stöver D., Columnar-structured thermal barrier coatings (TBCs) by thin film low-pressure plasma spraying (LPPS-TF), *Journal of Thermal Spray Technology*, 2011, **20**(1-2), p. 116-120

Huang Y., Song L., Huang T., Liu X., Xiao Y., Wu Y., Wu F., and Gu Z., Characterization and formation mechanism of nano-structured hydroxyapatite coatings deposited by the liquid precursor plasma spraying process, *Biomedical Materials*, 2010, **5**(5), p. 054113

Ilavsky J., Characterization of complex thermal barrier deposits pore microstructures by a combination of imaging, scattering, and intrusion techniques, *Journal of Thermal Spray Technology*, 2010, **19**(1-2), p. 178-189

Jaworski R., Pierlot C., Pawlowski L., Bigan M., and Martel M., Design of the synthesis of fine HA powder for suspension plasma spraying, *Surface and Coatings Technology*, 2009, **203**(15), p. 2092-2097

Jaworski R., Pawlowski L., Pierlot C., Roudet F., Kozerski S., and Petit F., Recent developments in suspension plasma sprayed titanium oxide and hydroxyapatite coatings, *Journal of Thermal Spray Technology*, 2010, **19**(1-2), p. 240-247

Jia L., and Gitzhofer F., Induction plasma synthesis of nano-structured SOFCs electrolyte using solution and suspension plasma spraying: a comparative study, *Journal of Thermal Spray Technology*, 2010, **19**(3), p. 566-574

Karger M., Vaßen R., and Stöver D., Atmospheric plasma sprayed thermal barrier coatings with high segmentation crack densities: spraying process, microstructure and thermal cycling behavior, *Surface and Coatings Technology*, 2011, **206**(1), p. 16-23

Kaßner H., Siegert R., Hathiramani D., Vaßen R., and Stöver D., Application of suspension plasma spraying (SPS) for manufacture of ceramic coatings, *Journal of Thermal Spray Technology*, 2008a, **17**(1), p. 115-123

Kaßner H., Stuke A., Vaßen R., and Stöver D., Influence of microstructure on thermal and optical properties of suspension plasma sprayed (SPS) and atmospheric plasma sprayed (APS) coatings, *Thermal Spray 2008: Crossing Borders*, editor Lugscheider

E., June 2-4, 2008 (Maastricht, The Netherlands), Verlag für Schweißen und verwandte Verfahren DVS-Verlag GmbH, Düsseldorf, Germany, 2008b, p. 573-577

Kaßner H., Vaßen R., and Stöver D., Study on instant droplet and particle stages during suspension plasma spraying (SPS), *Surface and Coatings Technology*, 2008c, **202**(18), p. 4355-4361

Kaßner H., Theoretische und experimentelle Untersuchungen zum Plasmaspritzen mit nanoskaligen Suspensionen, Ph.D. thesis, Ruhr-Universität Bochum, Germany, 2009a, in German

Kaßner H., Stuke A., Rödig M., Vaßen R., and Stöver D., Influence of porosity on thermal conductivity and sintering in suspension plasma sprayed thermal barrier coatings, *Advanced Ceramic Coatings and Interfaces III: Ceramic Engineering and Science Proceedings*, editors Lin H.-T., and Zhu D., John Wiley & Sons, Inc., Hoboken, New Jersey, USA, 2009b, **29**(4), p. 147-158

Killinger A., Gadow R., Mauer G., Guignard A., Vaßen R., and Stöver D., Review of new developments in suspension and solution precursor thermal spray processes, *Journal of Thermal Spray Technology*, 2011, **20**(4), p. 677-695

Kitamura J., Tang Z., Mizuno H., Sato K., and Burgess A., Structural, mechanical and erosion properties of yttrium oxide coatings by axial suspension plasma spraying for electronics applications, *Journal of Thermal Spray Technology*, 2011, **20**(1-2), p. 170-185

Kozerski S., Pawlowski L., Jaworski R., Roudet F., and Petit F., Two zones microstructure of suspension plasma sprayed hydroxyapatite coatings, *Surface and Coatings Technology*, 2010a, **204**(9-10), p. 1380-1387

Kozerski S., Toma F.-L., Pawlowski L., Leupolt B., Latka L., and Berger L.-M., Suspension plasma sprayed TiO_2 coatings using different injectors and their photocatalytic properties, *Surface and Coatings Technology*, 2010b, **205**(4), p. 980-986

Kucuk A., Lima R.S., and Berndt C.C., Influence of plasma spray parameters on formation and morphology of ZrO_2-8 wt% Y_2O_3 deposits, *Journal of the American Ceramic Society*, 2001, **84**(4), p. 693-700

Łatka L., Pawlowski L., Chicot D., Pierlot C., and Petit F., Mechanical properties of suspension plasma sprayed hydroxyapatite coatings submitted to simulated body fluid, *Surface and Coatings Technology*, 2010, **205**(4), p. 954-960

Łatka L., Goryachev S.B., Kozerski S., Pawłowski L., and Lampke T., Buildup mechanisms of suspension plasma sprayed ZrO_2 + 8 wt. % Y_2O_3 coatings, *Thermal Spray 2011*, editors Marple B.R., Agarwal A., Hyland M.M., Lau Y.-C., Li C.-J., Lima R.S., and McDonald A., September 27-29, 2011 (Hamburg, Germany), DVS Media GmbH, Düsseldorf, Germany, 2011, DVS-Berichte vol. 276, p. 104-108

Linsebigler A.L., Lu G., and Yates Jr J.T., Photocatalysis on TiO_2 surfaces: principles, mechanisms, and selected results, *Chemical Reviews*, 1995, **95**(3), p. 735-758

Marchand C., Chazelas C., Mariaux G., and Vardelle A., Liquid precursor plasma spraying: modeling the interactions between the transient plasma jet and the droplets, *Thermal Spray 2007: Global Coating Solutions*, editors Marple B.R., Hyland M.M., Lau Y.-C., Li C.-J., Lima R.S., and Montavon G., May 14-16, 2007 (Beijing, China), ASM International, Materials Park, Ohio, USA, 2007, p. 196-201

Marchand O., Bertrand P., Mougin J., Comminges C., Planche M.-P., and Bertrand G., Characterization of suspension plasma-sprayed solid oxide fuel cell electrodes, *Surface and Coatings Technology*, 2010, **205**(4), p. 993-998

Marchand O., Girardot L., Planche M.-P., Bertrand P., Bailly Y., and Bertrand G., An insight into suspension plasma spray: injection of the suspension and its interaction with the plasma flow, *Journal of Thermal Spray Technology*, 2011, **20**(6), p. 1310-1320

Mauer G., Vaßen R., and Stöver D., Atmospheric plasma spraying of yttria-stabilized zirconia coatings with specific porosity, *Surface and Coatings Technology*, 2009, **204**(1-2), p. 172-179

Mauer G., Guignard A., Vaßen R., and Stöver D., Process diagnostics in suspension plasma spraying, *Surface and Coatings Technology*, 2010, **205**(4), p. 961-966

Mauer G., and Vaßen R., Current developments and challenges in thermal barrier coatings, *Surface Engineering*, 2011, **27**(7), p. 477-479

Mauer G., Sebold D., Vaßen R., and Stöver D., Improving atmospheric plasma spraying of zirconate thermal barrier coatings based on particle diagnostics, *Journal of Thermal Spray Technology*, 2012a, **21**(3-4), p. 363-371

Mauer G., Guignard A., and Vaßen R., Plasma spraying of efficient photoactive TiO_2 coatings, *Surface and Coatings Technology*, 2012b, to be published (under review)

Meier S.M., Gupta D.K., and Sheffler K.D., Ceramic thermal barrier coatings for commercial gas turbine engines, *JOM*, 1991, **43**(3), p. 50-53

Meillot E., Vert R., Caruyer C., Damiani D., and Vardelle M., Manufacturing nanostructured YSZ coatings by suspension plasma spraying (SPS): effect of injection parameters, *Journal of Physics D: Applied Physics*, 2011, **44**(19), p. 194008

Meyer A., Kaßner H., Vaßen R., Stöver D., and Marqués-Lopez J.-L., Thermal barrier coating system and method for the production thereof, U.S. Patent Application, US 2011/0244216, issued 2011

Michaux P., Montavon G., Grimaud A., Denoirjean A., and Fauchais P., Elaboration of porous NiO/8YSZ layers by several SPS and SPPS routes, *Journal of Thermal Spray Technology*, 2010, **19**(1-2), p. 317-327

Miller R.A., Current status of thermal barrier coatings - an overview, *Surface and Coatings Technology*, 1987, **30**(1), p. 1-11

Miller R.A., Thermal barrier coatings for aircraft engines: history and directions, *Journal of Thermal Spray Technology*, 1997, **6**(1), p. 35-42

Moign A., Vardelle A., Themelis N.J., and Legoux J.G., Life cycle assessment of using powder and liquid precursors in plasma spraying: the case of yttria-stabilized zirconia, *Surface and Coatings Technology*, 2010, **205**(2), p. 668-673

Montavon G., Ilavsky J., Denoirjean A., Fauchais P., Bacciochini A., and Wittmann-Teneze K., Ultra-small angle X-ray scattering (USAXS) in-situ quantification of void network evolution during annealing of nanometer-sized YSZ plasma-sprayed coatings, *Thermal Spray 2011*, editors Marple B.R., Agarwal A., Hyland M.M., Lau Y.-C., Li C.-J., Lima R.S., and McDonald A., September 27-29, 2011 (Hamburg, Germany), DVS Media GmbH, Düsseldorf, Germany, 2011, DVS-Berichte vol. 276, p. 451-456

Moroz N., Umapathy H., and Mohanty P., Synthesis and microstructure evolution of nano-titania doped silicon coatings, *Journal of Thermal Spray Technology*, 2010, **19**(1-2), p. 294-302

Nazeeruddin M.K., Kay A., Rodicio I., Humphry-Baker R., Müller E., Liska P., Vlachopoulos N., and Grätzel M., Conversion of light to electricity by cis-X_2bis(2,2′-bipyridyl-4,4′-dicarboxylate)ruthenium(II) charge-transfer sensitizers (X = Cl^-, Br^-, I^-, CN^-, and SCN^-) on nanocrystalline TiO_2 electrodes, *Journal of the American Chemical Society*, 1993, **115**(14), p. 6382-6390

Oberste-Berghaus J., Bouaricha S., Legoux J.-G., and Moreau C., Injection conditions and in-flight particle states in suspension plasma spraying of alumina and zirconia nano-ceramics, *Proceedings of the International Thermal Spray Conference*, editors Berndt C., and Lugscheider E., May 2-4, 2005 (Basel, Switzerland), ASM International, Materials Park, Ohio, USA, 2005

Oberste-Berghaus J., Bouaricha S., Legoux J.-G., Moreau C., and Harvey B., Method and apparatus for fine particle liquid suspension feed for thermal spray system and coatings formed therefrom, U.S. Patent Application, US 2006/0289405, issued 2006

Oliker V.E., Terent'ev A.E., Shvedova L.K., and Martsenyuk I.S., Use of aqueous suspensions in plasma spraying of alumina coatings, *Powder Metallurgy and Metal Ceramics*, 2009, **48**(1-2), p. 115-120

Padture N.P., Gell M., and Jordan E.H., Thermal barrier coatings for gas-turbine engine applications, *Science*, 2002, **296**(5566), p. 280-284

Pawlowski L., The science and engineering of thermal spray coatings, Wiley, Chichester, England, 1995

Pawlowski L., Finely grained nanometric and submicrometric coatings by thermal spraying: a review, *Surface and Coatings Technology*, 2008, **202**(18), p. 4318-4328

Pawlowski L., Suspension and solution thermal spray coatings, *Surface and Coatings Technology*, 2009, **203**(19), p. 2807-2829

Perepezko J.H., The hotter the engine, the better, *Science*, 2009, **326**(5956), p. 1068-1069

Podlesak H., Pawlowski L., D'Haese R., Laureyns J., Lampke T., and Bellayer S., Advanced microstructural study of suspension plasma sprayed hydroxyapatite coatings, *Journal of Thermal Spray Technology*, 2010, **19**(3), p. 657-664

Qiu C., and Chen Y., Manufacturing process of nanostructured alumina coatings by suspension plasma spraying, *Journal of Thermal Spray Technology*, 2009, **18**(2), p. 272-283

Rabiei A., and Evans A.G., Failure mechanisms associated with the thermally grown oxide in plasma-sprayed thermal barrier coatings, *Acta Materialia*, 2000, **48**(15), p. 3963-3976

Rampon R., Filiatre C., and Bertrand G., Suspension plasma spraying of YPSZ coatings: suspension atomization and injection, *Journal of Thermal Spray Technology*, 2008a, **17**(1), p. 105-114

Rampon R., Marchand O., Filiatre C., and Bertrand G., Influence of suspension characteristics on coatings microstructure obtained by suspension plasma spraying, *Surface and Coatings Technology*, 2008b, **202**(18), p. 4337-4342

Rosenzweig L.S., Ruud J.A., Leblanc L.S., Thomas P.M., and Smith S.S., Protective coating with high adhesion and articles made herewith, U.S. Patent Application, US 2009/0280298, issued 2009

Schulz U., and Schmücker M., Microstructure of ZrO_2 thermal barrier coatings applied by EB-PVD, *Materials Science and Engineering: A*, 2000, **276**(1-2), p. 1-8

Schulz U., Saruhan B., Fritscher K., and Leyens C., Review on advanced EB-PVD ceramic topcoats for TBC applications, *International Journal of Applied Ceramic Technology*, 2004, **1**(4), p. 302-315

Siegert R., Döring J.-E., Hansch R., Stöver D., and Vaßen R., Method for producing gas-tight layers and layer systems by means of thermal spraying, International Patent Application, WO 2006/128424, issued 2006, in German

Siegert R., Alfaro J.M.S., Hansch R., Vaßen R., Stöver D., Corma-Canós A., Garcia-Gómez H., and Atienzar-Corvillo P., Thermal spraying method using a colloidal suspension, International Patent Application, WO 2007/090707, issued 2007, in German

Siegert R., Latzel S., Hansch R., Stöver D., and Vaßen R., Production of a gas-tight, crystalline mullite layer by using a thermal spraying method, U.S. Patent Application, US 2008/0193674, issued 2008

Skoog A.J., Murphy J.A., and Tomlinson T.J., Method for applying a plasma sprayed coating using liquid injection, U.S. Patent Application, US 2006/0222777, issued 2006

Stecura S., Optimization of the Ni-Cr-Al-Y/ZrO_2-Y_2O_3 thermal barrier system, *Advanced Ceramic Materials*, 1986, **1**(1), p. 68–76

Stöver D., Pracht G., Lehmann H., Dietrich M., Döring J., and Vaßen R., New material concepts for the next generation of plasma-sprayed thermal barrier coatings, *Journal of Thermal Spray Technology*, 2004, **13**(1), p. 76-83

Stöver D., Guignard A., Jarligo M.O., Karger M., Mack D.E., Mauer G., Steinke T., and Vaßen R., New materials and processing concepts for high performance thermal barrier coatings, *International Gas Turbine Congress 2011*, November 13-18, 2011 (Osaka, Japan)

Strutt P.R., Kear B.H., and Boland R.F., Thermal spray method for the formation of nanostructured coatings, U.S. Patent, US 6,277,448, issued 2001

Strutt P.R., Kear B.H., and Boland R.F., Nanostructured feeds for thermal spray systems, method of manufacture, and coatings formed therefrom, U.S. Patent, US 6,579,573, issued 2003

Stuke A., Optimierung der Reflektivität keramischer Wärmedämmschichten aus Yttrium-teilstabilisiertem Zirkoniumdioxid für den Einsatz auf metallischen Komponenten in Gasturbinen, Ph.D. thesis, Ruhr-Universität Bochum, Germany, 2007, in German

Tang Z., Hartell P., Masindo G., Bogdanovic N., Yaroslavski I., Kim H., Restrepo J., Ellsworth D., and Burgess A., Duration and reliability of axial suspension plasma spray process, *Thermal Spray 2010: Global Solutions for Future Applications*, editors Marple B.R., Agarwal A., Hyland M.M., Lau Y.-C., Li C.-J., Lima R.S., and Montavon G., May 3-5, 2010 (Singapore), DVS Media GmbH, Düsseldorf, Germany, 2010, DVS-Berichte vol. 264, p. 203-206

Tang Z., Kim H., Yaroslavski I., Masindo G., Celler Z., and Ellsworth D., Novel thermal barrier coatings produced by axial suspension plasma spray, *Thermal Spray 2011*, editors Marple B.R., Agarwal A., Hyland M.M., Lau Y.-C., Li C.-J., Lima R.S., and McDonald A., September, 27-29, 2011 (Hamburg, Germany), DVS Media GmbH, Düsseldorf, Germany, 2011, DVS-Berichte vol. 276, p. 571-575

Tarasi F., Medraj M., Dolatabadi A., Oberste-Berghaus J., and Moreau C., Phase formation and transformation in alumina/YSZ nanocomposite coating deposited by suspension plasma spray process, *Journal of Thermal Spray Technology*, 2010, **19**(4), p. 787-795

Tingaud O., Bacciochini A., Montavon G., Denoirjean A., and Fauchais P., Suspension DC plasma spraying of thick finely-structured ceramic coatings: process manufacturing mechanisms, *Surface and Coatings Technology*, 2009, **203**(15), p. 2157-2161

Tingaud O., Bertrand P., and Bertrand G., Microstructure and tribological behavior of suspension plasma sprayed Al_2O_3 and Al_2O_3-YSZ composite coatings, *Surface and Coatings Technology*, 2010a, **205**(4), p. 1004-1008

Tingaud O., Montavon G., Denoirjean A., Coudert J.-F., Rat V., and Fauchais P., Al_2O_3-ZrO_2 finely structured multilayer architectures from suspension plasma spraying, *Journal of Thermal Spray Technology*, 2010b, **19**(1-2), p. 207-218

Toma F.-L., Berger L.-M., Jacquet D., Wicky D., Villaluenga I., de Miguel Y.R., and Lindeløv J.S., Comparative study on the photocatalytic behaviour of titanium oxide thermal sprayed coatings from powders and suspensions, *Surface and Coatings Technology*, 2009, **203**(15), p. 2150-2156

Toma F.-L., Berger L.-M., Stahr C.C., Naumann T., and Langner S., Microstructures and functional properties of suspension-sprayed Al_2O_3 and TiO_2 coatings: an overview, *Journal of Thermal Spray Technology*, 2010, **19**(1-2), p. 262-274

VanEvery K., Krane M., Trice R., Wang H., Porter W., Besser M., Sordelet D., Ilavsky J., and Almer J., Column formation in suspension plasma-sprayed coatings and resultant thermal properties, *Journal of Thermal Spray Technology*, 2011, **20**(4), p. 817-828

Vaßen R., Cao X., Tietz F., Basu D., and Stöver D., Zirconates as new materials for thermal barrier coatings, *Journal of the American Ceramic Society*, 2000, **83**(8), p. 2023-2028

Vaßen R., Entwicklung neuer oxidischer Wärmedämmschichten für Anwendungen in stationären und Flug-Gasturbinen, Habilitation thesis, Ruhr-Universität-Bochum, Germany, 2004a, in German

Vaßen R., Traeger F., and Stöver D., Correlation between spraying conditions and microcrack density and their influence on thermal cycling life of thermal barrier coatings, *Journal of Thermal Spray Technology*, 2004b, **13**(3), p. 396-404

Vaßen R., Traeger F., and Stöver D., New thermal barrier coatings based on pyrochlore/YSZ double-layer systems, *International Journal of Applied Ceramic Technology*, 2004c, **1**(4), p. 351-361

Vaßen R., Guo H.B., and Stöver D., Manufacture and properties of segmented thermal barrier coatings, *Ceramic Engineering and Science Proceedings*, 2005, **26**(3), p. 37-45

Vaßen R., Hathiramani D., and Stöver D., Method for the production of thin dense ceramic layers, U.S. Patent Application, US 2007/0259126, issued 2007

Vaßen R., Kaßner H., Stuke A., Hauler F., Hathiramani D., and Stöver D., Advanced thermal spray technologies for applications in energy systems, *Surface and Coatings Technology*, 2008, **202**(18), p. 4432-4437

Vaßen R., Giesen S., and Stöver D., Lifetime of plasma-sprayed thermal barrier coatings: comparison of numerical and experimental results, *Journal of Thermal Spray Technology*, 2009a, **18**(5), p. 835-845

Vaßen R., Hathiramani D., Buchkremer H.P., Tietz F., Döring J.-E., Siegert R., Traeger F., and Stöver D., Method for producing a layer system comprising a metallic carrier and an anode functional layer, U.S. Patent, US 7,582,374, issued 2009b

Vaßen R., Stuke A., and Stöver D., Recent developments in the field of thermal barrier coatings, *Journal of Thermal Spray Technology*, 2009c, **18**(2), p. 181-186

Vaßen R., Yi Z., Kaßner H., and Stöver D., Suspension plasma spraying of TiO_2 for the manufacture of photovoltaic cells, *Surface and Coatings Technology*, 2009d, **203**(15), p. 2146-2149

Vaßen R., Jarligo M.O., Steinke T., Mack D.E., and Stöver D., Overview on advanced thermal barrier coatings, *Surface and Coatings Technology*, 2010a, **205**(4), p. 938-942

Vaßen R., Kaßner H., Mauer G., and Stöver D., Suspension plasma spraying: process characteristics and applications, *Journal of Thermal Spray Technology*, 2010b, **19**(1-2), p. 219-225

Vert R., Chicot D., Dublanche-Tixier C., Meillot E., Vardelle A., and Mariaux G., Adhesion of YSZ suspension plasma-sprayed coating on smooth and thin substrates, *Surface and Coatings Technology*, 2010, **205**(4), p. 999-1003

Waldbillig D., and Kesler O., The effect of solids and dispersant loadings on the suspension viscosities and deposition rates of suspension plasma sprayed YSZ coatings, *Surface and Coatings Technology*, 2009, **203**(15), p. 2098-2101

Wang J., and Gao L., Adsorption of polyethylenimine on nanosized zirconia particles in aqueous suspensions, *Journal of Colloid and Interface Science*, 1999, **216**(2), p. 436-439

Wang X.-M., Li C.-X., Li C.-J., Tian L.-H., Song B., and Yang G.-J., Microstructure and electrochemical behavior of $Sm_{0.5}Sr_{0.5}CoO_3$ deposited by solution precursor plasma spraying, *Thermal Spray 2010: Global Solutions for Future Applications*, editors Marple B.R., Agarwal A., Hyland M.M., Lau Y.-C., Li C.-J., Lima R.S., and Montavon G., May 3-5, 2010 (Singapore), DVS Media GmbH, Düsseldorf, Germany, 2010a, DVS-Berichte vol. 264, p. 890-894

Wang Y., Legoux J.-G., Neagu R., Hui R., Maric R., and Marple B.R., Deposition of NiO/YSZ composite and YSZ by suspension plasma spray on porous metal, *Thermal Spray 2010: Global Solutions for Future Applications*, editors Marple B.R., Agarwal A., Hyland M.M., Lau Y.-C., Li C.-J., Lima R.S., and Montavon G., May 3-5, 2010 (Singapore), DVS Media GmbH, Düsseldorf, Germany, 2010b, DVS-Berichte vol. 264, p. 431-438

7. Acknowledgment

My gratitude goes to Prof. Dr. Robert Vaßen, who supervised my research work during these three years and gave me the opportunity of working in his group. I warmly thank Prof. Dr. Detlev Stöver for having followed the progress of my work and for having accepted to evaluate my thesis. I am grateful to Dr. Georg Mauer, who accompanied my investigations and was constantly interested in my results. I cordially thank Prof. Dr. Viktor Scherer, who accepted to be the president of the doctoral commission.

The experimental research I conducted would not have been possible without the support of many colleagues at the Institute for Energy and Climate Research, Materials Synthesis and Processing (IEK-1) at Forschungszentrum Jülich. I thank particularly Karl-Heinz Rauwald, Ralf Laufs and Frank Vondahlen for their support in thermal spray operations and in the manufacture of mechanical parts. Thank you to Dr. Doris Sebold for the numerous microscopical analyses, to Sigrid Schwartz-Lückge for several mercury porosimetry measurements and to Mark Kappertz for his assistance in metallographic preparations. My gratitude goes particularly to Dr. Maria Ophelia Jarligo and Svenja Ebert for their constant support on several aspects of the research and for being such kind office colleagues and friends.

I would like to thank Nicole Adels and Dr. Daniel Mack for their supervision of thermal cycling tests, Dr. Robert Mücke for his significant help in the measurements of elastic properties, Hiltrud Moitroux for the numerous photographs of coating specimens and the challenging photographs of the suspension atomization, Andrea Hilgers for particle size measurements, Dr. Nikolai Zotov for his support on questions related to lanthanum zirconate, Mirko Ziegner for X-ray diffraction analyses, Gerd Mattonet for his supervision of several mechanical manufacturing works, Volker Bader for his support on isothermal annealing, Michaela Andreas for the preparation of lanthanum zirconate feedstocks, and many other colleagues for their daily support during my work at Jülich. Thank you to Hannelore Rüther, Vicky Rostin and Stefan Weitz for their assistance in various administrative matters, and to Stefan Giesen and Rainer Kriescher for computer-related questions. I thank Dr. Holger Kaßner for his

previous achievements in this research topic. I am grateful to Zachary Hopkins and Vincent Dalbert, who provided a friendly and significant support for my laboratory work.

My activities at IEK-1 during these three years enabled me to meet many kind colleagues having diverse personalities and cultural backgrounds, and with whom I exchanged a lot. They all enriched this experience and a lot of them became friends. In this regard, I would like to thank additionally Dr. Janika Boltz, Joon-Yong Choi, Linnan Du, Andreas Franke, Florian Frey, Dr. Feng Han, Dr. Andreas Hospach, Bo-Ouk Hur, Jiyeon Kim, Dr. Vadym Kochubey, Felix Kunzelmann, Dr. Qianli Ma, Dr. Fernanda Marzano, Dr. Li Meng, Dr. Hyo-Jeong Moon, Prof. Daniel Mumm, Christian Nordhorn, Dr. Mitsutoshi Okada, Dr. Balasundaram Rajasekaran, Stefan Rezanka, Nadin Schlegel, Yaping Song, Magali Thomas-Desessarts, Emmanuel Vachon Lachance, Tobias Wegener, Cornelia Weiler, Dr. Ye Xing, Gengchen Yang and Dr. Yanfei Zhang. I am also grateful to all colleagues of IEK-1, who always contribute to the warm working atmosphere and with whom I was glad to work and to exchange.

I also had a great time taking part in further activities with the PhD students of Studium Universale. Special thanks go to my friends at Forschungszentrum Jülich who shared my daily life, shared theirs and are too many to be cited individually. I thank my family in France who supported me during my study and in my decision of going to Germany. I also thank my in-laws for their precious advice in many aspects. Finally, my deep gratitude goes to my wife Carole Babelot. Sharing our simultaneous experiences as doctoral candidates was priceless for both of us and I heartily thank Carole for her unconditional support and love for many years.

1. **Einsatz von multispektralen Satellitenbilddaten in der Wasserhaushalts- und Stoffstrommodellierung – dargestellt am Beispiel des Rureinzugsgebietes**
   von C. Montzka (2008), XX, 238 Seiten
   ISBN: 978-3-89336-508-1

2. **Ozone Production in the Atmosphere Simulation Chamber SAPHIR**
   by C. A. Richter (2008), XIV, 147 pages
   ISBN: 978-3-89336-513-5

3. **Entwicklung neuer Schutz- und Kontaktierungsschichten für Hochtemperatur-Brennstoffzellen**
   von T. Kiefer (2008), 138 Seiten
   ISBN: 978-3-89336-514-2

4. **Optimierung der Reflektivität keramischer Wärmedämmschichten aus Yttrium-teilstabilisiertem Zirkoniumdioxid für den Einsatz auf metallischen Komponenten in Gasturbinen**
   von A. Stuke (2008), X, 201 Seiten
   ISBN: 978-3-89336-515-9

5. **Lichtstreuende Oberflächen, Schichten und Schichtsysteme zur Verbesserung der Lichteinkopplung in Silizium-Dünnschichtsolarzellen**
   von M. Berginski (2008), XV, 171 Seiten
   ISBN: 978-3-89336-516-6

6. **Politikszenarien für den Klimaschutz IV – Szenarien bis 2030**
   hrsg.von P. Markewitz, F. Chr. Matthes (2008), 376 Seiten
   ISBN 978-3-89336-518-0

7. **Untersuchungen zum Verschmutzungsverhalten rheinischer Braunkohlen in Kohledampferzeugern**
   von A. Schlüter (2008), 164 Seiten
   ISBN 978-3-89336-524-1

8. **Inorganic Microporous Membranes for Gas Separation in Fossil Fuel Power Plants**
   by G. van der Donk (2008), VI, 120 pages
   ISBN: 978-3-89336-525-8

9. **Sinterung von Zirkoniumdioxid-Elektrolyten im Mehrlagenverbund der oxidkeramischen Brennstoffzelle (SOFC)**
   von R. Mücke (2008), VI, 165 Seiten
   ISBN: 978-3-89336-529-6

10. **Safety Considerations on Liquid Hydrogen**
    by K. Verfondern (2008), VIII, 167 pages
    ISBN: 978-3-89336-530-2

11. **Kerosinreformierung für Luftfahrtanwendungen**
von R. C. Samsun (2008), VII, 218 Seiten
ISBN: 978-3-89336-531-9

12. **Der 4. Deutsche Wasserstoff Congress 2008 – Tagungsband**
hrsg. von D. Stolten, B. Emonts, Th. Grube (2008), 269 Seiten
ISBN: 978-3-89336-533-3

13. **Organic matter in Late Devonian sediments as an indicator for environmental changes**
by M. Kloppisch (2008), XII, 188 pages
ISBN: 978-3-89336-534-0

14. **Entschwefelung von Mitteldestillaten für die Anwendung in mobilen Brennstoffzellen-Systemen**
von J. Latz (2008), XII, 215 Seiten
ISBN: 978-3-89336-535-7

15. **RED-IMPACT**
Impact of Partitioning, Transmutation and Waste Reduction Technologies on the Final Nuclear Waste Disposal
SYNTHESIS REPORT
ed. by W. von Lensa, R. Nabbi, M. Rossbach (2008), 178 pages
ISBN 978-3-89336-538-8

16. **Ferritic Steel Interconnectors and their Interactions with Ni Base Anodes in Solid Oxide Fuel Cells (SOFC)**
by J. H. Froitzheim (2008), 169 pages
ISBN: 978-3-89336-540-1

17. **Integrated Modelling of Nutrients in Selected River Basins of Turkey**
Results of a bilateral German-Turkish Research Project
project coord. M. Karpuzcu, F. Wendland (2008), XVI, 183 pages
ISBN: 978-3-89336-541-8

18. **Isotopengeochemische Studien zur klimatischen Ausprägung der Jüngeren Dryas in terrestrischen Archiven Eurasiens**
von J. Parplies (2008), XI, 155 Seiten, Anh.
ISBN: 978-3-89336-542-5

19. **Untersuchungen zur Klimavariabilität auf dem Tibetischen Plateau - Ein Beitrag auf der Basis stabiler Kohlenstoff- und Sauerstoffisotope in Jahrringen von Bäumen waldgrenznaher Standorte**
von J. Griessinger (2008), XIII, 172 Seiten
ISBN: 978-3-89336-544-9

20. **Neutron-Irradiation + Helium Hardening & Embrittlement Modeling of 9%Cr-Steels in an Engineering Perspective (HELENA)**
by R. Chaouadi (2008), VIII, 139 pages
ISBN: 978-3-89336-545-6

21. **in Bearbeitung**

22. **Verbundvorhaben APAWAGS (AOEV und Wassergenerierung) – Teilprojekt: Brennstoffreformierung – Schlussbericht**
von R. Peters, R. C. Samsun, J. Pasel, Z. Porš, D. Stolten (2008), VI, 106 Seiten
ISBN: 978-3-89336-547-0

23. **FREEVAL**
Evaluation of a Fire Radiative Power Product derived from Meteosat 8/9 and Identification of Operational User Needs
Final Report
project coord. M. Schultz, M. Wooster (2008), 139 pages
ISBN: 978-3-89336-549-4

24. **Untersuchungen zum Alkaliverhalten unter Oxycoal-Bedingungen**
von C. Weber (2008), VII, 143, XII Seiten
ISBN: 978-3-89336-551-7

25. **Grundlegende Untersuchungen zur Freisetzung von Spurstoffen, Heißgaschemie, Korrosionsbeständigkeit keramischer Werkstoffe und Alkalirückhaltung in der Druckkohlenstaubfeuerung**
von M. Müller (2008), 207 Seiten
ISBN: 978-3-89336-552-4

26. **Analytik von ozoninduzierten phenolischen Sekundärmetaboliten in *Nicotiana tabacum* L. cv Bel W3 mittels LC-MS**
von I. Koch (2008), III, V, 153 Seiten
ISBN 978-3-89336-553-1

27. **IEF-3 Report 2009. Grundlagenforschung für die Anwendung**
(2009), ca. 230 Seiten
ISBN: 978-3-89336-554-8

28. **Influence of Composition and Processing in the Oxidation Behavior of MCrAlY-Coatings for TBC Applications**
by J. Toscano (2009), 168 pages
ISBN: 978-3-89336-556-2

29. **Modellgestützte Analyse signifikanter Phosphorbelastungen in hessischen Oberflächengewässern aus diffusen und punktuellen Quellen**
von B. Tetzlaff (2009), 149 Seiten
ISBN: 978-3-89336-557-9

30. **Nickelreaktivlot / Oxidkeramik – Fügungen als elektrisch isolierende Dichtungskonzepte für Hochtemperatur-Brennstoffzellen-Stacks**
von S. Zügner (2009), 136 Seiten
ISBN: 978-3-89336-558-6

31. **Langzeitbeobachtung der Dosisbelastung der Bevölkerung in radioaktiv kontaminierten Gebieten Weißrusslands – Korma-Studie**
von H. Dederichs, J. Pillath, B. Heuel-Fabianek, P. Hill, R. Lennartz (2009), Getr. Pag.
ISBN: 978-3-89336-532-3

32. **Herstellung von Hochtemperatur-Brennstoffzellen über physikalische Gasphasenabscheidung**
von N. Jordán Escalona (2009), 148 Seiten
ISBN: 978-3-89336-532-3

33. **Real-time Digital Control of Plasma Position and Shape on the TEXTOR Tokamak**
by M. Mitri (2009), IV, 128 pages
ISBN: 978-3-89336-567-8

34. **Freisetzung und Einbindung von Alkalimetallverbindungen in kohlebefeuerten Kombikraftwerken**
von M. Müller (2009), 155 Seiten
ISBN: 978-3-89336-568-5

35. **Kosten von Brennstoffzellensystemen auf Massenbasis in Abhängigkeit von der Absatzmenge**
von J. Werhahn (2009), 242 Seiten
ISBN: 978-3-89336-569-2

36. **Einfluss von Reoxidationszyklen auf die Betriebsfestigkeit von anodengestützten Festoxid-Brennstoffzellen**
von M. Ettler (2009), 138 Seiten
ISBN: 978-3-89336-570-8

37. **Großflächige Plasmaabscheidung von mikrokristallinem Silizium für mikromorphe Dünnschichtsolarmodule**
von T. Kilper (2009), XVII, 154 Seiten
ISBN: 978-3-89336-572-2

38. **Generalized detailed balance theory of solar cells**
by T. Kirchartz (2009), IV, 198 pages
ISBN: 978-3-89336-573-9

39. **The Influence of the Dynamic Ergodic Divertor on the Radial Electric Field at the Tokamak TEXTOR**
von J. W. Coenen (2009), xii, 122, XXVI pages
ISBN: 978-3-89336-574-6

40. **Sicherheitstechnik im Wandel Nuklearer Systeme**
von K. Nünighoff (2009), viii, 215 Seiten
ISBN: 978-3-89336-578-4

41. **Pulvermetallurgie hochporöser NiTi-Legierungen für Implanat- und Dämpfungsanwendungen**
von M. Köhl (2009), XVII, 199 Seiten
ISBN: 978-3-89336-580-7

42. **Einfluss der Bondcoatzusammensetzung und Herstellungsparameter auf die Lebensdauer von Wärmedämmschichten bei zyklischer Temperaturbelastung**
von M. Subanovic (2009), 188, VI Seiten
ISBN: 978-3-89336-582-1

43. **Oxygen Permeation and Thermo-Chemical Stability of Oxygen Permeation Membrane Materials for the Oxyfuel Process**
by A. J. Ellett (2009), 176 pages
ISBN: 978-3-89336-581-4

44. **Korrosion von polykristallinem Aluminiumoxid (PCA) durch Metalljodidschmelzen sowie deren Benetzungseigenschaften**
von S. C. Fischer (2009), 148 Seiten
ISBN: 978-3-89336-584-5

45. **IEF-3 Report 2009. Basic Research for Applications**
(2009), 217 Seiten
ISBN: 978-3-89336-585-2

46. **Verbundvorhaben ELBASYS (Elektrische Basissysteme in einem CFK-Rumpf) - Teilprojekt: Brennstoffzellenabgase zur Tankinertisierung - Schlussbericht**
von R. Peters, J. Latz, J. Pasel, R. C. Samsun, D. Stolten
(2009), xi, 202 Seiten
ISBN: 978-3-89336-587-6

47. **Aging of ^{14}C-labeled Atrazine Residues in Soil: Location, Characterization and Biological Accessibility**
by N. D. Jablonowski (2009), IX, 104 pages
ISBN: 978-3-89336-588-3

48. **Entwicklung eines energetischen Sanierungsmodells für den europäischen Wohngebäudesektor unter dem Aspekt der Erstellung von Szenarien für Energie- und CO_2 - Einsparpotenziale bis 2030**
von P. Hansen (2009), XXII, 281 Seiten
ISBN: 978-3-89336-590-6

49. **Reduktion der Chromfreisetzung aus metallischen Interkonnektoren für Hochtemperaturbrennstofzellen durch Schutzschichtsysteme**
von R. Trebbels (2009), iii, 135 Seiten
ISBN: 978-3-89336-591-3

50. **Bruchmechanische Untersuchung von Metall / Keramik-Verbundsystemen für die Anwendung in der Hochtemperaturbrennstoffzelle**
von B. Kuhn (2009), 118 Seiten
ISBN: 978-3-89336-592-0

51. **Wasserstoff-Emissionen und ihre Auswirkungen auf den arktischen Ozonverlust**
Risikoanalyse einer globalen Wasserstoffwirtschaft
von T. Feck (2009), 180 Seiten
ISBN: 978-3-89336-593-7

52. **Development of a new Online Method for Compound Specific Measurements of Organic Aerosols**
by T. Hohaus (2009), 156 pages
ISBN: 978-3-89336-596-8

53. **Entwicklung einer FPGA basierten Ansteuerungselektronik für Justageeinheiten im Michelson Interferometer**
von H. Nöldgen (2009), 121 Seiten
ISBN: 978-3-89336-599-9

54. **Observation – and model – based study of the extratropical UT/LS**
by A. Kunz (2010), xii, 120, xii pages
ISBN: 978-3-89336-603-3

55. **Herstellung polykristalliner Szintillatoren für die Positronen-Emissions-Tomographie (PET)**
von S. K. Karim (2010), VIII, 154 Seiten
ISBN: 978-3-89336-610-1

56. **Kombination eines Gebäudekondensators mit H2-Rekombinatorelementen in Leichtwasserreaktoren**
von S. Kelm (2010), vii, 119 Seiten
ISBN: 978-3-89336-611-8

57. **Plant Leaf Motion Estimation Using A 5D Affine Optical Flow Model**
by T. Schuchert (2010), X, 143 pages
ISBN: 978-3-89336-613-2

58. **Tracer-tracer relations as a tool for research on polar ozone loss**
by R. Müller (2010), 116 pages
ISBN: 978-3-89336-614-9

59. **Sorption of polycyclic aromatic hydrocarbon (PAH) to Yangtze River sediments and their components**
by J. Zhang (2010), X, 109 pages
ISBN: 978-3-89336-616-3

60. **Weltweite Innovationen bei der Entwicklung von CCS-Technologien und Möglichkeiten der Nutzung und des Recyclings von CO_2**
Studie im Auftrag des BMWi
von W. Kuckshinrichs et al. (2010), X, 139 Seiten
ISBN: 978-3-89336-617-0

61. **Herstellung und Charakterisierung von sauerstoffionenleitenden Dünnschichtmembranstrukturen**
von M. Betz (2010), XII, 112 Seiten
ISBN: 978-3-89336-618-7

62. **Politikszenarien für den Klimaschutz V – auf dem Weg zum Strukturwandel, Treibhausgas-Emissionsszenarien bis zum Jahr 2030**
hrsg. von P. Hansen, F. Chr. Matthes (2010), 276 Seiten
ISBN: 978-3-89336-619-4

63. **Charakterisierung Biogener Sekundärer Organischer Aerosole mit Statistischen Methoden**
von C. Spindler (2010), iv, 163 Seiten
ISBN: 978-3-89336-622-4

64. **Stabile Algorithmen für die Magnetotomographie an Brennstoffzellen**
von M. Wannert (2010), ix, 119 Seiten
ISBN: 978-3-89336-623-1

65. **Sauerstofftransport und Degradationsverhalten von Hochtemperaturmembranen für CO2-freie Kraftwerke**
von D. Schlehuber (2010), VII, 139 Seiten
ISBN: 978-3-89336-630-9

66. **Entwicklung und Herstellung von foliengegossenen, anodengestützten Festoxidbrennstoffzellen**
von W. Schafbauer (2010), VI, 164 Seiten
ISBN: 978-3-89336-631-6

67. **Disposal strategy of proton irradiated mercury from high power spallation sources**
by S. Chiriki (2010), xiv, 124 pages
ISBN: 978-3-89336-632-3

68. **Oxides with polyatomic anions considered as new electrolyte materials for solid oxide fuel cells (SOFCs)**
by O. H. Bin Hassan (2010), vii, 121 pages
ISBN: 978-3-89336-633-0

69. **Von der Komponente zum Stack: Entwicklung und Auslegung von HT-PEFC-Stacks der 5 kW-Klasse**
von A. Bendzulla (2010), IX, 203 Seiten
ISBN: 978-3-89336-634-7

70. **Satellitengestützte Schwerewellenmessungen in der Atmosphäre und Perspektiven einer zukünftigen ESA Mission (PREMIER)**
von S. Höfer (2010), 81 Seiten
ISBN: 978-3-89336-637-8

71. **Untersuchungen der Verhältnisse stabiler Kohlenstoffisotope in atmosphärisch relevanten VOC in Simulations- und Feldexperimenten**
von H. Spahn (2010), IV, 210 Seiten
ISBN: 978-3-89336-638-5

72. **Entwicklung und Charakterisierung eines metallischen Substrats für nanostrukturierte keramische Gastrennmembranen**
von K. Brands (2010), vii, 137 Seiten
ISBN: 978-3-89336-640-8

73. **Hybridisierung und Regelung eines mobilen Direktmethanol-Brennstoffzellen-Systems**
von J. Chr. Wilhelm (2010), 220 Seiten
ISBN: 978-3-89336-642-2

74. **Charakterisierung perowskitischer Hochtemperaturmembranen zur Sauerstoffbereitstellung für fossil gefeuerte Kraftwerksprozesse**
von S.A. Möbius (2010) III, 208 Seiten
ISBN: 978-3-89336-643-9

75. **Characterization of natural porous media by NMR and MRI techniques: High and low magnetic field studies for estimation of hydraulic properties**
by L.-R. Stingaciu (2010), 96 pages
ISBN: 978-3-89336-645-3

76. **Hydrological Characterization of a Forest Soil Using Electrical Resistivity Tomography**
by Chr. Oberdörster (2010), XXI, 151 pages
ISBN: 978-3-89336-647-7

77. **Ableitung von atomarem Sauerstoff und Wasserstoff aus Satellitendaten und deren Abhängigkeit vom solaren Zyklus**
von C. Lehmann (2010), 127 Seiten
ISBN: 978-3-89336-649-1

78. **18th World Hydrogen Energy Conference 2010 – WHEC2010 Proceedings**
Speeches and Plenary Talks
ed. by D. Stolten, B. Emonts (2012)
ISBN: 978-3-89336-658-3

78-1. **18th World Hydrogen Energy Conference 2010 – WHEC2010 Proceedings**
Parallel Sessions Book 1:
Fuel Cell Basics / Fuel Infrastructures
ed. by D. Stolten, T. Grube (2010), ca. 460 pages
ISBN: 978-3-89336-651-4

78-2. **18th World Hydrogen Energy Conference 2010 – WHEC2010 Proceedings**
Parallel Sessions Book 2:
Hydrogen Production Technologies – Part 1
ed. by D. Stolten, T. Grube (2010), ca. 400 pages
ISBN: 978-3-89336-652-1

78-3. **18th World Hydrogen Energy Conference 2010 – WHEC2010 Proceedings**
Parallel Sessions Book 3:
Hydrogen Production Technologies – Part 2
ed. by D. Stolten, T. Grube (2010), ca. 640 pages
ISBN: 978-3-89336-653-8

78-4. **18th World Hydrogen Energy Conference 2010 – WHEC2010 Proceedings**
Parallel Sessions Book 4:
Storage Systems / Policy Perspectives, Initiatives and Cooperations
ed. by D. Stolten, T. Grube (2010), ca. 500 pages
ISBN: 978-3-89336-654-5

78-5. **18th World Hydrogen Energy Conference 2010 – WHEC2010 Proceedings**
Parallel Sessions Book 5:
Stategic Analysis / Safety Issues / Existing and Emerging Markets
ed. by D. Stolten, T. Grube (2010), ca. 530 pages
ISBN: 978-3-89336-655-2

78-6. **18th World Hydrogen Energy Conference 2010 – WHEC2010 Proceedings**
Parallel Sessions Book 6:
Stationary Applications / Transportation Applications
ed. by D. Stolten, T. Grube (2010), ca. 330 pages
ISBN: 978-3-89336-656-9

78 Set (complete book series)

18th World Hydrogen Energy Conference 2010 – WHEC2010 Proceedings
ed. by D. Stolten, T. Grube, B. Emonts (2010)
ISBN: 978-3-89336-657-6

79. **Ultrafast voltex core dynamics investigated by finite-element micromagnetic simulations**
by S. Gliga (2010), vi, 144 pages
ISBN: 978-3-89336-660-6

80. **Herstellung und Charakterisierung von keramik- und metallgestützten Membranschichten für die CO_2-Abtrennung in fossilen Kraftwerken**
von F. Hauler (2010), XVIII, 178 Seiten
ISBN: 978-3-89336-662-0

81. **Experiments and numerical studies on transport of sulfadiazine in soil columns**
by M. Unold (2010), xvi, 115 pages
ISBN: 978-3-89336-663-7

82. **Prompt-Gamma-Neutronen-Aktivierungs-Analyse zur zerstörungsfreien Charakterisierung radioaktiver Abfälle**
von J.P.H. Kettler (2010), iv, 205 Seiten
ISBN: 978-3-89336-665-1

83. **Transportparameter dünner geträgerter Kathodenschichten der oxidkeramischen Brennstoffzelle**
von C. Wedershoven (2010), vi, 137 Seiten
ISBN: 978-3-89336-666-8

84. **Charakterisierung der Quellverteilung von Feinstaub und Stickoxiden in ländlichem und städtischem Gebiet**
von S. Urban (2010), vi, 211 Seiten
ISBN: 978-3-89336-669-9

85. **Optics of Nanostructured Thin-Film Silicon Solar Cells**
by C. Haase (2010), 150 pages
ISBN: 978-3-89336-671-2

86. **Entwicklung einer Isolationsschicht für einen Leichtbau-SOFC-Stack**
von R. Berhane (2010), X, 162 Seiten
ISBN: 978-3-89336-672-9

87. **Hydrogen recycling and transport in the helical divertor of TEXTOR**
by M. Clever (2010), x, 172 pages
ISBN: 978-3-89336-673-6

88. **Räumlich differenzierte Quantifizierung der N- und P-Einträge in Grundwasser und Oberflächengewässer in Nordrhein-Westfalen unter besonderer Berücksichtigung diffuser landwirtschaftlicher Quellen**
von F. Wendland et. al. (2010), xii, 216 Seiten
ISBN: 978-3-89336-674-3

89. **Oxidationskinetik innovativer Kohlenstoffmaterialien hinsichtlich schwerer Lufteinbruchstörfälle in HTR´s und Graphitentsorgung oder Aufarbeitung**
von B. Schlögl (2010), ix, 117 Seiten
ISBN: 978-3-89336-676-7

90. **Chemische Heißgasreinigung bei Biomassenvergasungsprozessen**
von M. Stemmler (2010), xv, 196 Seiten
ISBN: 978-3-89336-678-1

91. **Untersuchung und Optimierung der Serienverschaltung von Silizium-Dünnschicht-Solarmodulen**
von S. Haas (2010), ii, 202 Seiten
ISBN: 978-3-89336-680-4

92. **Non-invasive monitoring of water and solute fluxes in a cropped soil**
by S. Garré (2010), xxiv, 133 pages
ISBN: 978-3-89336-681-1

93. **Improved hydrogen sorption kinetics in wet ball milled Mg hydrides**
by L. Meng (2011), II, 119 pages
ISBN: 978-3-89336-687-3

94. **Materials for Advanced Power Engineering 2010**
ed. by J. Lecomte-Beckers, Q. Contrepois, T. Beck and B. Kuhn
(2010), 1327 pages
ISBN: 978-3-89336-685-9

95. **2D cross-hole MMR – Survey design and sensitivity analysis for cross-hole applications of the magnetometric resistivity**
by D. Fielitz (2011), xvi, 123 pages
ISBN: 978-3-89336-689-7

96. **Untersuchungen zur Oberflächenspannung von Kohleschlacken unter Vergasungsbedingungen**
von T. Melchior (2011), xvii, 270 Seiten
ISBN: 978-3-89336-690-3

97. **Secondary Organic Aerosols: Chemical Aging, Hygroscopicity, and Cloud Droplet Activation**
by A. Buchholz (2011), xiv, 134 pages
ISBN: 978-3-89336-691-0

98. **Chrom-bezogene Degradation von Festoxid-Brennstoffzellen**
von A. Neumann (2011), xvi, 218 Seiten
ISBN: 978-3-89336-692-7

99. **Amorphous and microcrystalline silicon applied in very thin tandem solar cells**
by S. Schicho (2011), XII, 190 pages
ISBN: 978-3-89336-693-4

100. **Sol-gel and nano-suspension electrolyte layers for high performance solid oxide fuel cells**
by F. Han (2011), iv, 131 pages
ISBN: 978-3-89336-694-1

101. **Impact of different vertical transport representations on simulating processes in the tropical tropopause layer (TTL)**
by F. Plöger (2011), vi, 104 pages
ISBN: 978-3-89336-695-8

102. **Untersuchung optischer Nanostrukturen für die Photovoltaik mit Nahfeldmikroskopie**
von T. Beckers (2011), xiii, 128 Seiten
ISBN: 978-3-89336-696-5

103. **Impact of contamination on hydrogenated amorphous silicon thin films & solar cells**
by J. Wördenweber (2011), XIV, 138 pages
ISBN: 978-3-89336-697-2

104. **Water and Organic Nitrate Detection in an AMS: Laboratory Characterization and Application to Ambient Measurements**
by A. Mensah (2011), XI, 111 pages
ISBN: 978-3-89336-698-9

105. **Entwicklung eines neuen Konzepts zur Steuerung der thermischen Ausdehnung von glaskeramischen Verbundwerkstoffen mit angepasster Fließfähigkeit am Beispiel der Hochtemperatur-Brennstoffzelle**
von E. Wanko (2011), xi, 134 Seiten
ISBN: 978-3-89336-705-4

106. **Tomographic reconstruction of atmospheric volumes from infrared limb-imager measurements**
by J. Ungermann (2011), xiv, 153 pages
ISBN: 978-3-89336-708-5

107. **Synthese und Identifizierung von substituierten Mg-Al-Cl Doppelhydroxidverbindungen mit Schwerpunkt IR-Spektroskopie**
von B. Hansen (2011), XII, 121 Seiten
ISBN: 978-3-89336-709-2

108. **Analysis of spatial soil moisture dynamics using wireless sensor networks**
by U. Rosenbaum (2011), xxii, 120 pages
ISBN: 978-3-89336-710-8

109. **Optimierung von APS-ZrO2-Wärmedämmschichten durch Variation der Kriechfestigkeit und der Grenzflächenrauhigkeit**
von M. E. Schweda (2011), 168 Seiten
ISBN: 978-3-89336-711-5

110. **Sorption of a branched nonylphenol isomer and perfluorooctanoic acid on geosorbents and carbon nanotubes**
by C. Li (2011), X, 102 pages
ISBN: 978-3-89336-716-0

111. **Electron Transport in the Plasma Edge with Rotating Resonant Magnetic Perturbations at the TEXTOR Tokamak**
by H. Stoschus (2011), iv, 113 pages
ISBN: 978-3-89336-718-4

112. **Diffusion and Flow Investigations in Natural Porous Media by Nuclear Magnetic Resonance**
by N. Spindler (2011), viii, 144 pages
ISBN: 978-3-89336-719-1

113. **Entwicklung und Erprobung des Hygrometer for Atmospheric Investigations**
von T. Klostermann (2011), IV, 118 Seiten
ISBN: 978-3-89336-723-8

114. **Application of functional gene arrays for monitoring influences of plant/seasons on bacterial functions and community structures in constructed wetlands (Bitterfeld, Germany)**
by J. Ning (2011), xiv, 157 pages
ISBN: 978-3-89336-724-5

115. **Wasseraustrag aus den Kathodenkanälen von Direkt-Methanol-Brennstoffzellen**
von A. Schröder (2011), VII, 228 Seiten
ISBN: 978-3-89336-727-6

116. **CITYZEN Climate Impact Studies**
ed. by M. Schultz (2011), 45 pages
ISBN: 978-3-89336-729-0

117. **Software Tools zum interoperablen Austausch und zur Visualisierung von Geodatensätzen über das Internet**
von M. Schultz, M. Decker, S. Lührs (2011), iv, 156 Seiten
ISBN: 978-3-89336-730-6

118. **Optimierung eines Leichtbaudesigns für ein SOFC-Brennstoffzellenstack**
von T. Nguyen-Xuan (2011), III, 154 Seiten
ISBN: 978-3-89336-732-0

119. **Institute of Energy and Climate Research IEK-6:**
Nuclear Waste Management & Reactor Safety Report 2009/2010
Material Science for Nuclear Waste Management
ed. by M. Klinkenberg, S. Neumeier, D. Bosbach (2011), 242 pages
ISBN: 978-3-89336-735-1

120. **Fate of the Antibiotic Sulfadiazine in Yangtze River Sediments: Transformation, Sorption and Transport**
by N. Meng (2011), XII, 111 pages
ISBN: 978-3-89336-736-8

121. **Thermodynamische Eigenschaften gasförmiger und kondensierter Verbindungen für Hochtemperaturanwendungen**
von T. Markus (2011), II, 131 Seiten
ISBN: 978-3-89336-728-3

122. **Ein neues LIF-Instrument für flugzeug- und bodengebundene Messungen von OH- und HO_2-Radikalen in der Troposphäre**
von S. Broch (2011), IV, 160 Seiten
ISBN: 978-3-89336-742-9

123. **Processes in the Yangtze River System - Experiences and Perspectives**
Workshop-Proceedings
ed. by S. Küpper, G. Subklew, R.-D. Wilken (2011), 83 pages
ISBN: 978-3-89336-744-3

124. **Thermo-Mechanical Properties of Mixed Ion-Electron Conducting Membrane Materials**
by B. Huang (2011), 130 pages
ISBN: 978-3-89336-746-7

125. **Growth, Etching, and Stability of Sputtered ZnO:Al for Thin-Film Silicon Solar Cells**
by J. I. Owen (2011), xv, 192 pages
ISBN: 978-3-89336-749-8

126. **Entwicklung geträgerter $Ba_{0,5}Sr_{0,5}Co_{0,8}Fe_{0,2}O_{3-\delta}$ Sauerstoff-Permeationsmembranen**
von F. Schulze-Küppers (2011), ii, 119 Seiten
ISBN: 978-3-89336-752-8

127. **Development of the 2-Component-Injection Moulding for Metal Powders**
by A. P. Cysne Barbosa (2011), XIV, 150 pages
ISBN: 978-3-89336-753-5

128. **Performance of Tungsten-Based Materials and Components under ITER and DEMO Relevant Steady-State Thermal Loads**
by G. H. Ritz (2011), X, 128 pages
ISBN: 978-3-89336-755-9

129. **Experimentelle Bestimmung und numerische Simulation von Viskositäten in Schlackesystemen unter Vergasungsbedingungen**
von T. Nentwig (2011), 156 Seiten
ISBN: 978-3-89336-756-6

130. **Development of Thin Film Oxygen Transport Membranes on Metallic Supports**
by Y. Xing (2012), iv, 117 pages
ISBN: 978-3-89336-765-8

131. **Release of Inorganic Trace Elements from High-Temperature Gasification of Coal**
by M. Bläsing (2012), XVIII, 145 pages
ISBN: 978-3-89336-772-6

132. **Rauchgasseitige Korrosion von Nickelbasislegierungen für zukünftige 700°C-Dampfkraftwerke**
von F. Lüttschwager (2012), 145 Seiten
ISBN: 978-3-89336-773-3

133. **In-Situ Raman Spectroscopy: A Method to Study and Control the Growth of Microcrystalline Silicon for Thin-Film Solar Cells**
by S. Muthmann (2012), x, 134 pages
ISBN: 978-3-89336-774-0

134. **Remote sensing of sun-induced fluorescence for improved modeling of gross primary productivity in a heterogeneous agricultural area**
by A. Schickling (2012), xvi, 135 pages
ISBN: 978-3-89336-775-7

135. **Untersuchung der Ladungsträgerkonzentration und -beweglichkeit in mikrokristallinen Siliziumlegierungen mit Hall-Effekt undThermokraft**
von C. Sellmer (2012), 159 Seiten
ISBN: 978-3-89336-778-8

136. **Development of thin film inorganic membranes for oxygen separation**
by H. J. Moon (2012), XII, 118 pages
ISBN: 978-3-89336-781-8

137. **Influence of Material and Testing Parameters on the Lifetime of TBC Systems with MCrAlY and NiPtAl Bondcoats**
by P. Song (2012), V, 126 pages
ISBN: 978-3-89336-783-2

138. **Strömungsmechanische Modellierung eines Brenngaserzeugungssystems**
von F. Scharf (2012), vi, 223 Seiten
ISBN: 978-3-89336-784-9

139. **Clouds and aerosol in infrared radiative transfer calculations for the analysis of satellite observations**
by S. Grießbach (2012), viii, 169 pages
ISBN: 978-3-89336-785-6

140. **Untersuchung zum Thin Film Low Pressure Plasma Spraying (LPPS-TF) Prozess**
von A. Hospach (2012), 165 Seiten
ISBN: 978-3-89336-787-0

141. **Development of thermal spray processes with liquid feedstocks**
by A. Guignard (2012), 128 pages
ISBN: 978-3-89336-788-7

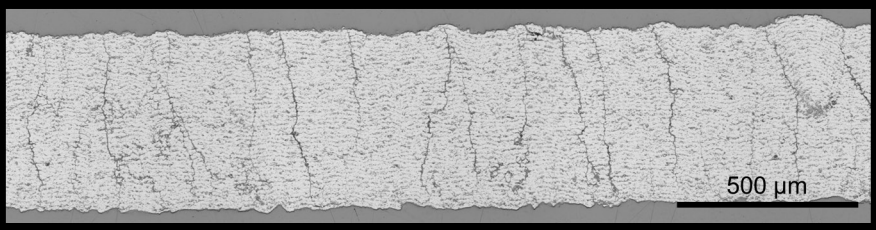

Energie & Umwelt / Energy & Environment
Band / Volume 141
ISBN 978-3-89336-788-7

JÜLICH
FORSCHUNGSZENTRUM